

AD-A086 734

MOTOROLA INC SCOTTSDALE ARIZ GOVERNMENT ELECTRONICS DIV F/6 20/2
DOUBLY ROTATED CUT SAW DEVICES.(U)
JUN 80 D F WILLIAMS, F Y CHO

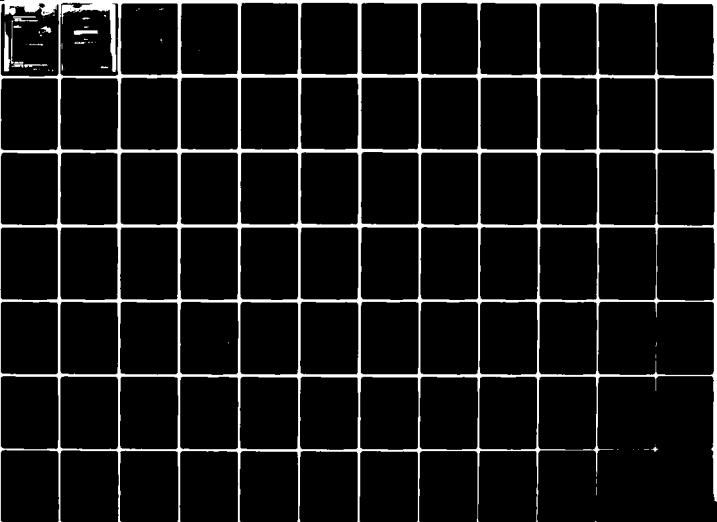
DAAK20-79-C-0275

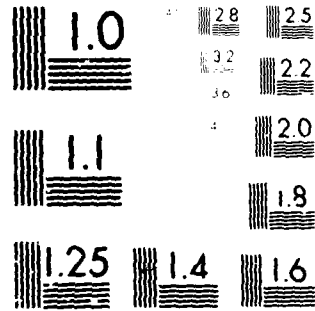
NL

UNCLASSIFIED

DELET-TR-79-0275-1

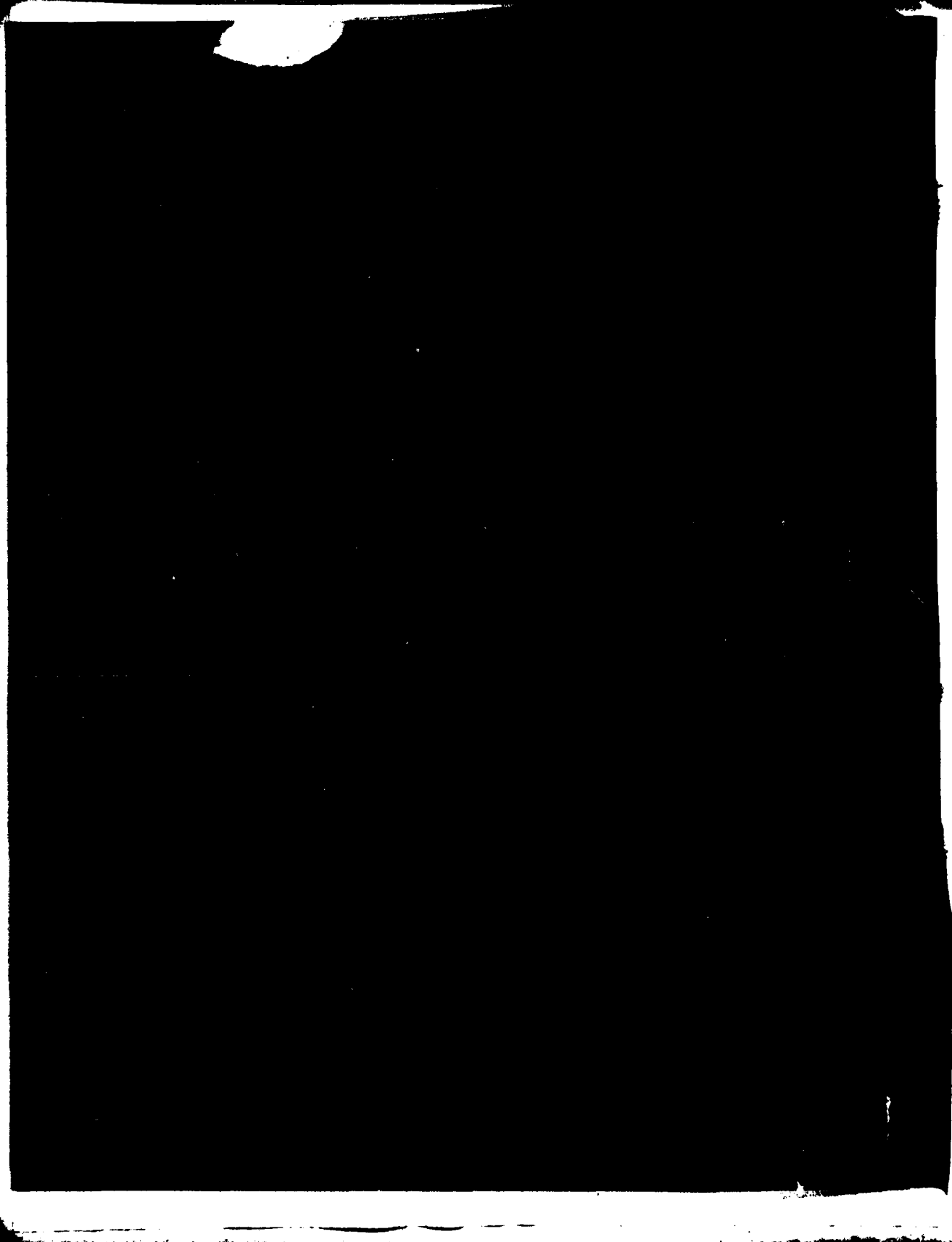
1 of 2
AD
20-79-734





MICROCOPY RESOLUTION TEST CHART
NBS 1963-A





UNCLASSIFIED

SECURITY CLASSIFICATION OF THIS PAGE (When Data Entered)

REPORT DOCUMENTATION PAGE		READ INSTRUCTIONS BEFORE COMPLETING FORM	
1. REPORT NUMBER DELET-TR-79-8275-1	2. GOVT ACCESSION NO. AD-A086 734	3. RECIPIENT'S CATALOG NUMBER (14) G.C.S.	
4. TITLE (and Subtitle) Doubly Rotated Cut SAW Devices		5. DATE OF REPORT (and Period Covered) Interim Report 15 August 1979 - May 1 March 1980	
6. AUTHOR(s) D.F. Williams, F.Y. Cho		7. CONTRACT OR GRANT NUMBER(s) DAAK20-79-C-8275 (New)	
8. PERFORMING ORGANIZATION NAME AND ADDRESS Motorola, GED 8201 E. McDowell Rd. Scottsdale, AZ 85252		9. PROGRAM ELEMENT, PROJECT, TASK AREA & WORK UNIT NUMBER 612705.H94.09.11.01	
10. CONTROLLING OFFICE NAME AND ADDRESS Director, US Army Electronics Tech & Devices Lab ATTN: DELET-MM Fort Monmouth, NJ 07703		11. REPORT DATE June 1980	
12. PERFORMING AGENCY NAME & ADDRESS (if different from Controlling Office)		13. NUMBER OF PAGES 119	
		14. SECURITY CLASS. (of this report) UNCLASSIFIED	
		15. DECLASSIFICATION/DEREGISTRATION SCHEDULE	
16. DISTRIBUTION STATEMENT (of this Report) Approved for Public Release; Distribution Unlimited.			
17. DISTRIBUTION STATEMENT (of the abstract entered in Block 20, if different from Report) DTIC ELECTE JUL 14 1980 S C D			
18. SUPPLEMENTARY NOTES			
19. KEY WORDS (Continue on reverse side if necessary and identify by block number) Surface Acoustic Waves, Quartz, Temperature Coefficient of Frequency, X-Ray Orientation			
20. ABSTRACT (Continue on reverse side if necessary and identify by block number) The objective of this program is the exploratory development of doubly rotated cuts of quartz possessing superior Surface Acoustic Wave (SAW) properties for applications involving environmentally hardened devices. The key properties examined and optimized both theoretically and experimentally are: first, second and third order Temperature Coefficients of Delay (TCD), piezoelectric coupling factor, power flow angle, Bulk Acoustic Wave (BAW) inverse velocity surfaces, degeneracies and leaky waves, and sensitivities of the above quantities to misorientations and manufacturing tolerances. →			

DD FORM 1 JAN 79 1473 EDITION OF 1 NOV 65 IS OBSOLETE

UNCLASSIFIED

SECURITY CLASSIFICATION OF THIS PAGE (When Data Entered)

4011071

UNCLASSIFIED

SECURITY CLASSIFICATION OF THIS PAGE(When Data Entered)

The program consists of two major task areas comprising an interactive numerical/experimental approach. Task I involves the numerical computation of the key SAW properties for doubly rotated quartz substrates for the purpose of locating promising angular ranges with properties superior to the singly rotated cuts now in existence. More detailed calculations follow to refine the angular coordinates in order to specify cuts for experimental verification in Task II. In Task II, sets of substrates with promising orientations identified in Task I will be prepared and SAW device patterns will be fabricated for evaluation of the key SAW properties. The experimental results of this task will be correlated with the theoretical predictions and an iterative process develops for refinement of both theoretical and experimental parameters. As the program proceeds, working SAW device models will be delivered as a demonstration of progress and an indication of the future potential of the doubly rotated cuts. Depending upon the progress made and time and budget limitations, additional properties in the area of nonlinear elasticity will be investigated. This report contains the result of Task I and part of Task II.

Accession For	
NTIS GRA&I	<input checked="" type="checkbox"/>
DDC TAB	<input type="checkbox"/>
Unannounced	
Justification	
By _____	
Distribution/	
Availability Codes	
Dist.	Avail and/or special
A	

UNCLASSIFIED

SECURITY CLASSIFICATION OF THIS PAGE(When Data Entered)

TABLE OF CONTENTS

Section	Page
I INTRODUCTION	1
1 PROGRAM OBJECTIVE	1
2 PROGRAM SCOPE	1
3 TECHNICAL APPROACH SUMMARY	1
II TECHNICAL DISCUSSION	3
1 INTRODUCTION	3
a. Calculation of Temperature Coefficients	4
b. Rayleigh Wave	5
c. Methods for Calculating the Temperature Dependence of the Rayleigh Velocity	6
d. Piezoelectric Coupling Factor	58
e. Power Flow Angle	60
f. Proximity and Excitation Strength of Bulk Waves (BAW) Spectrum	61
g. Degeneracies	64
h. Sensitivities Due to Crystal Misorientation	66
2 WAFER FABRICATION	68
a. Face Definitions	69
b. Running the X-Ray Program	69
c. Analysis of X-Ray Program	71
d. Determination of Actual ψ Angle	73
e. Determination of α and β	74
f. Procedure Used to Zero X-Ray Machine	75
g. Cutting Techniques for Doubly Rotated Orientations	77
h. Wafer Polishing	77
III CONCLUSION	79
APPENDIX A — VOLUME PERTURBATION OF AULD	81
APPENDIX B — VOLUME PERTURBATION FORMULA OF SINHA AND TIERSTEN	85
APPENDIX C — THE DIFFERENTIATION METHOD	87
APPENDIX D — SOLUTION METHOD	91
APPENDIX E — EQUIVALENCE OF TEMPERATURE COEFFICIENTS OF FREQUENCY AND DELAY	93
APPENDIX F — X-RAY RUN	95
APPENDIX G — X-RAY PROGRAM	99

LIST OF FIGURES

Figure	Page
1 Finite Difference Method Versus Experiment ST-Cut (Quartz)	9
2 Finite Difference Method Calculation for Hauden's Cut (YXwlt) $56^\circ/40^\circ/27^\circ$	10
3 Tiersten's Method Versus Finite Difference and Experiment	11
4 Calculated Values of TCF ⁽¹⁾ Versus Propagation Angles	13
5 TCF Map of SAW Device on Quartz	53
6 Temperature Coefficients of the Fundamental Constants of Quartz	55
7 Nonzero Power Flow Angle	61
8 Bragg Condition for Excitation of BAW	62
9 Polar Plots of Inverse Velocities for a (YXwlt) $0/27/137.8$	63
10 Polar Plots of Inverse Velocities for a (YXwlt) $7/27/135.59$	64
11 Flow Diagram of Calculation for Reflected Angles in Doubly Rotated Cut of Quartz	70
12 Two Possible Ways of Defining the Crystal Axes on a Lumbered Bar	71
13 X-ray Position Chart	72
14 Direction of Mask Alignment Angle Rotation	73
15 Crystal Rotation (YXwlt) $\phi/\theta/0$	73
16 Actual -Z Face, Crystalline Axes, α , β , and $\Delta\psi$	74
17 Mask Rotation to Obtain Desired ψ	75
18 Position of Step 3, 10.1 Alignment Wafer	76
19 Position of Step 5, 10.1 Alignment Wafer Rotated by 180 Degrees About -Y Axis	76

LIST OF TABLES

Table	Page
1. Crystal Elastic Constants' Temperature Derivatives	54
2 Propagation Characteristics of Selected Orientations.....	57
3 Propagation Characteristics of Selected Orientations.....	59
4 Power Flow Angles ST-Cut	61
5 $\partial TCF^{(1)}/\partial\psi$ For Selected Cuts	67
6 $\partial TCF^{(1)}/\partial\phi$ and $\partial TCF^{(1)}/\partial\theta$ For Selected Cuts	68

SECTION 1

INTRODUCTION

1. PROGRAM OBJECTIVE

The objective of this program is the exploratory development of doubly rotated cuts of quartz possessing superior Surface Acoustic Wave (SAW) properties for applications involving environmentally hardened devices. The key properties examined and optimized both theoretically and experimentally are: first, second and third order Temperature Coefficients of Delay (TCD), piezoelectric coupling factor, power flow angle, Bulk Acoustic Wave (BAW) inverse velocity surfaces, leaky waves, and sensitivities of the above quantities to misorientations and manufacturing tolerances.

2. PROGRAM SCOPE

The program consists of two major task areas comprising an interactive numerical/experimental approach. Task I involves the numerical computation of the key SAW properties for doubly rotated quartz substrates for the purpose of locating promising angular ranges with properties superior to the singly rotated cuts now in existence. More detailed calculations follow to refine the angular coordinates in order to specify cuts for experimental verification in Task II. In Task II, sets of substrates with promising orientations identified in Task I are prepared and SAW device patterns fabricated for evaluation of the key SAW properties. The experimental results of this task are correlated with the theoretical predictions and an iterative process develops for refinement of both theoretical and experimental parameters. As the program proceeds, working SAW device models will be delivered as a demonstration of progress and an indication of the future potential of the doubly rotated cuts. Depending upon the progress made and time and budget limitations, additional properties in the area of nonlinear elasticity will be investigated.

3. TECHNICAL APPROACH SUMMARY

To accurately characterize the properties of doubly rotated quartz, three basic capabilities are essential:

- a. Theoretical approach and associated computer software which will accurately and quickly locate promising zero TCD cut angles and characterize the other key SAW parameters
- b. Source of rotated quartz substrates of superior quality which can be quickly fabricated and the angular orientation which can be determined with a high degree of precision
- c. Required fabrication facilities and measurement tools to accurately determine the key SAW device parameters.

In the theoretical area, this program has characterized two basic theoretical approaches for the identification of zero TCDs on rotated cuts of quartz. For this study, two computer programs available at Motorola are used. The first program calculates the first, second and third order TCDs of rotated cuts using a finite difference method. This technique is simple, well established, and has been used for analytically determining the temperature coefficient curves for singly and doubly rotated cuts of quartz. To more accurately refine the temperature coefficient properties, a second program which encompasses lattice skewing effects is used. This more complete theoretical approach is based on the work of Sinha and Tiersten¹; its utility has been verified.

The final theoretical work is the characterization of the other key parameters with standard SAW programs used routinely for material characterization and device development.

Accurately oriented quartz bars, supplied by Motorola, Carlisle, are cut, lapped and finely polished at Motorola. A mechanical polishing procedure is used. During this program, several substrates from a single bar with incremental angular deviations about a promising angular position are fabricated. By careful organization of the angle selection and cut procedures, a substantial savings in time and money is achieved.

The angular orientation of the doubly rotated substrates are defined to an accuracy of within ± 5 minutes using X-ray diffractometry. Equipment used includes Laue pattern X-ray equipment, X-ray diffractometers, and precision wafer cut and polishing equipment.

A complete SAW test area and optical laboratory form the basis for evaluating the key SAW parameters of the doubly rotated quartz delay lines, oscillators and resonators. The equipment will be set up for rapid display and recording of the SAW parameters.

¹"On The Temperature Dependence of the Velocity of Surface Waves in Quartz", B.K. Sinha and H.F. Tiersten, Proceedings of the 32nd Annual Symposium on Frequency Control, 1978, pp. 150 - 153.

SECTION II

TECHNICAL DISCUSSION

The following section discusses the technical approaches used in this program. A comparison of numerical approaches is made and the numerical approach used is described in paragraph 1 (Task I). Experimental techniques (Task II) will be outlined in paragraph 2.

1. INTRODUCTION

Quartz is the most commonly used substrate for fabricating Surface Acoustic Wave (SAW) devices. In SAW narrowband filter, oscillator, and resonator applications, the temperature stability of the device is an important design parameter. Currently, almost all SAW devices fabricated on quartz use the ST-Cut, which exhibits a parabolic frequency dependence in temperature. For many applications, the temperature dependence of devices fabricated on ST quartz is too large. Thus it is desirable to find crystal cuts with superior temperature performance. Of course, many other design parameters must be considered when choosing a crystal cut. Some of the more important ones are the piezoelectric coupling coefficient, acoustic losses, dependence of device performance on cut misorientation, excitation of bulk modes, and beam steering angle. These parameters are all easily determined for a given cut.

The objectives of this program are to find crystal cuts which exhibit zero temperature coefficients of delay so that there will be no frequency-temperature dependence observed in temperature stable oscillators, resonators and filters. We have used computer models to investigate the temperature dependence of different cuts of crystal for SAW devices.

Defining τ as the delay time for an acoustic wave to propagate between two points on the surface of the crystal, we wish to find orientations for which τ is constant in temperature, or more formally $(1/\tau)(d\tau/dT)|_{T=25 \text{ degrees C}} = 0$.

If F is the frequency of a SAW resonator, we have $(1/F)(dF/dT) = -(1/\tau)(d\tau/dT)$. Of course, we would also like the higher order derivatives to be as close to zero as possible, or $(1/2\tau)(d^2\tau/dT^2)|_{T=25 \text{ degrees C}} = 0$, etc.

Letting ρ be the length between two points, (τ) is simply given by $\tau = (\rho/V)$, $(1/\tau)(d\tau/dT) = (1/\rho)(d\rho/dT) - (1/V)(dV/dT)$.

We have computer programs for calculating τ as a function of the stress, the dielectric and piezoelectric constants of a substrate material. Furthermore, we have at our disposal the temperature variation of those constants for quartz allowing one to calculate $(1/V)(dV/dT)$ by a finite difference method (note that higher order terms can be calculated the same way). If the crystal expansion coefficients are known, it is then a simple matter to calculate $(1/\tau)(d\tau/dT)$ for any particular orientation. Perturbation

programs developed by Sinha and Tiersten to calculate $(1/\tau)(d\tau/dT)$ are also available. Combined with a search method, we are able to find cuts for which first order temperature coefficient of frequency vanishes.

a. Calculation of Temperature Coefficients

It has been shown that determining the temperature dependence of τ (time delay) is equivalent to determining the temperature dependence of F (frequency) via the relation $F \propto 1/\tau$.

Since our experimental data is derived from frequency measurements, we determine the frequency characteristics of the devices. The relation between the temperature coefficient of frequency (TCF) and temperature coefficient of delay (TCD) are related as follows (See Appendix E):

$$\alpha_F^{(1)} = -\alpha_\tau^{(1)} \quad (1)$$

$$\alpha_F^{(2)} = -\alpha_\tau^{(2)} + (\alpha_\tau^{(1)})^2 \quad (2)$$

$$\alpha_F^{(3)} = -\alpha_\tau^{(3)} + 2\alpha_\tau^{(1)} \alpha_\tau^{(2)} - (\alpha_\tau^{(1)})^3 \quad (3)$$

where $\alpha_F^{(i)}$ is the i th order TCF, $\alpha_\tau^{(i)}$ is the i th order TCD.

Using the relations above, one can always relate one set of the temperature coefficients to the other.

The various procedures outlined in the following sections will yield the quantities $\alpha_v^{(i)}$, $i = 1, 2, 3$, with $V_s(T) \cong V_s(T_0)(1 + \alpha_v^{(1)} dT + \alpha_v^{(2)} dT^2 + \alpha_v^{(3)} dT^3)$ and $dT = T - T_0$.

The problem of interest is not only, however, in finding the $\alpha_v^{(i)}$'s but in finding the delay time τ and the frequency dependence F of a device. The frequency dependence $F(T) = F(T_0)(1 + \alpha_F^{(1)} dT + \alpha_F^{(2)} dT^2 + \alpha_F^{(3)} dT^3)$ is a function of not only V_s , but of $l(T_0) = l(T_0)(1 + \alpha_l^{(1)} dT + \alpha_l^{(2)} dT^2 + \alpha_l^{(3)} dT^3)$, the spacing between reflectors in a resonator (or the length of the delay line in an oscillator)

From the above relations and $(1 + X)^{-1} \cong 1 - X + X^2 - X^3$ if $X \ll 1$, we see that:

$$F = V_s \cdot g \cong \{ V_s \cdot (1 + \alpha_v^{(1)} dT + \alpha_v^{(2)} dT^2 + \alpha_v^{(3)} dT^3) \} / l_0 \cdot (1 + \alpha_l^{(1)} dT + \alpha_l^{(2)} dT^2 + \alpha_l^{(3)} dT^3) \quad (4)$$

$$\cong F(T_0) \{ 1 + \alpha_v^{(1)} dT + \alpha_v^{(2)} dT^2 + \alpha_v^{(3)} dT^3 \quad (5)$$

$$- \alpha_l^{(1)} dT - \alpha_l^{(1)} \alpha_v^{(1)} dT^2 - \alpha_l^{(1)} \alpha_v^{(2)} dT^3$$

$$- \alpha_l^{(2)} dT^2 - \alpha_l^{(2)} \alpha_v^{(1)} dT^3 - \alpha_l^{(3)} dT^3$$

$$+ (\alpha_l^{(1)})^2 dT^2 + (\alpha_l^{(1)})^2 \alpha_v^{(1)} dT^3$$

$$+ 2\alpha_l^{(1)} \alpha_l^{(2)} dT^3 - (\alpha_l^{(1)} dT)^3 \} \quad (6)$$

or

$$\alpha_1^{(1)} = \alpha_1^{(1)} - \alpha_1^{(1)} \quad (7)$$

$$\alpha_1^{(2)} = \alpha_1^{(2)} - \alpha_1^{(1)} \alpha_1^{(1)} + (\alpha_1^{(1)})^2 - \alpha_1^{(2)} \quad (8)$$

$$\alpha_1^{(3)} = \alpha_1^{(3)} - \alpha_1^{(1)} \alpha_1^{(2)} + \alpha_1^{(1)} (\alpha_1^{(1)})^2 \quad (9)$$

$$-(\alpha_1^{(1)})^3 + 2\alpha_1^{(1)} \alpha_1^{(2)} - \alpha_1^{(1)} \alpha_1^{(2)} - \alpha_1^{(3)}$$

giving the frequency dependence directly. The calculation of the temperature coefficients of velocity, $\alpha_1^{(1)}$, is achieved by calculating the phase velocity with the Finite Difference Technique or other techniques discussed below for a variety of temperatures. As the velocity is a function of temperature, a linear regression program is used in the finite difference technique to curve fit the data to a third order polynomial. The constants $\alpha_1^{(1)}$, $\alpha_1^{(2)}$ and $\alpha_1^{(3)}$ are thus obtained by optimum curve fitting of the data points to the polynomial. The temperature coefficients of length, $\alpha_1^{(1)}$, are found in standard references. It should be noted that the α_1 's also depend on the direction of propagation, and must be calculated for each direction of propagation considered by a simple geometrical transformation analogous to that used to rotate all of the other physical constants.

b. Rayleigh Wave

We will briefly discuss the Rayleigh wave solutions in their general form in this section. The coordinate system is defined with the Z or 1 axis being the direction of propagation and the -Y or 3 axis normal to the crystal surface. V_R will denote the Rayleigh wave velocity, $\beta_R = \omega/V_R$, the wave number, u_i (i = 1, 2, 3), the particle displacements along the 1, 2, or 3 axis, $u_4 = \phi$, the electric potential. Also, T_{ij} denotes the stress tensor.

$S_{ii} = (1/2)(du_i/dx_i + du_j/dx_j)$, the strain tensor, c_{ijkl} , the elastic tensor, ρ the density of the substrate, D, the electric displacement, E, the electric field, ϵ_{ij} the dielectric constant, e_{ijk} the piezoelectric constant. We also use Δ for the difference, where, for example,

$$\Delta\rho = \rho(T) - \rho(T_0) = \rho(T_0)(\alpha \rho^{(1)}dT + \alpha \rho^{(2)}dT^2 + \alpha \rho^{(3)}dT^3), \text{ and let } P = \text{power/unit width in the } x \text{ direction.}$$

We assume relations such as

$$T = -e \cdot E + c^E : S \text{ or } S = e \cdot E + S^E : T \quad (10)$$

$$D = \epsilon^S \cdot E + e : S \quad D = \epsilon^T \cdot E + d : T$$

$$\rho \partial^2 u_j / \partial t^2 - c_{ijkl} \partial^2 u_k / \partial x_j \partial x_l - e_{kij} \partial^2 \phi / \partial x_i \partial x_k = 0 \quad (11)$$

$$e_{ik} \partial^2 u_k / \partial x_i \partial x_l - \epsilon_{ik} \partial^2 \phi / \partial x_i \partial x_k = 0$$

The general solution for a wave traveling on the surface can be written

$$u_j = \left[\sum_m C_m \alpha_j^{(m)} \exp(-i\omega/V_j) \sum_{i=1}^3 b_i^{(m)} x_i \right] \exp(i\omega t) \text{ for } j = 1 \text{ to } 4 \quad (12)$$

For the Rayleigh wave, this reduces to $U_1 = \sum_{m=1}^4 C_m \alpha_j^{(m)} \exp(-i\beta_R b^{(m)} y) \exp(i\beta_R z - i\omega t)$ (13)

where the coefficient c_m , $\alpha_j^{(m)}$ (weighting factors), β_R (wave number), and $b^{(m)}$ (complex decay constants) are to be calculated by the standard iterative procedure on a computer.

The fields are calculated as $E = \nabla u_4$ with $E_x = 0$, $E_y = (-i\beta_R b^{(m)})u_4$ and $E_z = (i\beta_R)u_4$.

c. Methods for Calculating the Temperature Dependence of the Rayleigh Velocity

In the following sections, four methods for calculating the temperature characteristics of the Rayleigh wave are discussed.

(1) Finite Difference Technique of Calculating Temperature Dependence of the Rayleigh Velocity

Before $TCD^{(1)} = (1/\tau)(d\tau/dT)$ can be calculated, one must first calculate the dependence of the Rayleigh wave velocity on temperature. The most straightforward method for doing this is the finite difference method. The Rayleigh wave velocities are calculated for different temperatures, yielding the values $V_i(T_i)$, $i = 1, 2, \dots, n$. This is done by first calculating the fundamental constants at the temperature T_1 of interest. The fundamental constants are then rotated into the coordinate system of interest. An iterative procedure is used to calculate a velocity V_i for which Christoffel's equation and the boundary conditions are satisfied simultaneously (see Appendix D). Simple finite difference techniques can be used to calculate $(1/V_i)(dV_i/dT)$, $(1/2V_i)(d^2V_i/dT^2)$, etc. For example, after calculating $V_i(T_i)$ for $T_1 = T_0$, $T_2 = T_0 + \Delta T$, $T_3 = T_0 - \Delta T$, we can use $(1/V_i)(dV_i/dT)$ at $T_0 \cong (1/V_0(T_0))(V_i(T_0 + \Delta T) - V_i(T_0 - \Delta T))/2\Delta$. Alternately, standard linear regression of polynomials may be employed to yield those coefficients. Another approach consists of calculating directly the frequency-temperature characteristics of the orientation for several widely differing temperatures. A measure of the temperature stability is then used. Letting $F(T)$ be the frequency of the device, the measure of deviation is calculated as

$$\begin{aligned} \text{RMS frequency deviation} = \\ \left[\left(\sum_{i=1}^n (F(T_i) - F(T_0))^2 \right) / n \cdot F(T_0)^2 \right]^{1/2} \text{ with} \quad (14) \\ F(T) = V_r(T) / \lambda_0 (1 + \alpha_L^{(1)}(\Delta T) + \alpha_L^{(2)}(\Delta T)^2 + \alpha_L^{(3)}(\Delta T)^3), \end{aligned}$$

although $\alpha_L^{(1)}$, $\alpha_L^{(2)}$, and $\alpha_L^{(3)}$ are calculated for purposes of comparison.

In much of the earlier work, the SAW velocities were calculated at three temperature points, $T_1 = -50^\circ\text{C}$, $T_2 = 25^\circ\text{C}$, and $T_3 = 100^\circ\text{C}$, to save on computer time. The following formulas were used for the calculations of first and second order temperature coefficients of velocity.

$$\begin{aligned}\alpha_V^{(1)} &= [V(T_1) - V(T_3)]/[V(T_2) (T_1 - T_3)] & (15) \\ &= [V(100) - V(-50)]/[V(25) \cdot 150]\end{aligned}$$

$$\begin{aligned}\alpha_V^{(2)} &= [V(T_1) + V(T_3) - 2 \cdot V(T_2)]/[V(T_2) \cdot 2 (T_3 - T_2)(T_2 - T_1)] & (16) \\ &= [V(100 + V(-50) - 2 \cdot V(25)]/[V(25) \cdot 2 (75)(75)]\end{aligned}$$

In the more recent works, six temperature points were calculated for each orientation to provide data for the linear regression analysis. The six temperature points were 100°C , 85°C , 75°C , -25°C , -10°C , and -50°C . The results were used to calculate $\text{TCF}^{(1)}$, $\text{TCF}^{(2)}$ and $\text{TCF}^{(3)}$.

(2) Perturbation Technique of Calculating Temperature Dependence of the Rayleigh Velocity

Perturbation theory may be applied to the problem of calculating the first, second and third order dependence of the Rayleigh velocity V , of a piezoelectric substrate, once the solution to the Rayleigh wave propagation at a temperature reference T_0 is known.

Perturbation techniques allow calculations of small changes in the solutions to a problem caused by small changes in the physical parameters of the problem, once the solution to the unperturbed problem is known. One can apply perturbation techniques either to boundary perturbation such as mass loading on the surface or to volume perturbations such as adding a thin conducting layer to the interior of piezoelectric substrates. As the boundary conditions are unaffected by changes in temperature while material constants such as c_{ij} are temperature dependent, one can apply the volume perturbation theory to the problem.

The general approach to the problem of determining the temperature dependence of V , will be as follows. First, the Rayleigh wave propagation problem will be solved in the standard way in its entirety at room temperature, T_0 . Given the solution of the problem at T_0 and the dependence of the physical constants (such as c_{ij}) on temperature at T_0 , one will apply the volume perturbation formula, calculating the temperature dependence of V . The dependence of V , on T is then used to calculate the frequency characteristics of the actual device given the thermal expansion coefficients as a function of temperature. At this point, the frequency temperature dependence of the substrate as a function of the crystal cut and direction can be thoroughly explored. See Appendix A for a complete discussion of this method.

(3) Approach of Sinha and Tiersten

The primary difficulty with the perturbation technique is that it does not take into account the change of coordinate systems induced by the thermal expansion in the material. This comes about because the material distorts as temperature changes. Thus, the set of axis is to which the *fundamental elastic constants refer, which is fixed to the crystal, is no longer equivalent to the axis used to calculate V.* This problem is elegantly solved by Sinha and Tiersten^{1,2}. The first simplification which occurs is that the density of the material remains constant with temperature. Furthermore, the $\alpha_i^{(0)}$ simply become $\alpha_i^{(0)} = \alpha_i^{(0)}$, as the length in this coordinate system does not change. The only difficulty is that the elastic constants previously used no longer refer to the proper coordinate system and must be rederived from the original experimental data. This procedure has already been carried out for the first order temperature derivation of quartz³ but has not been done for the second and third order coefficients. Nonetheless, the procedure yields more accurate results for the first order dependence. See Appendix B for a mathematical description of the salient features of this technique.

(4) Differentiation Method

A method for determining the theoretical temperature dependence of Rayleigh Surface Waves consists of formally differentiating the wave equation and boundary conditions. The boundary conditions and wave equation must be true at all temperatures, placing constraints on how the parameters of the wave equation may vary. In this technique, the derivatives of these equations with respect to temperature are set to zero and solved for the velocity-temperature dependence. This method follows the methods used by Bechmann, Ballato, and Lukaszek to compute the temperature dependence of the fundamental elastic constants from frequency data, except that the simplifying assumptions of assuming bulk wave solutions cannot be made. This method was later used by Hauden³ to search for temperature stable cuts of quartz. See Appendix C for a discussion of this method.

(5) Summary of Approaches

Of all the techniques presented, the finite difference technique satisfies all of the basic requirements for calculating temperature coefficients of delay. Arbitrary crystal structures may be

¹"On the Temperature Dependence of the Velocity of Surface Waves in Quartz," Sinha and Tiersten, 1978 Ultrasonics Symposium Proceedings, pp. 662-665.

²"Temperature Dependence of the Fundamental Elastic Constants of Quartz," Sinha and Tiersten, Proceedings of the 32nd Annual Symposium on Frequency Control, 1978, pp. 150-153.

³"Higher Order Temperature Coefficients of Quartz SAW Oscillators," D. Hauden, M. Michael, J. J. Gagnepain, Frequency Control Symposium (1978), pp. 77-86.

investigated once the density, piezoelectric, elastic, and dielectric constants and their temperature variation are known. When double precision on the computer is used and when the velocity over a large temperature range is calculated, it becomes a very accurate numerical approach. The computational efficiency of the finite difference method is not as high as some of the other techniques, owing to the need for repeated calculation of the surface wave velocity.

A comparison between the experimental results of Schulz¹ and Motorola's finite difference program adapted from Jones et al.² as shown in Figure 1. The results for this cut and many other orientations studied have been found to be very good. The slight shift of the analytical curve versus experimental curve can be explained by a crystal misorientation.

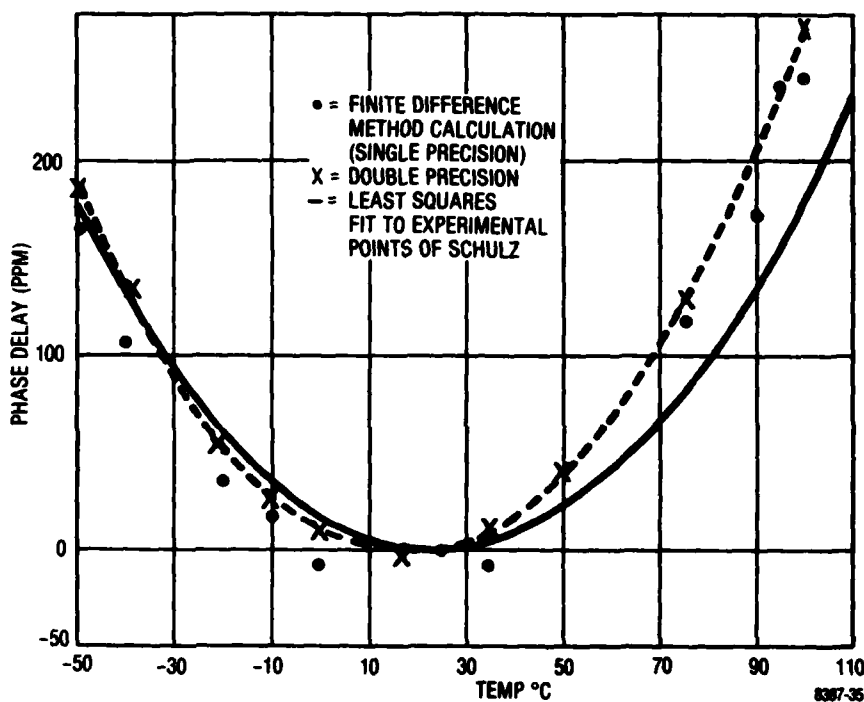


Figure 1. Finite Difference Method Versus Experiment ST-Cut (Quartz)

¹"Surface Acoustic Wave Delay Lines with Small Temperature Coefficient," Schulz, Manfred B., Proc. IEEE, Sept. 1970, pp. 1361-1362.

²"Numerical Computation of Acoustic Surface Waves in Layered Piezoelectric Media - Computer Program Descriptions", Jones, Smith, and Perry, Hughes Aircraft Company, Final Report, Air Force Cambridge Research Laboratories, Contract No. F19628-70-C-0027.

Figure 2 displays a phase delay versus temperature plot for the orientation (YXwlt) 56/40/27 in quartz obtained from Hauden's graphs². Using the differentiation approach, he calculated $\alpha_T^{(1)} = 0$, $\alpha_T^{(2)} = -0.04 \times 10^{-1}$ ppm/°C², $\alpha_T^{(3)} = -22.7 \times 10^{-6}$ ppm/°C³ for a cut close to (YXwlt) 56/40/27. The Finite Difference approach was used to verify his first order calculation but is in disagreement on the second and third order calculations. This can be resolved by experiment.

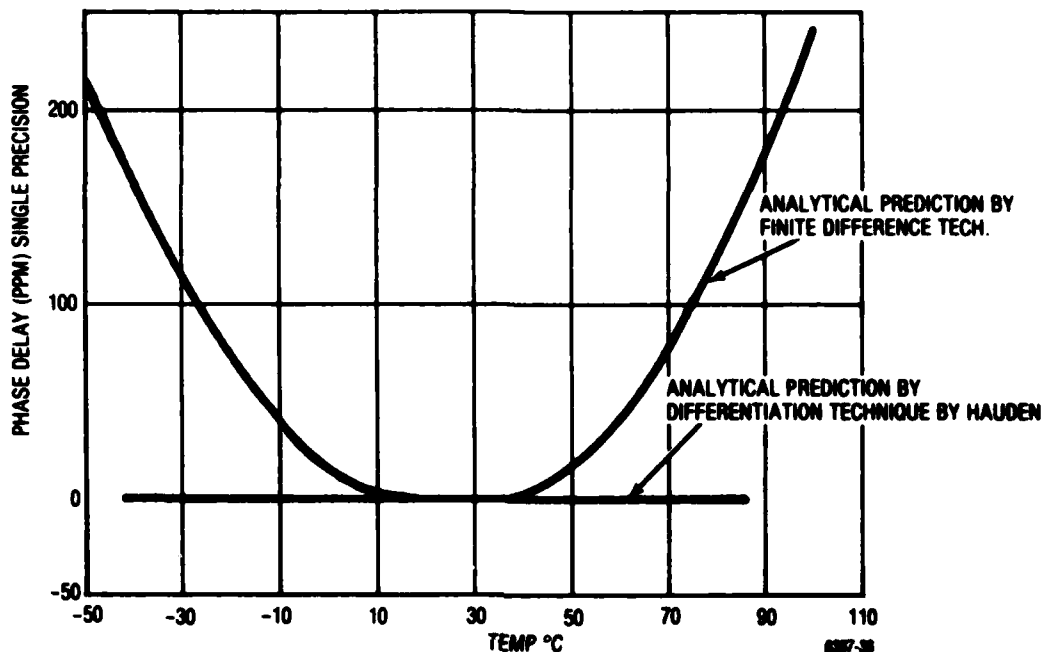


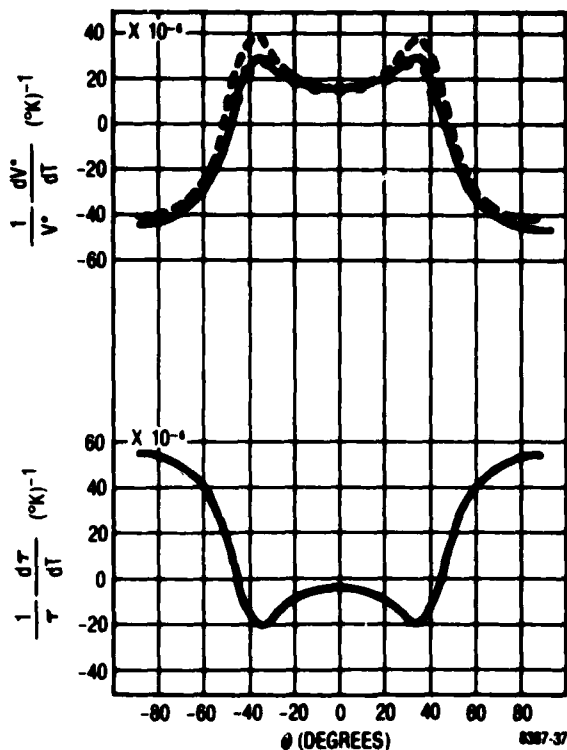
Figure 2. Finite Difference Method Calculation for Hauden's Cut (YXwlt) 56°/40°/27°

Tiersten's Perturbation program, while very difficult to extend to higher orders, is available for calculating the first order TCD.

Figure 3 shows the results of Tiersten's calculation¹ and compares those results with the Finite Difference method as well as experiment. The cut used for comparison is the AT-Cut. The improvement in accuracy is substantial. It offers the significant advantages of being quite cost efficient, as well as being more accurate in the first order on off-axis cuts, our primary area of interest. In the task of making quartz cuts along the surface of zero TCD, accurate values for the first order TCD prove more useful than the less exact values for the first, second, and third order TCD's provided by other methods, because it is a necessary (but not sufficient) condition for zero TCD cut to get a zero first order. Since it is the dominating term, it is important to first get an accurate first order zero TCD locus. Then one may search for the intersection of this locus with the zero second and third order terms with the finite difference technique.

¹"Temperature Dependence of the Fundamental Elastic Constants of Quartz," B. K. Sinha and H. F. Tiersten, Proceedings of the 32nd Annual Symposium on Frequency Control, 1978, pp. 150-153.

²"Higher Order Temperature Coefficients of Quartz SAW Oscillators," D. Hauden, M. Michael, J. J. Gagnepain, Frequency Control Symposium (1978), pp. 77-86.



TEMPERATURE COEFFICIENTS OF ACTUAL VELOCITY AND DELAY FOR SURFACE WAVES ON AT-CUT QUARTZ AS A FUNCTION OF PROPAGATION DIRECTION RELATIVE TO THE DIAGONAL AXIS AT 25°C. THE DOTTED CURVE SHOWS THE AVERAGE OF THE CALCULATED VALUES AT 0°C AND 50°C FROM REF. 1. THE CIRCLES ARE THE AVERAGE OF THE EXPERIMENTAL VALUES AT 0°C AND 50°C. GRAPH OBTAINED FROM REF 1

Figure 3. Tiersten's Method Versus Finite Difference and Experiment

(6) Investigative Approach

A necessary but not sufficient condition to find a temperature stable cut of quartz is that $\alpha_F^{(1)} = 0$. In practice, a sufficient condition for finding a zero temperature cut is that $\alpha_F^{(1)} = \alpha_F^{(2)} = \alpha_F^{(3)} = 0$. Thus every zero temperature cut must be on the locus of angles which satisfy the condition $\alpha_F^{(1)} = 0$. Thus the first problem is to locate accurately such cuts. Both the finite difference approach and Tiersten's method are being used now to calculate the TCF.

The approach used in this program is to identify the areas (angles) where $TCF^{(1)}$, $TCF^{(2)}$ and $TCF^{(3)}$ are relatively low by using the Finite Difference Approach and then define the exact orientation that has zero $TCF^{(1)}$ in those areas by the Sinha and Tiersten approach.

In case the condition $TCF^{(1)} = TCF^{(2)} = TCF^{(3)} = 0$ cannot be met, a compromise approach would be to find an orientation where the first and third order effects tend to cancel out in the temperature range of interest and to find the minimum second order effect orientation amount for those cuts. This approach would provide an effective low TCF cut of quartz for SAW application.

(7) Analytical Results on Zero TCF on Quartz

IRE standard angle definitions (YX wlt) PHI/THETA/PSI for quartz were used throughout the investigation¹. Consider the TCFs to be functions of these angles, which define an angular volume $0 \leq \text{PHI} \leq 30^\circ$, $-90^\circ \leq \text{THETA} \leq 90^\circ$, $0 \leq \text{PSI} \leq 180^\circ$, which spans the space of possible cuts and propagation directions. The set of points at which $\text{TCF}^{(1)}(\text{PHI}, \text{THETA}, \text{PSI}) = 0$ forms a surface in this angular volume. Likewise, the set of points at which $\text{TCF}^{(2)}(\text{PHI}, \text{THETA}, \text{PSI}) = 0$ also form surfaces in this angular volume.

Our object is to find a point where $\text{TCF}^{(1)} = \text{TCF}^{(2)} = \text{TCF}^{(3)} = 0$. If the surface of zero $\text{TCF}^{(1)}$ intersected with the surface of zero $\text{TCF}^{(2)}$, the result would be a line (or a point if the two surfaces are tangent to each other) of angular points on which $\text{TCF}^{(1)} = \text{TCF}^{(2)} = 0$. The intersection of this line with the surface on which $\text{TCF}^{(3)} = 0$ would yield a single point at which $\text{TCF}^{(1)} = \text{TCF}^{(2)} = \text{TCF}^{(3)} = 0$. Neglecting higher order terms, we would have found a temperature stable cut.

The calculated values of $\text{TCF}^{(1)}$ versus propagation angles are shown in Figure 4. The zero $\text{TCF}^{(1)}$ is identified by the areas where $\text{TCF}^{(1)}$ changes sign.

Using the Finite Difference approach with the available crystal constants, the calculated results show that the zero $\text{TCF}^{(1)}$ surfaces do not intersect with the zero $\text{TCF}^{(2)}$ surfaces, based on the interpolated results of the $10^\circ \times 10^\circ \times 10^\circ$ resolution. It is not likely that a finer resolution will provide contrary information because $\text{TCF}^{(1)}$ and $\text{TCF}^{(2)}$ are relatively slow varying functions as shown in Figure 4.

¹"Standards on Piezoelectric Crystals 1949," Proc. IRE 14, Dec. 1949, pp. 1378-1395.

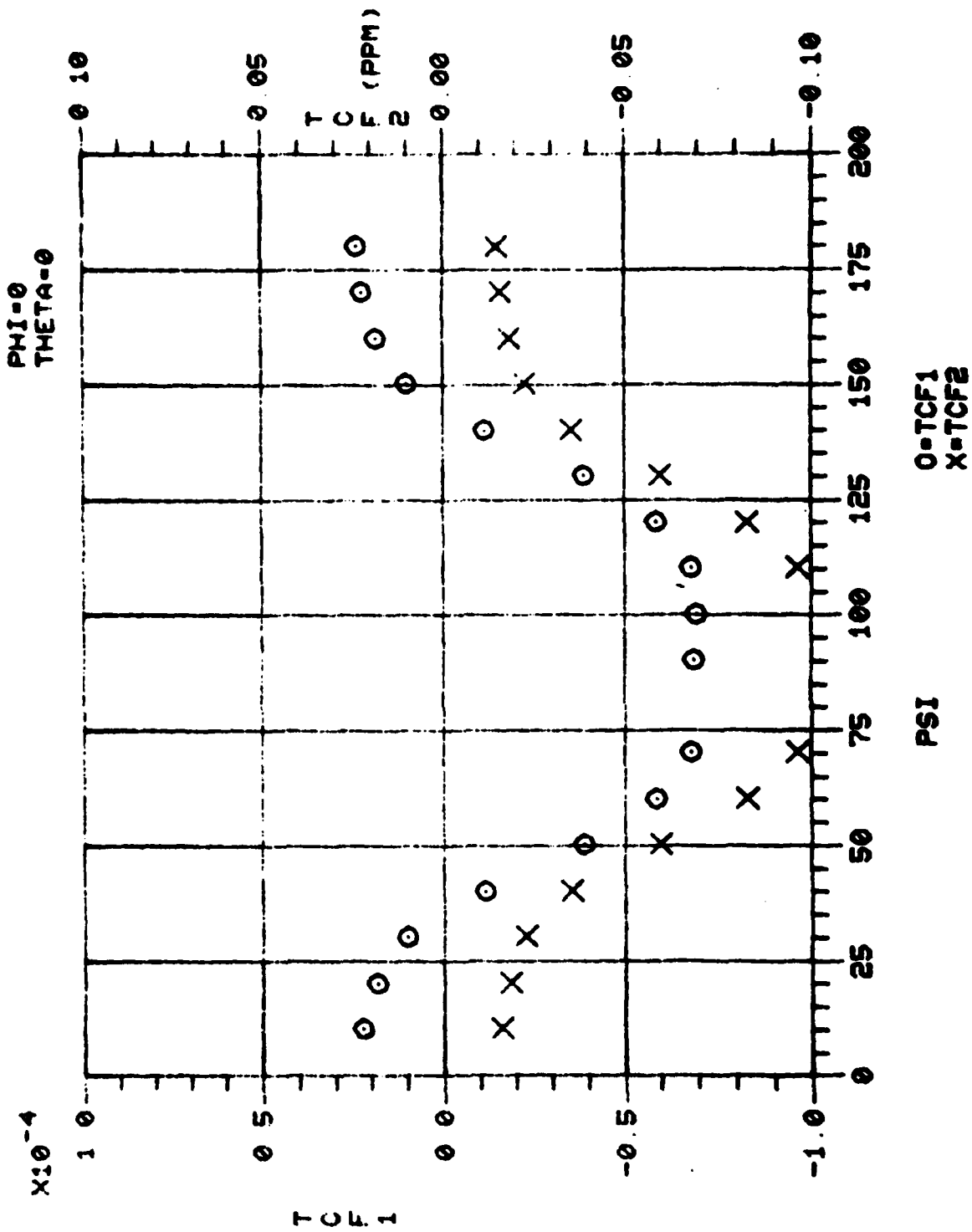


Figure 4A. Calculated Values of TCF_1 Versus Propagation Angles

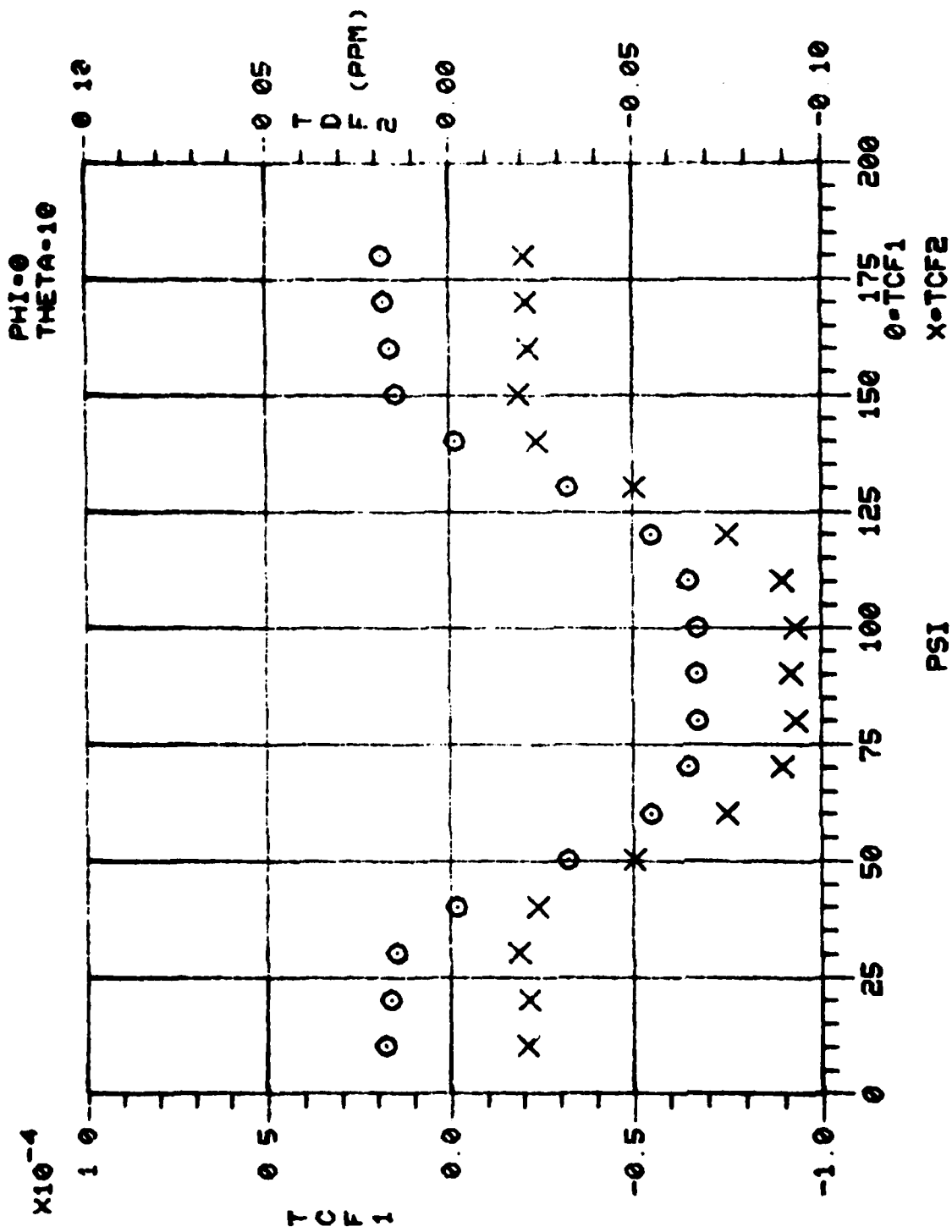


Figure 4B. Calculated Values of TCF⁽¹⁾ Versus Propagation Angles

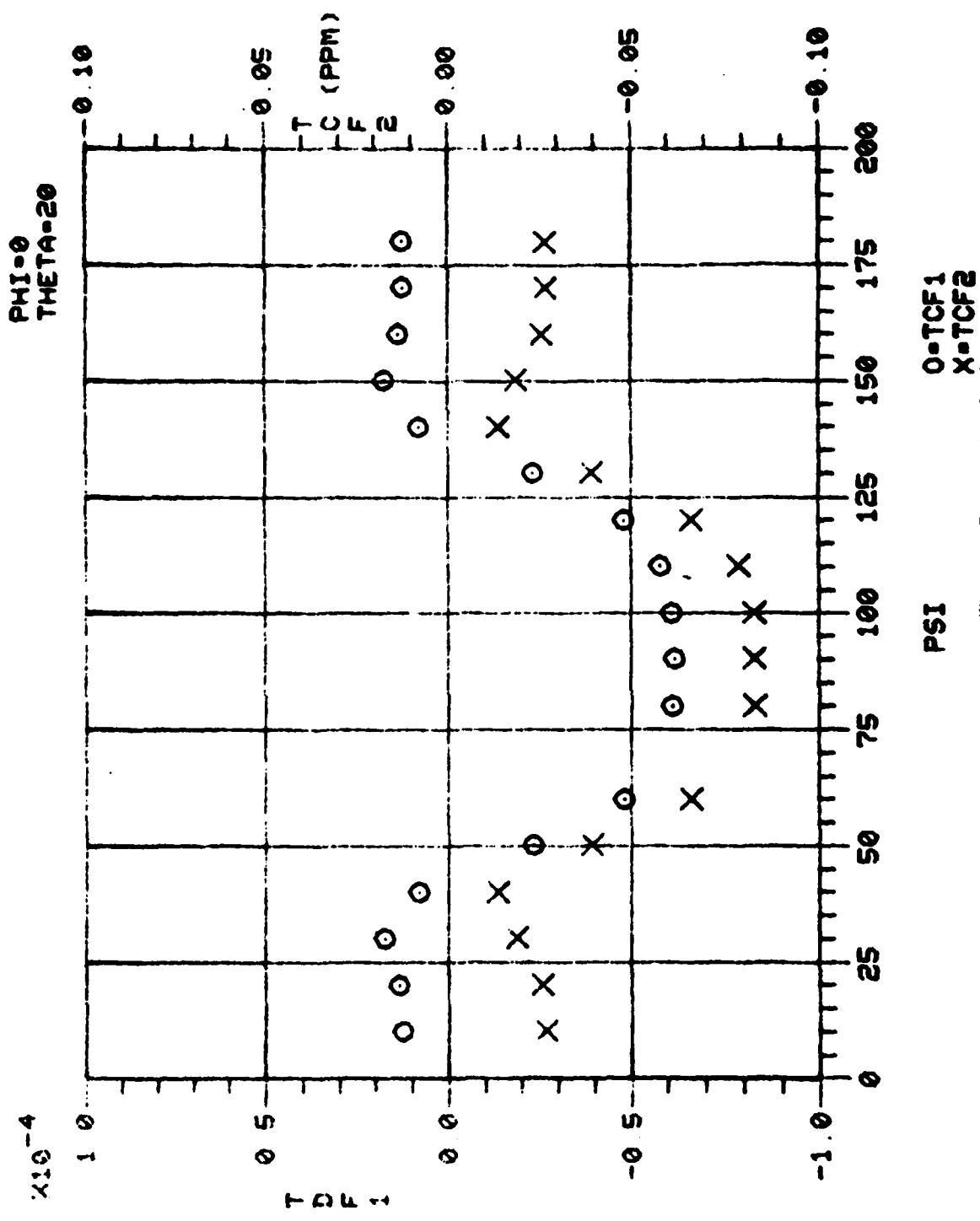


Figure 4C. Calculated Values of TCF⁽¹⁾ Versus Propagation Angles

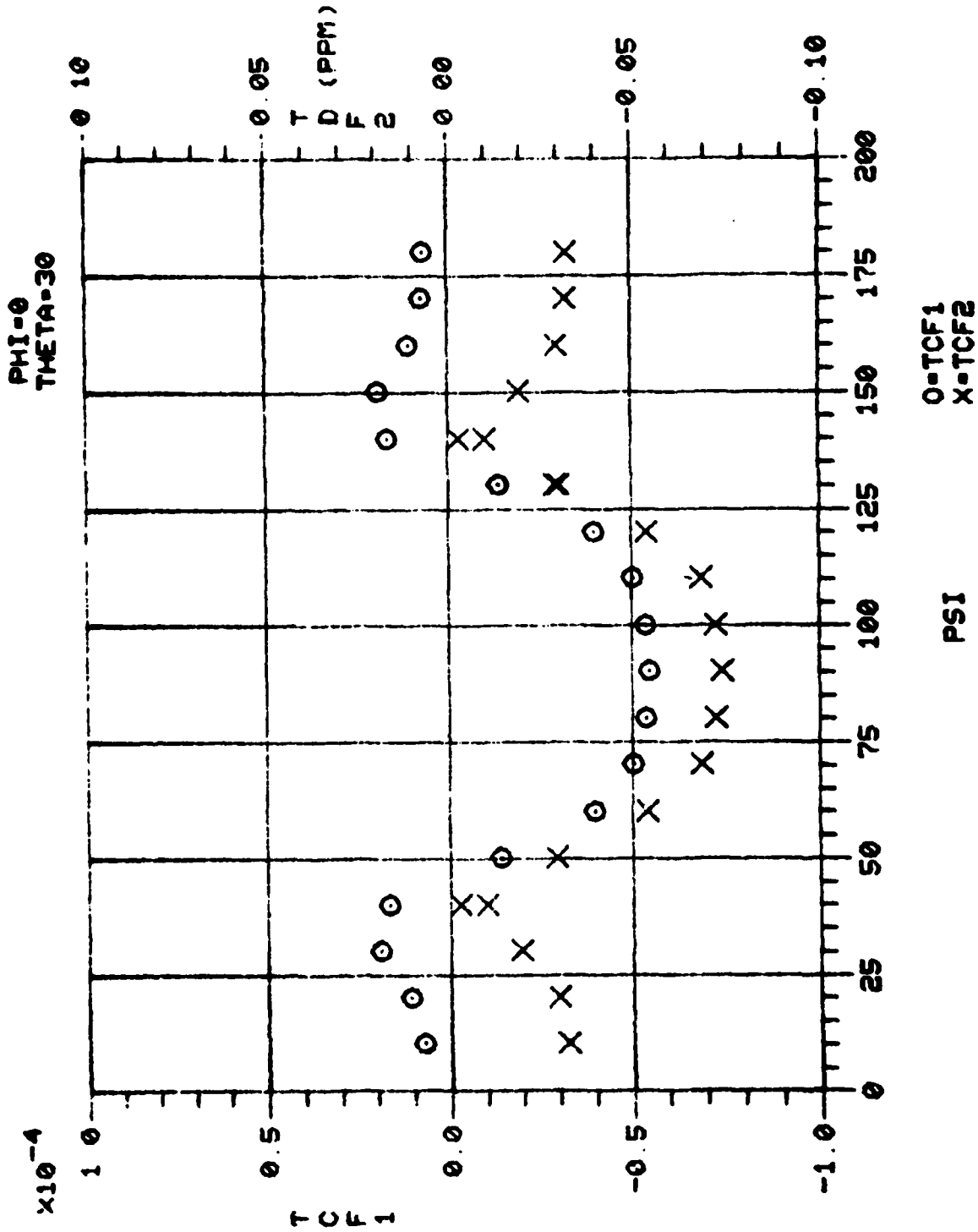


Figure 4D. Calculated Values of TCF⁽¹⁾ Versus Propagation Angles

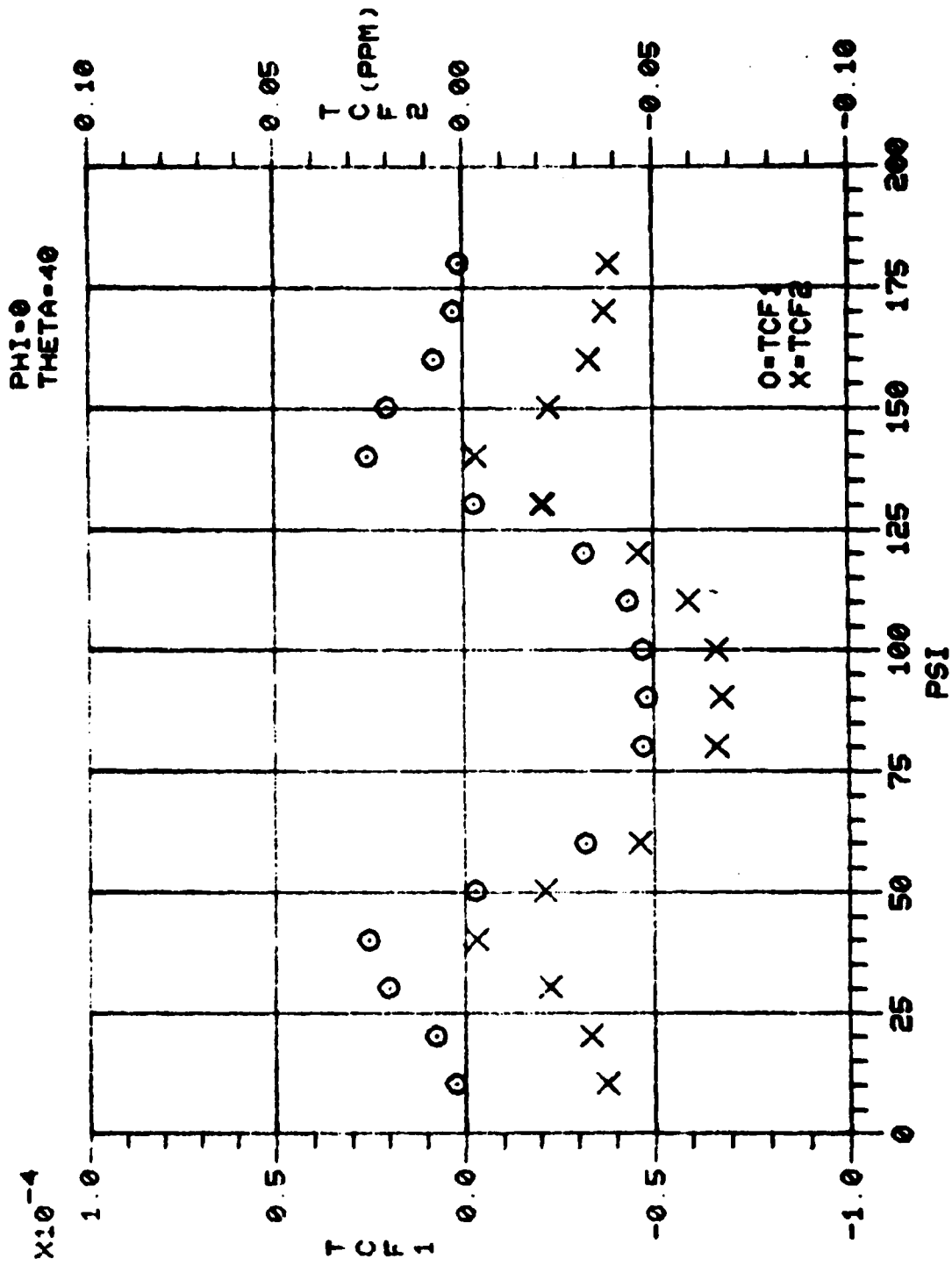


Figure 4E. Calculated Values of TCF⁽¹⁾ Versus Propagation Angles

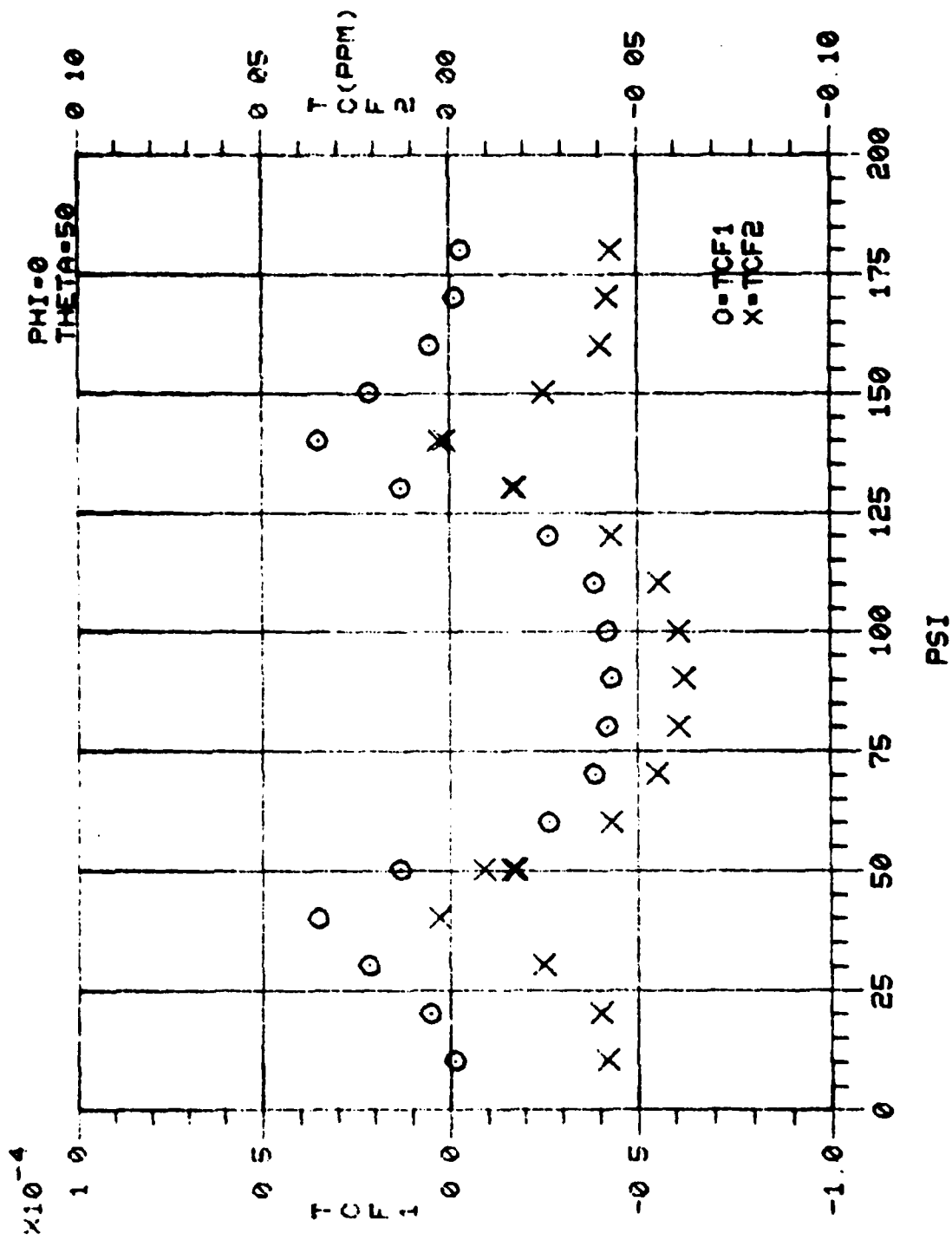


Figure 4F. Calculated Values of TCF⁽¹⁾ Versus Propagation Angles

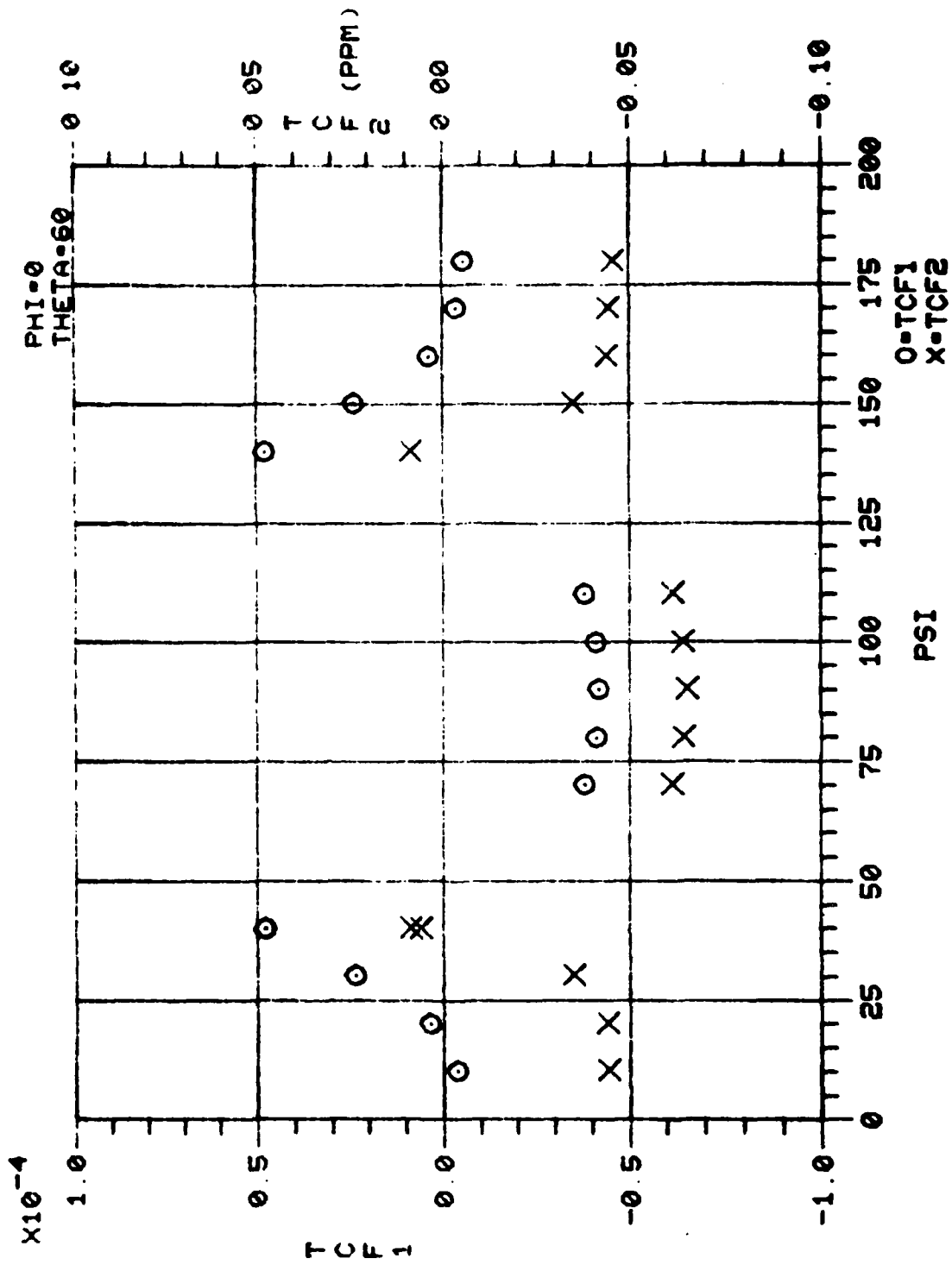


Figure 4G. Calculated Values of TCF⁽¹⁾ Versus Propagation Angles

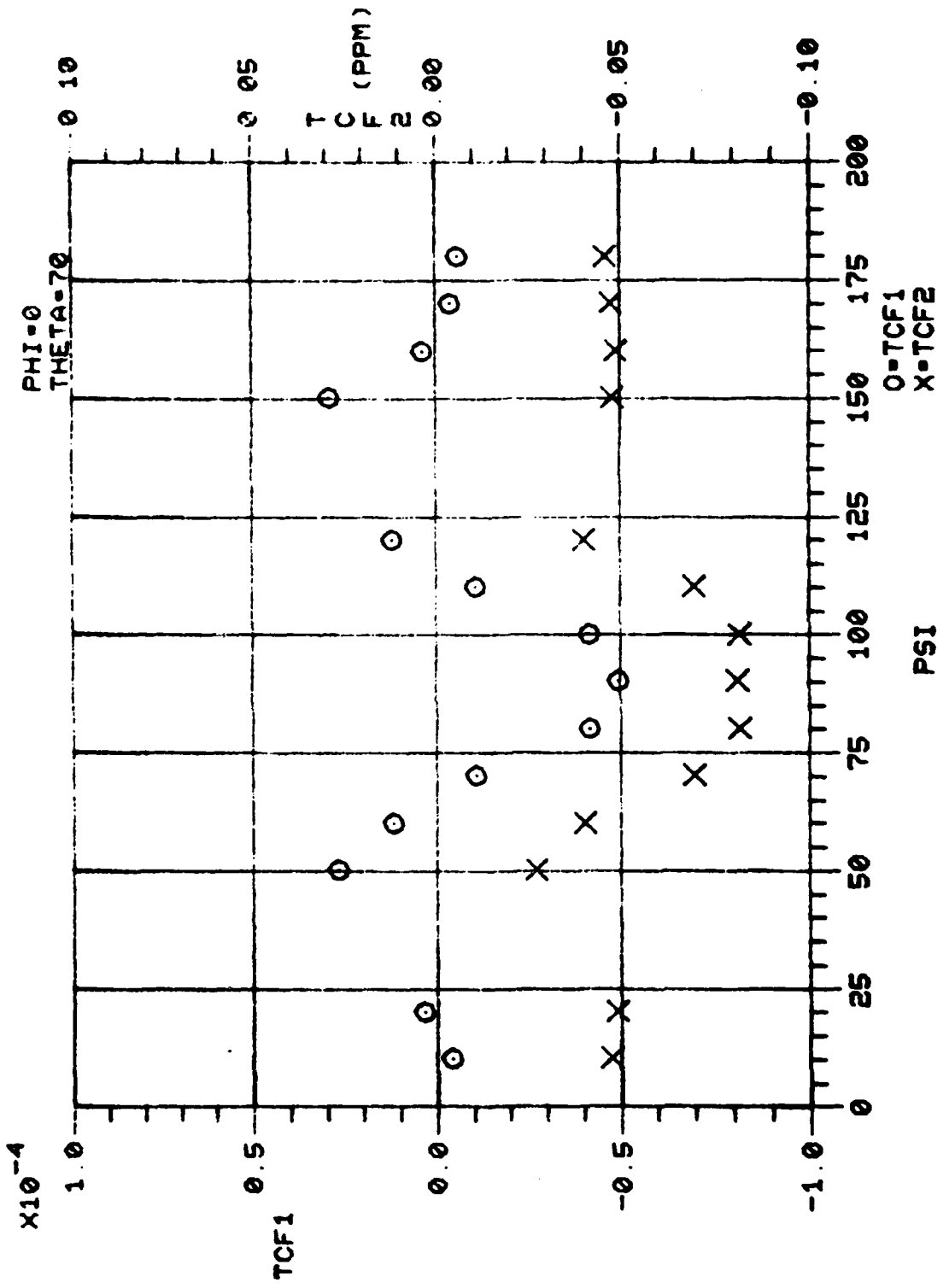


Figure 4H. Calculated Values of TCF⁽¹⁾ Versus Propagation Angles

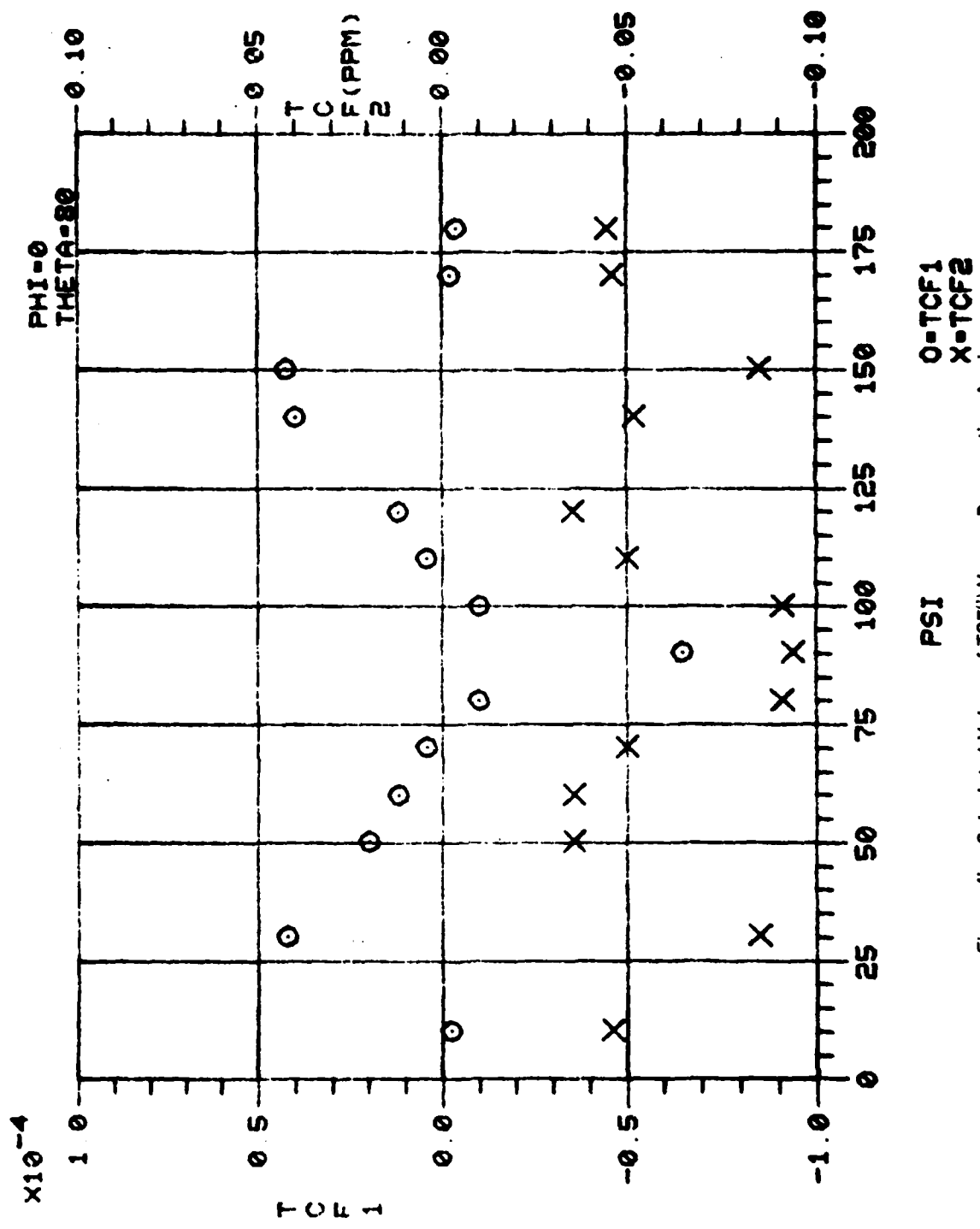


Figure 4I. Calculated Values of TCF⁽¹⁾ Versus Propagation Angles

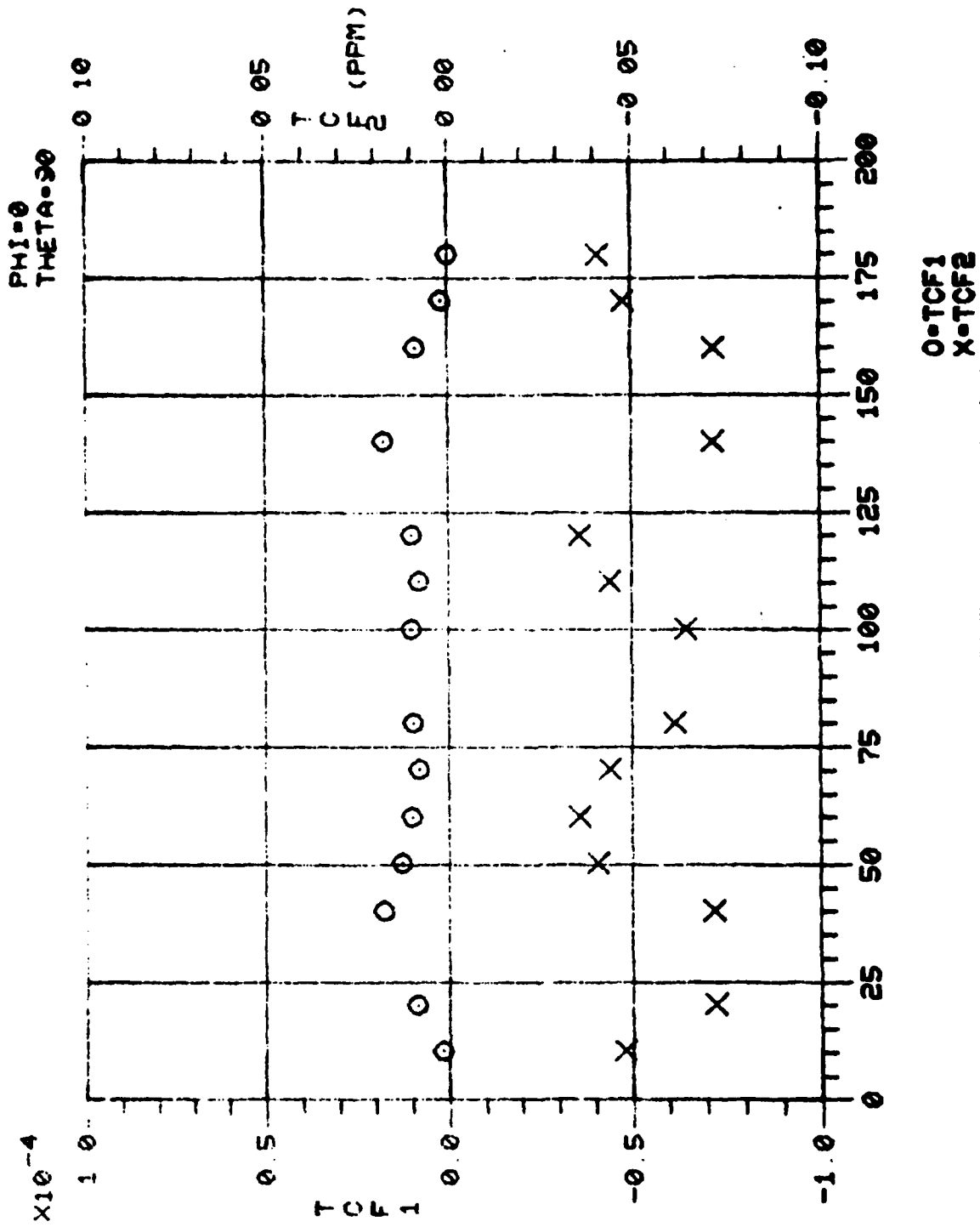
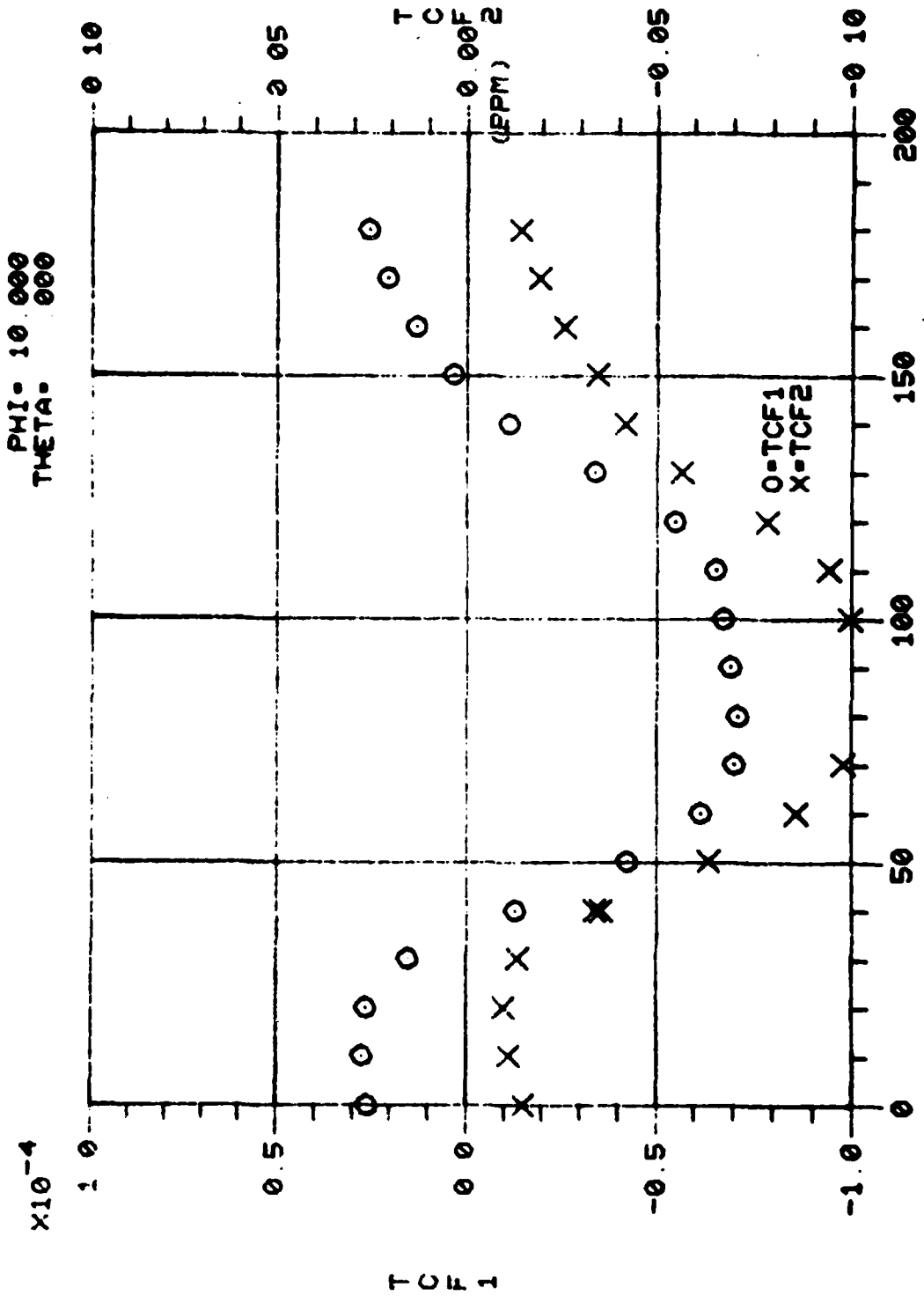


Figure 4J. Calculated Values of TCF⁽¹⁾ Versus Propagation Angles



PSI
Figure 4K. Calculated Values of TCF⁽¹⁾ Versus Propagation Angles

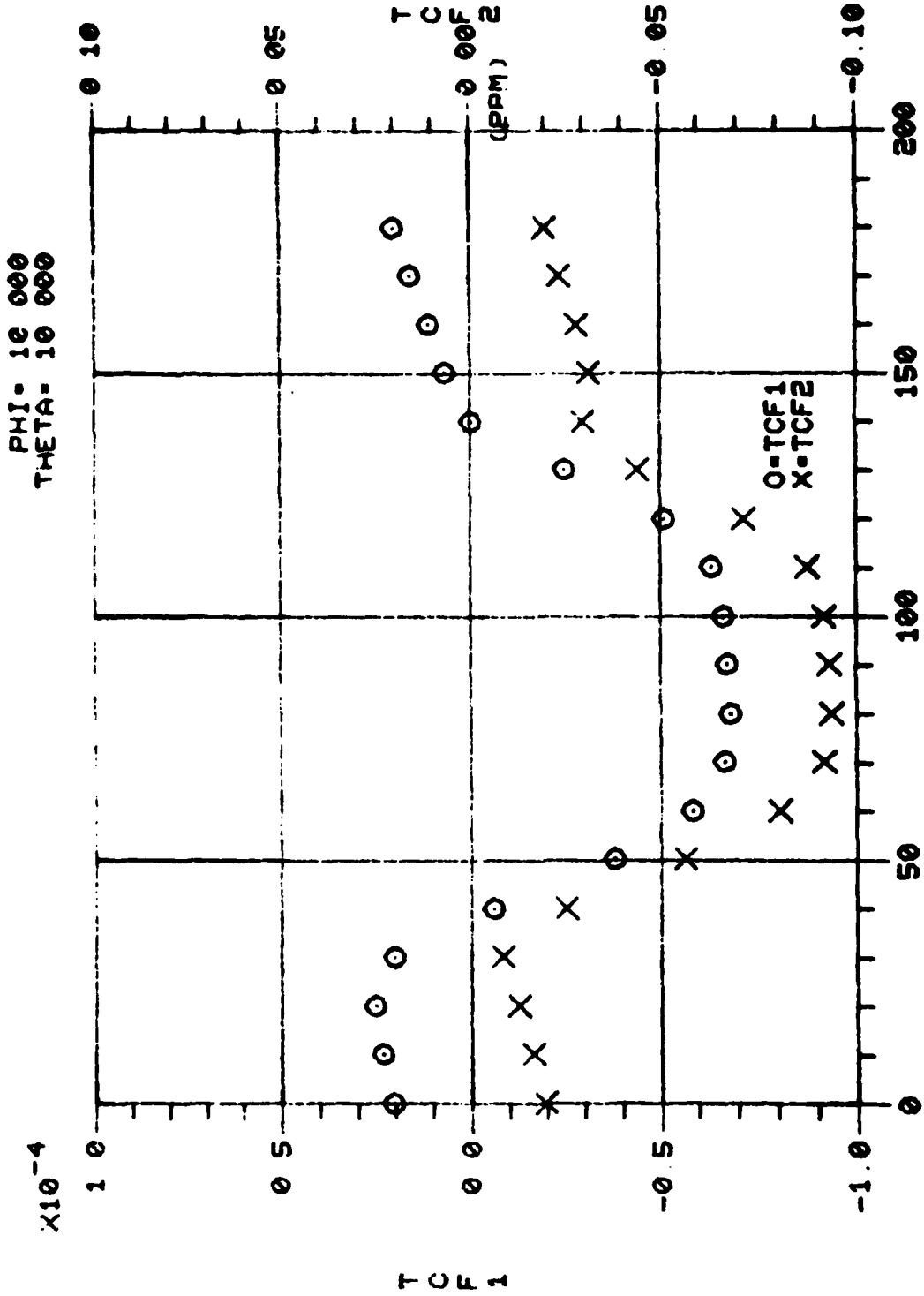


Figure 4L. Calculated Values of TCF⁽¹⁾ Versus Propagation Angles

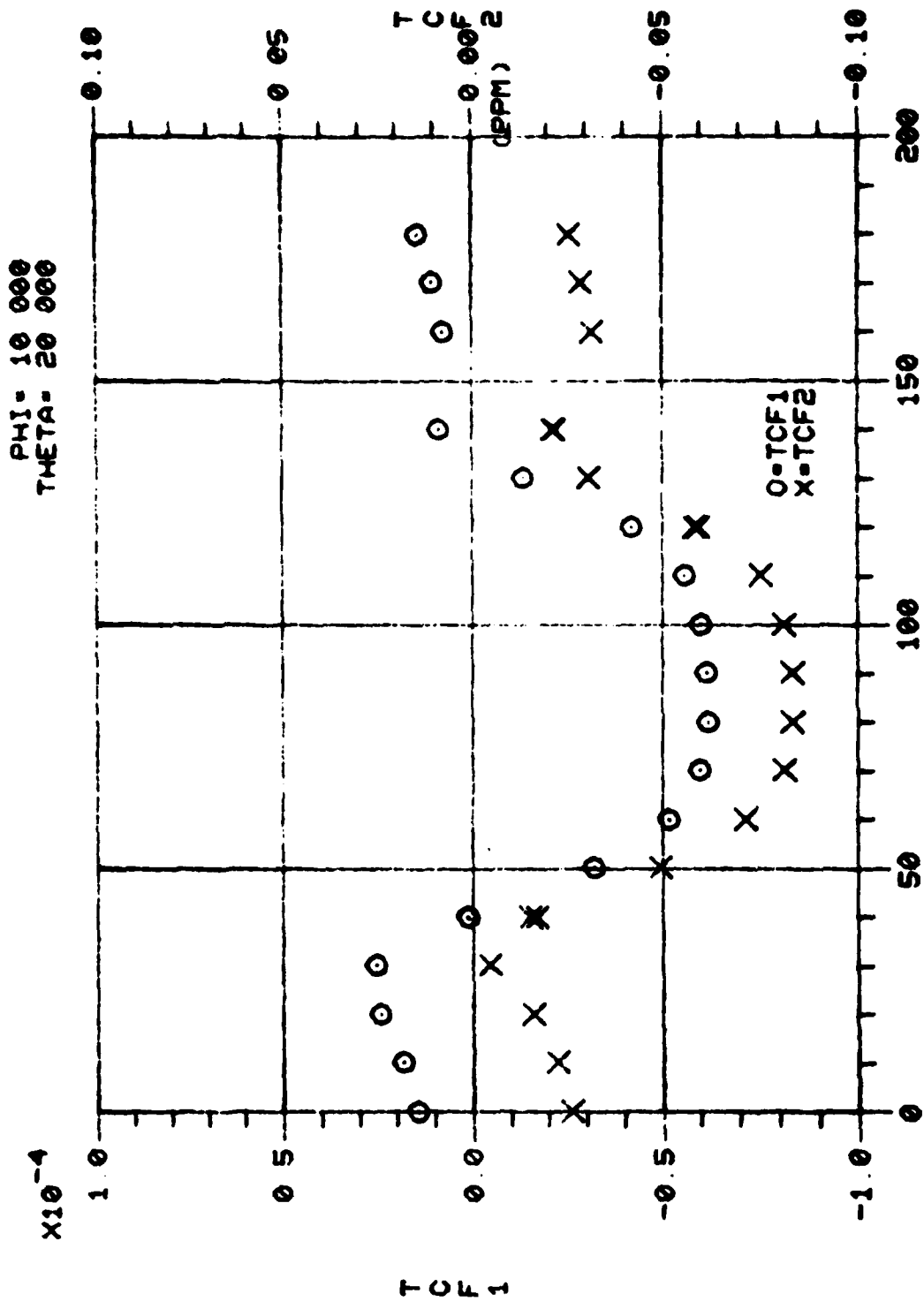


Figure 4M. Calculated Values of TCF⁽¹⁾ Versus Propagation Angles

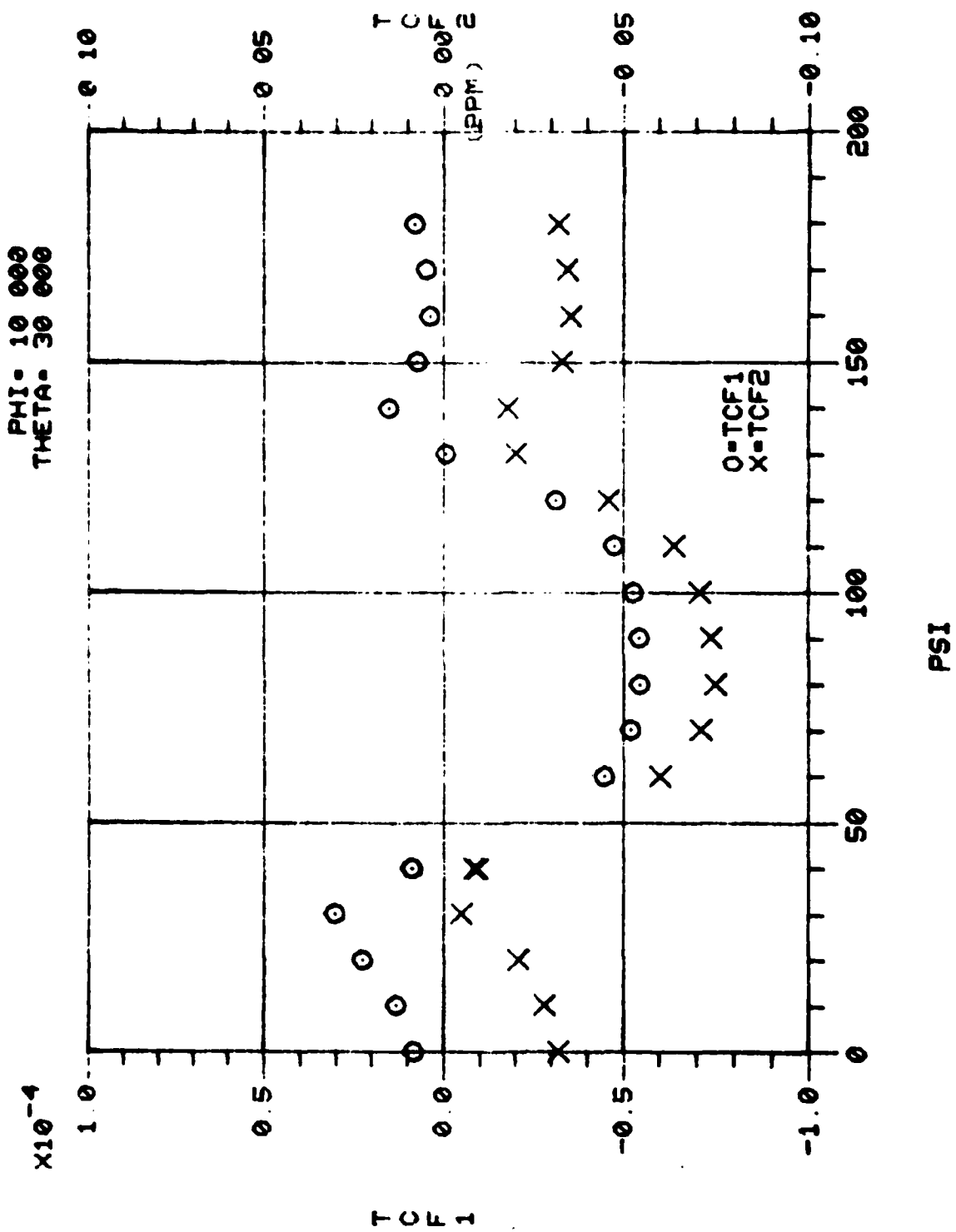
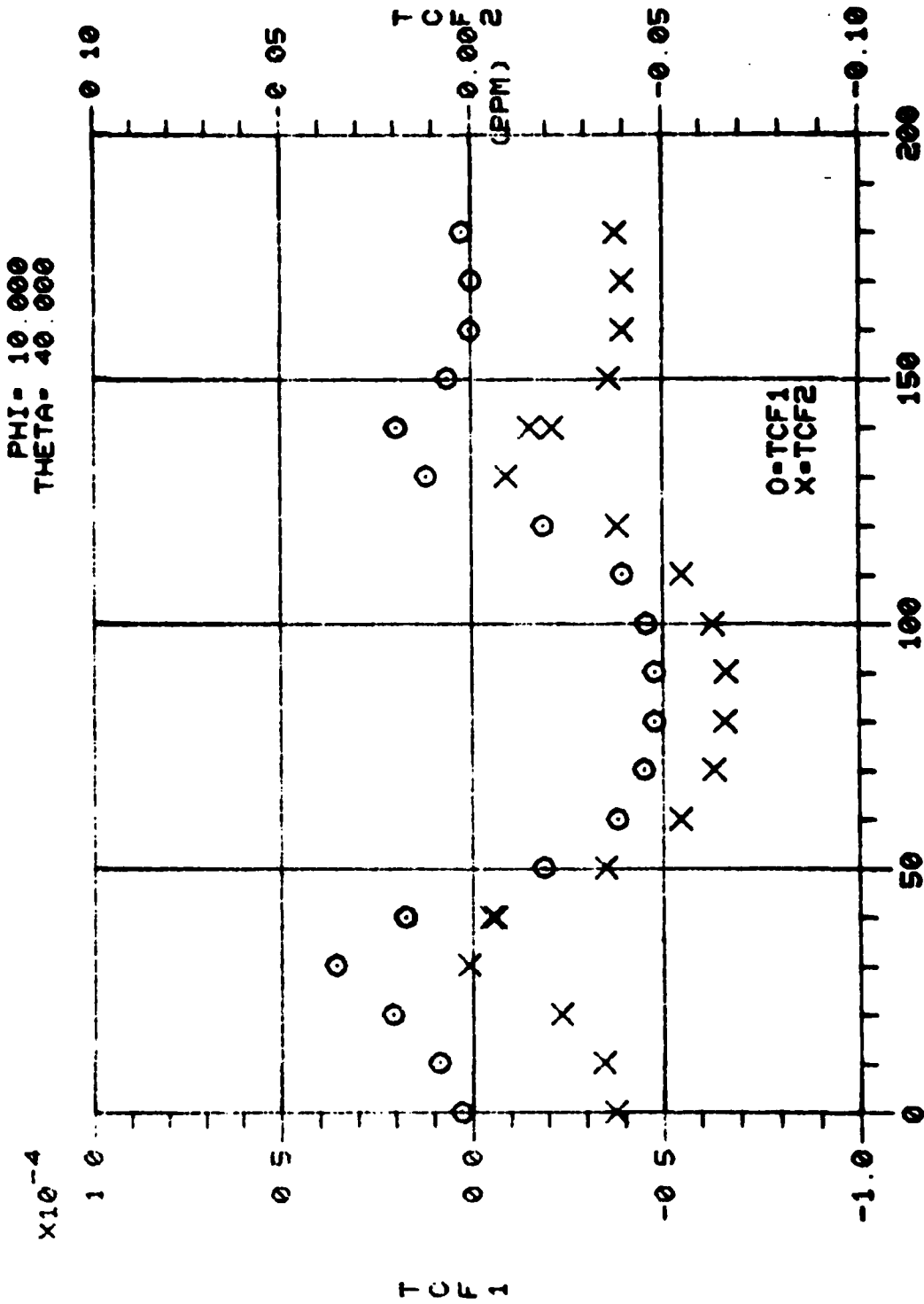


Figure 4N. Calculated Values of TCF⁽¹⁾ Versus Propagation Angles



PSI

Figure 40. Calculated Values of TCF⁽¹⁾ Versus Propagation Angles

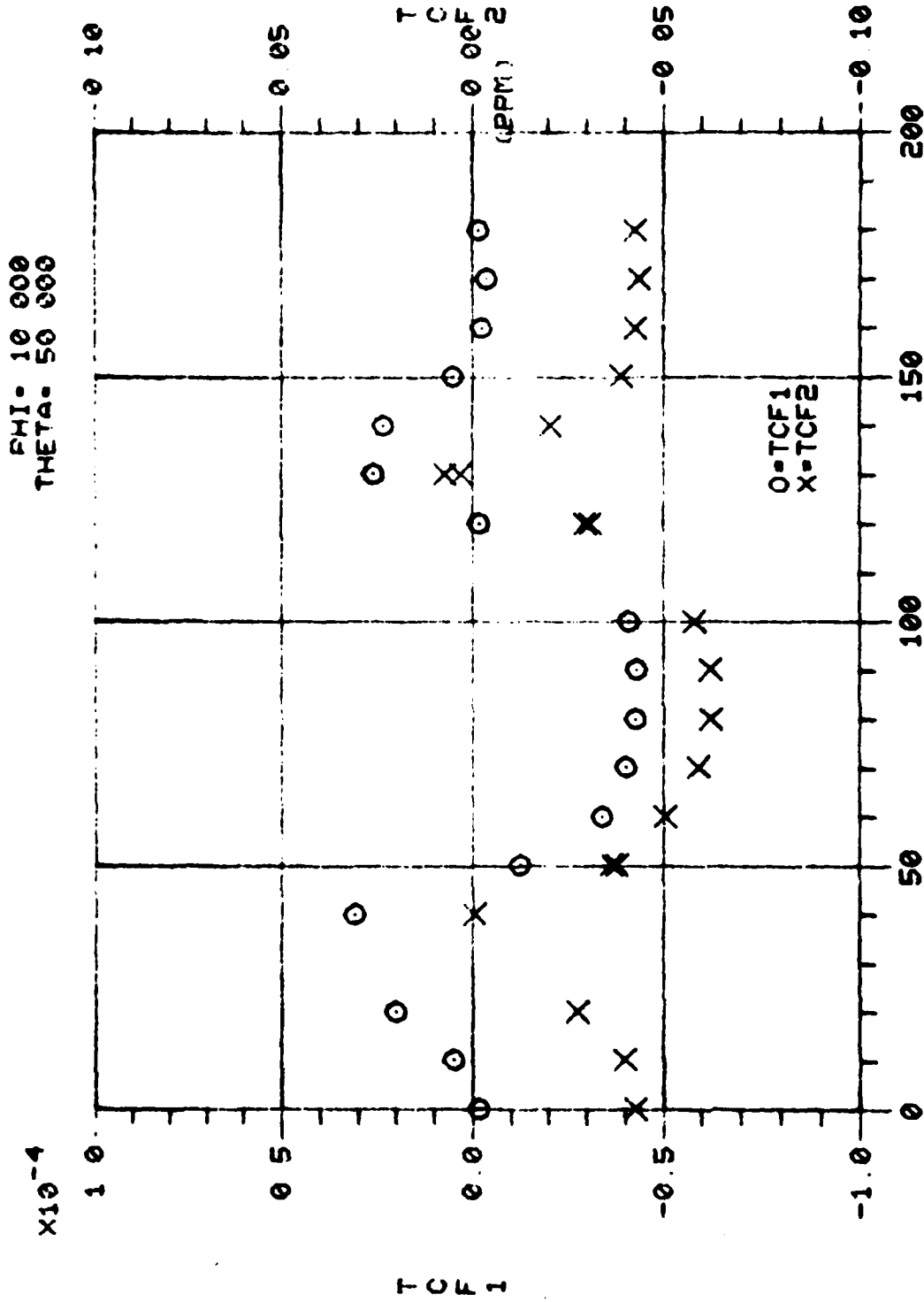


Figure 4P. Calculated Values of TCF⁽¹⁾ Versus Propagation Angles

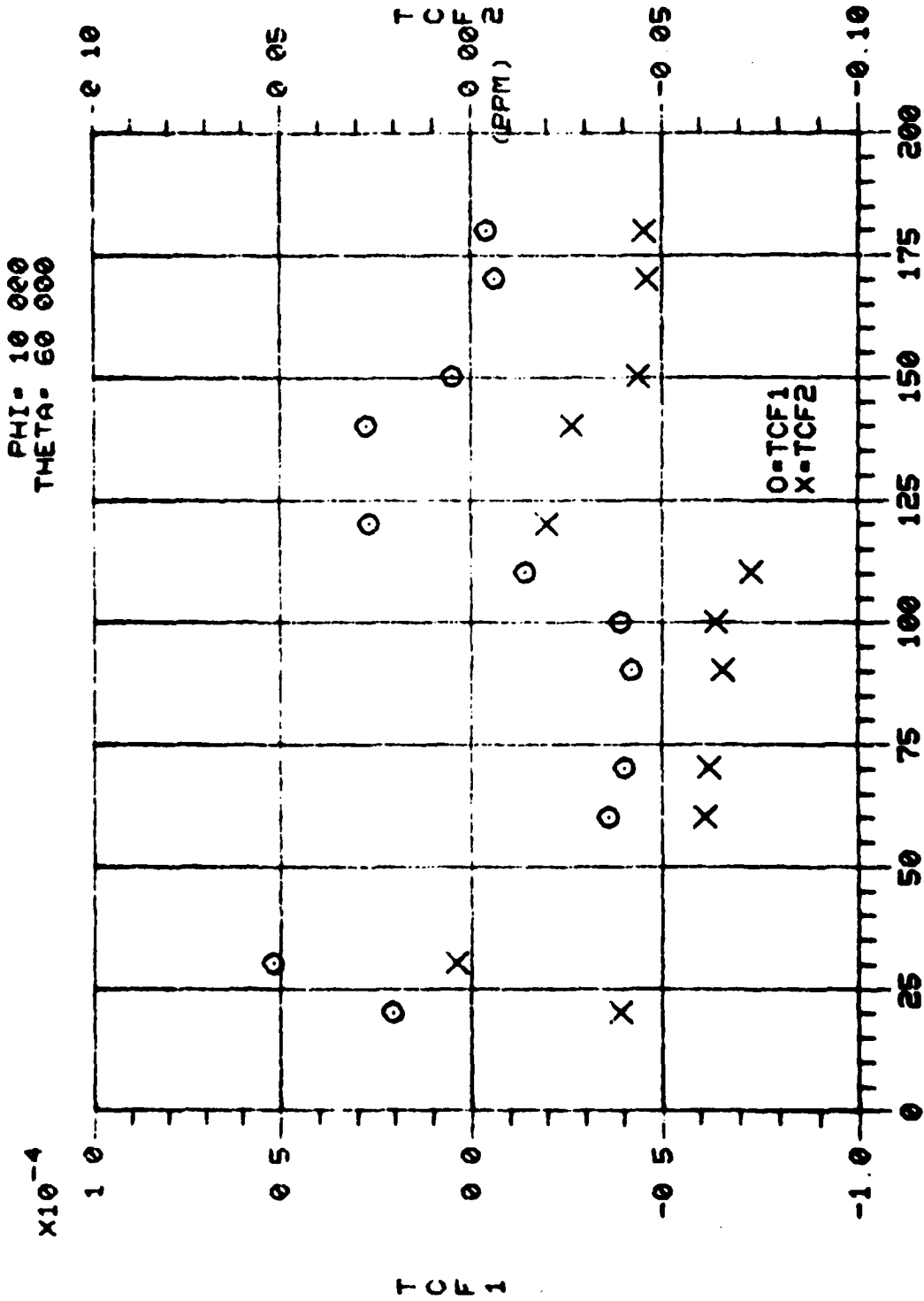
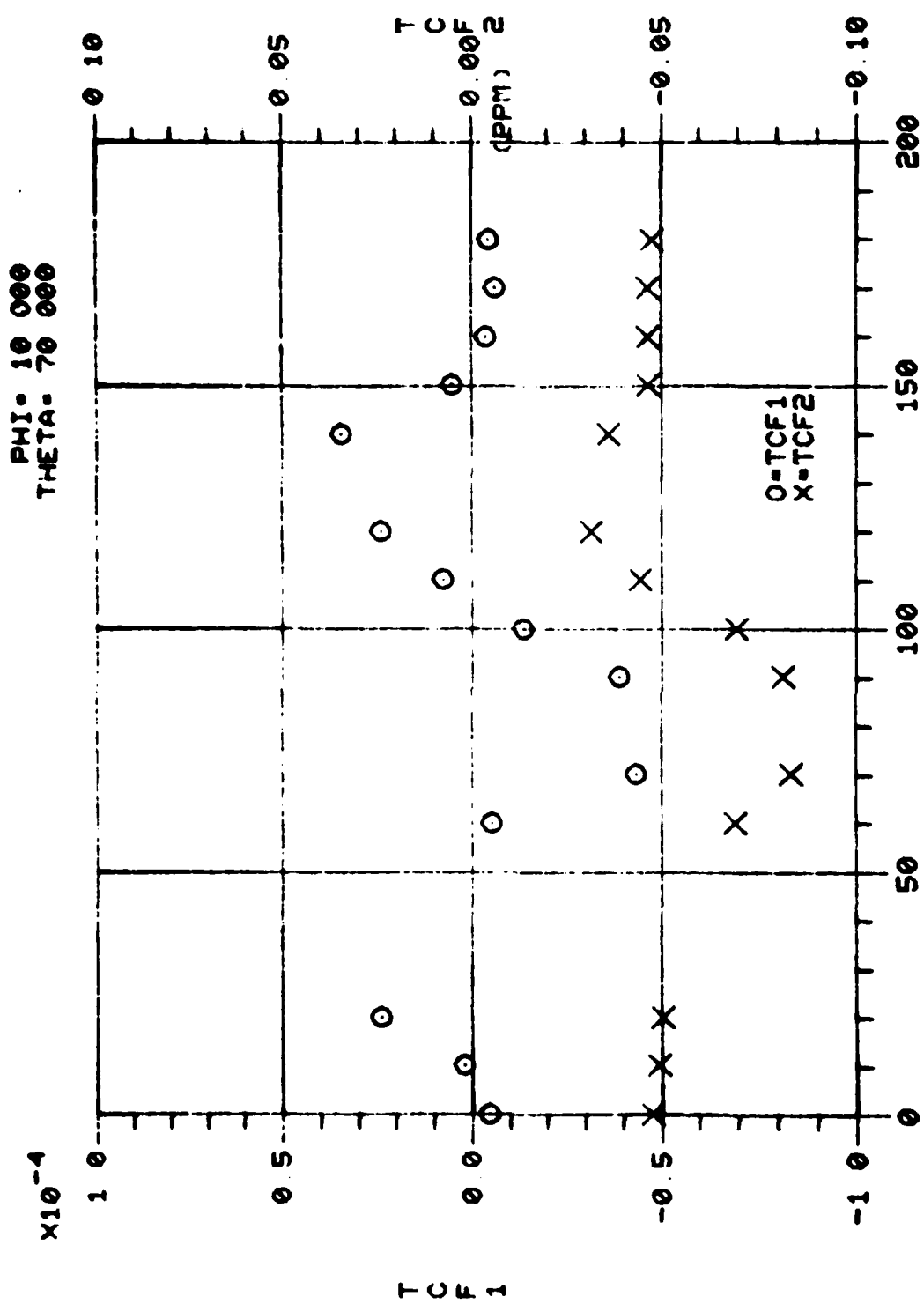


Figure 40. Calculated Values of TCF⁽¹⁾ Versus Propagation Angles



PSI

Figure 4R. Calculated Values of TCF⁽¹⁾ Versus Propagation Angles

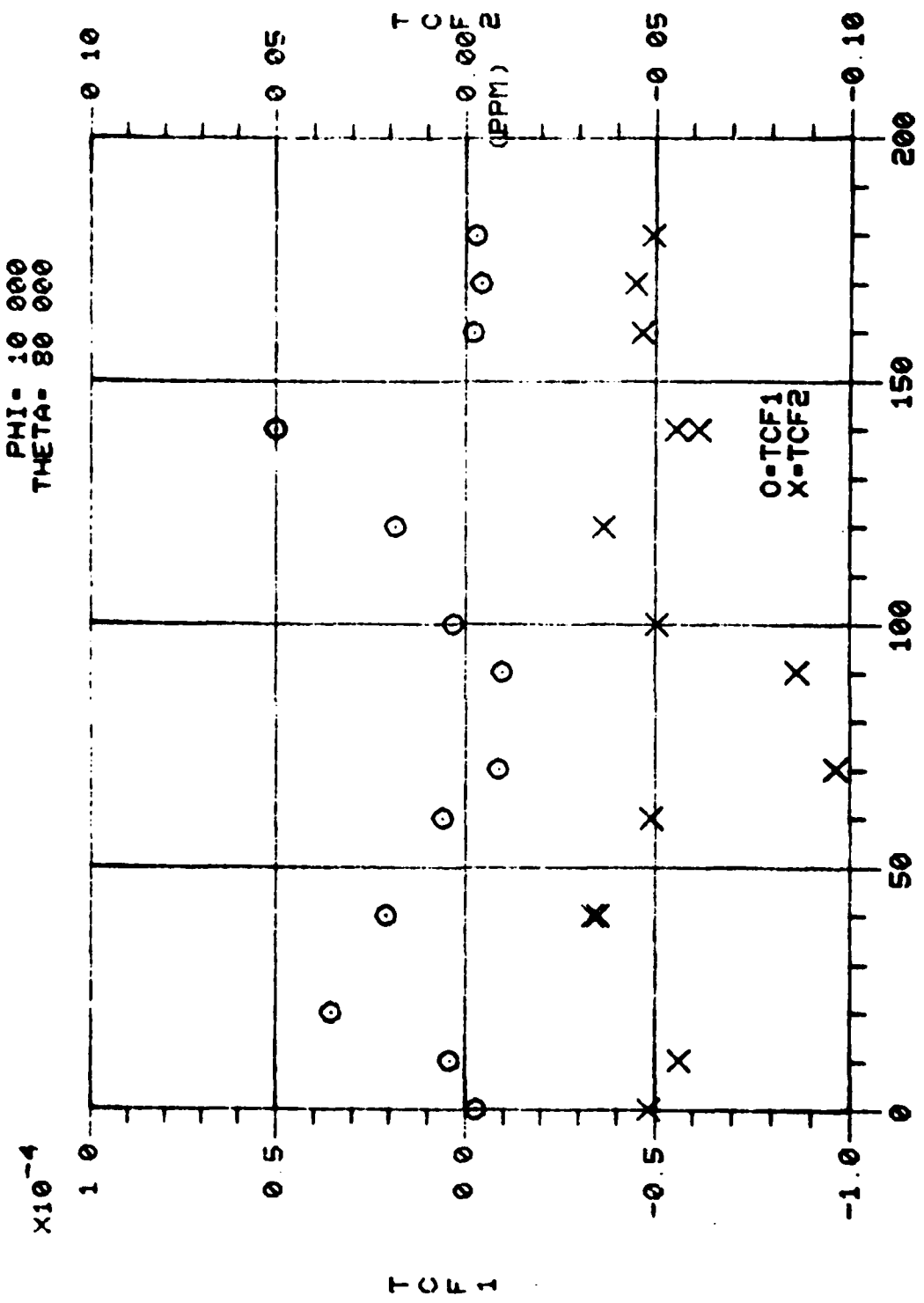


Figure 4S. Calculated Values of TCF⁽¹⁾ Versus Propagation Angles

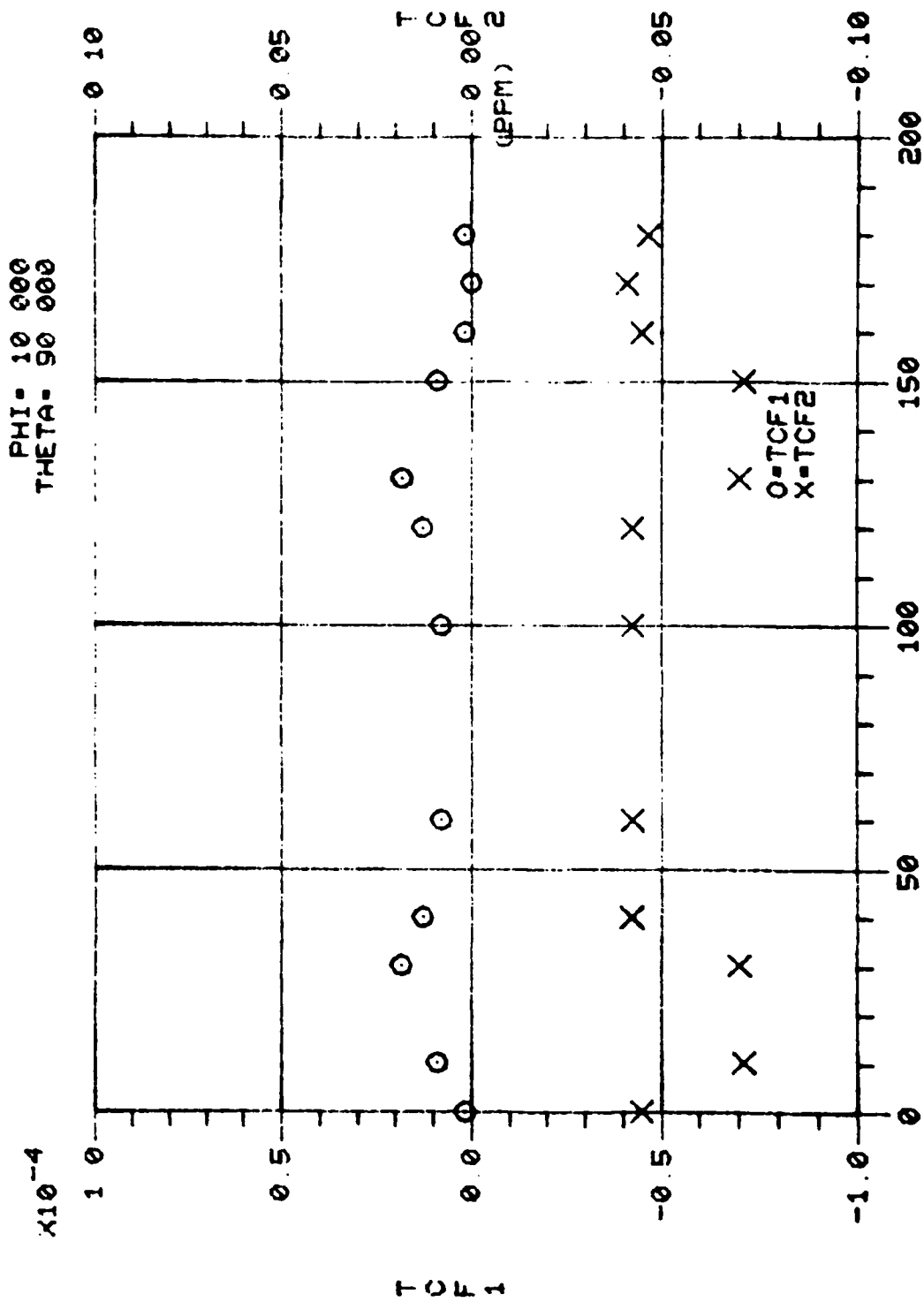


Figure 4T. Calculated Values of TCF⁽¹⁾ Versus Propagation Angles

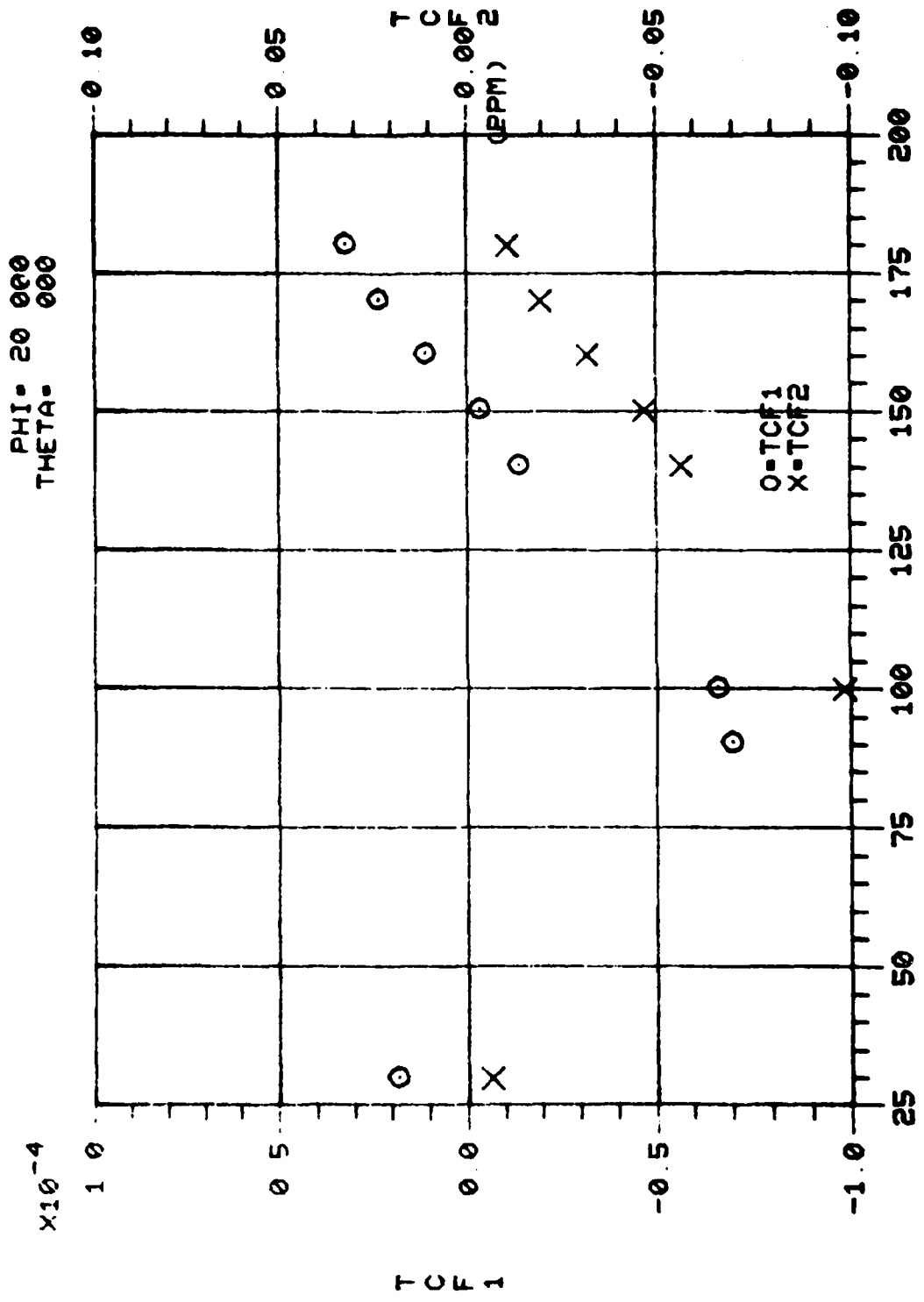


Figure 4U. Calculated Values of TCF⁽¹⁾ Versus Propagation Angles

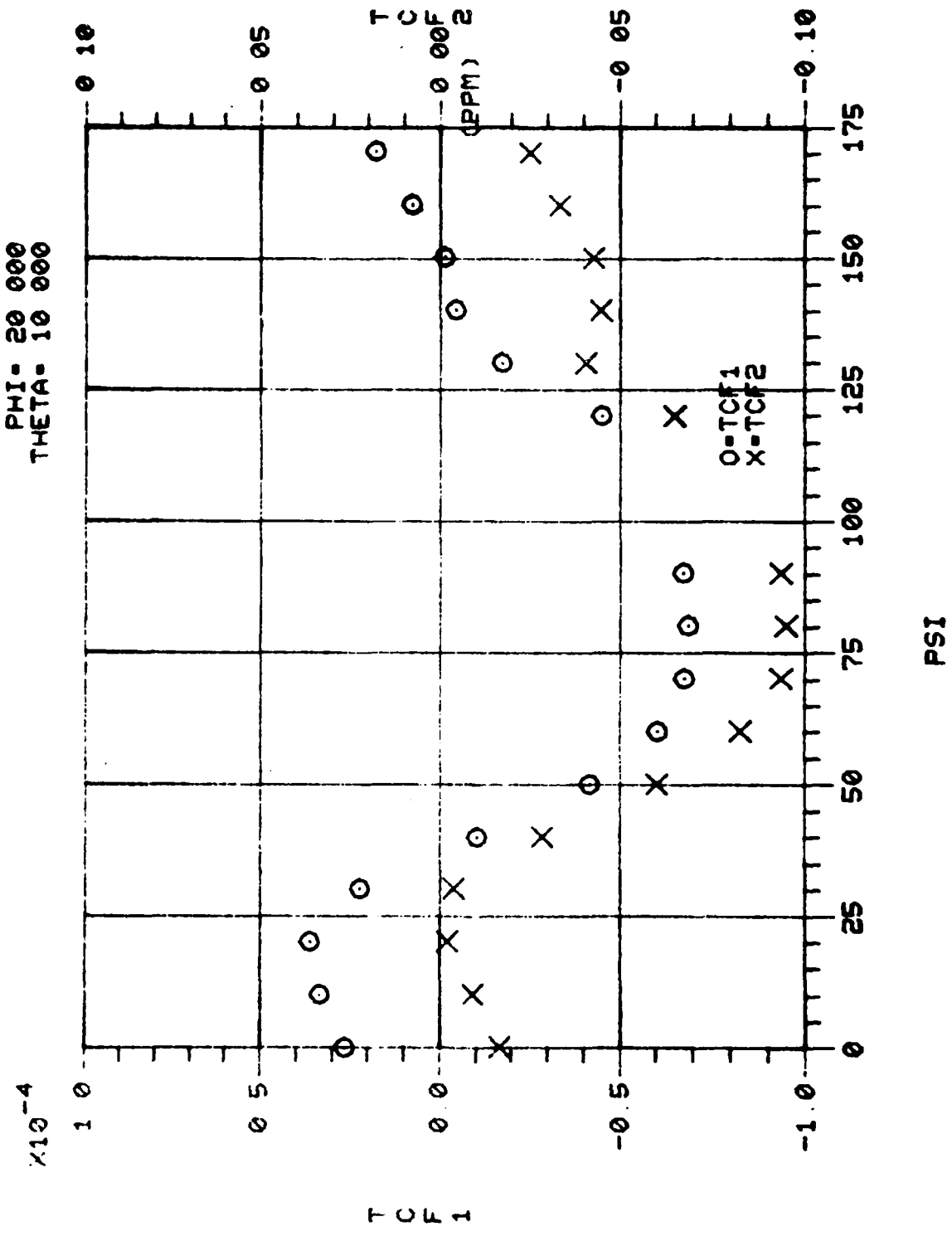


Figure 4V. Calculated Values of TCF⁽¹⁾ Versus Propagation Angles

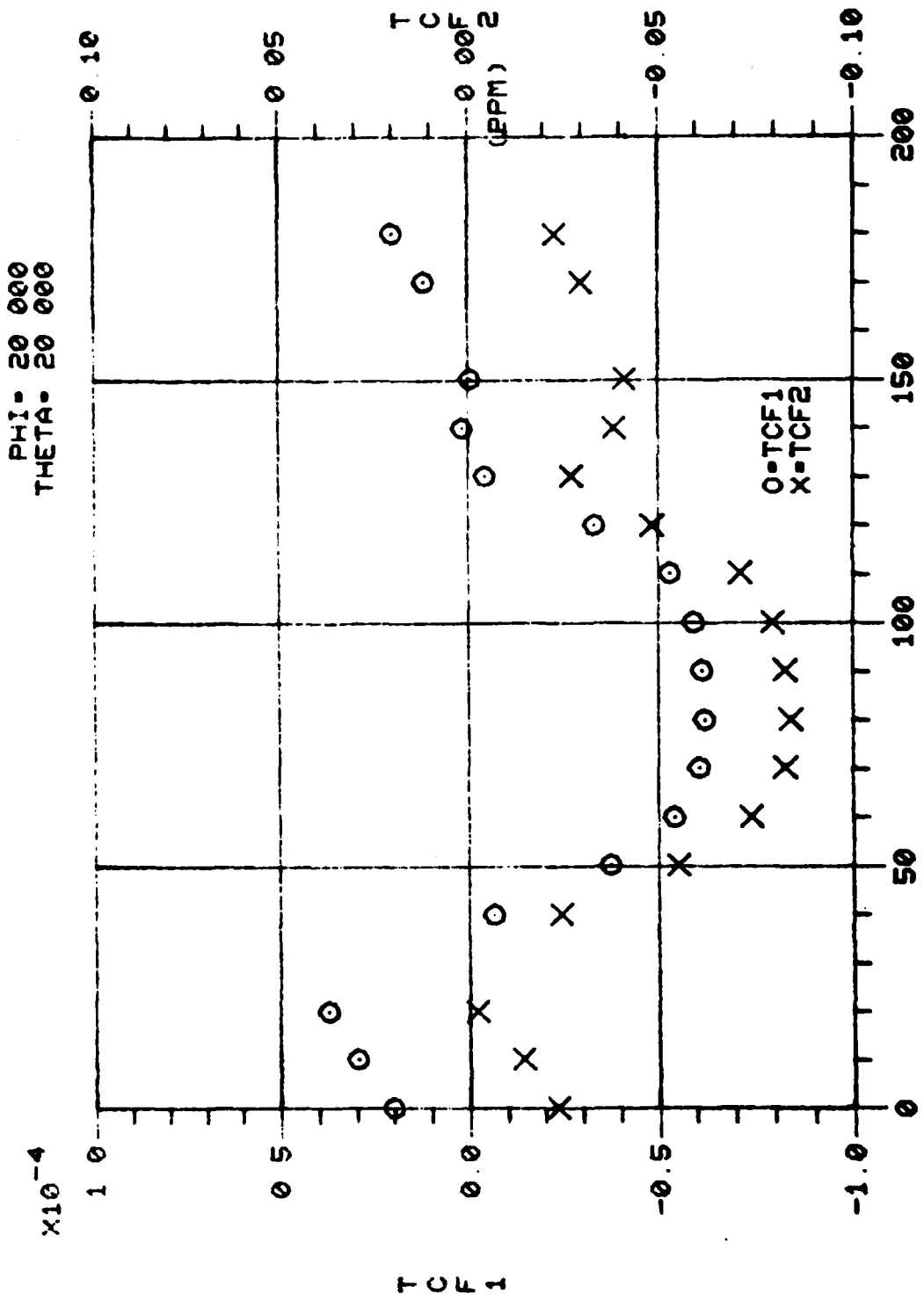
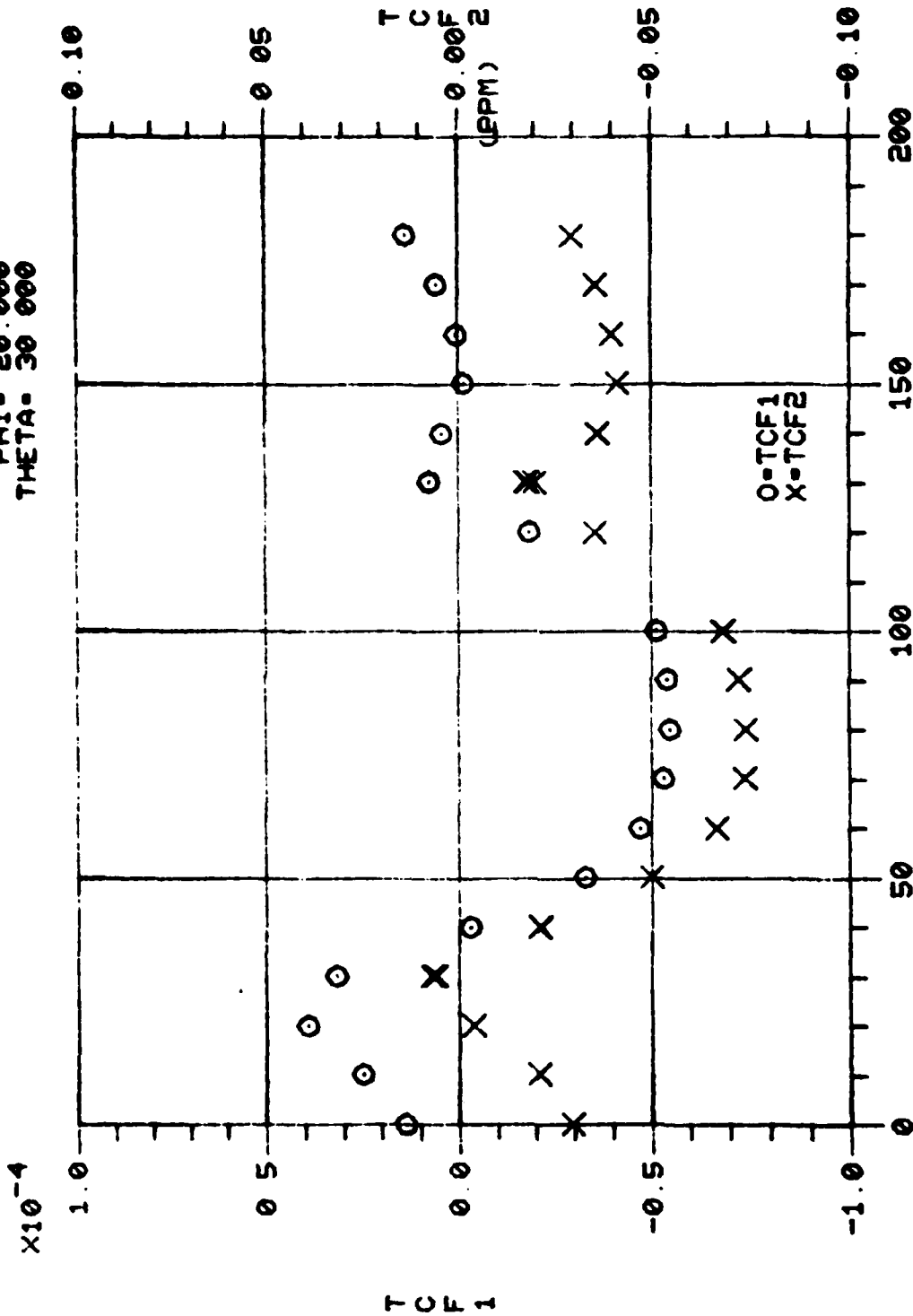


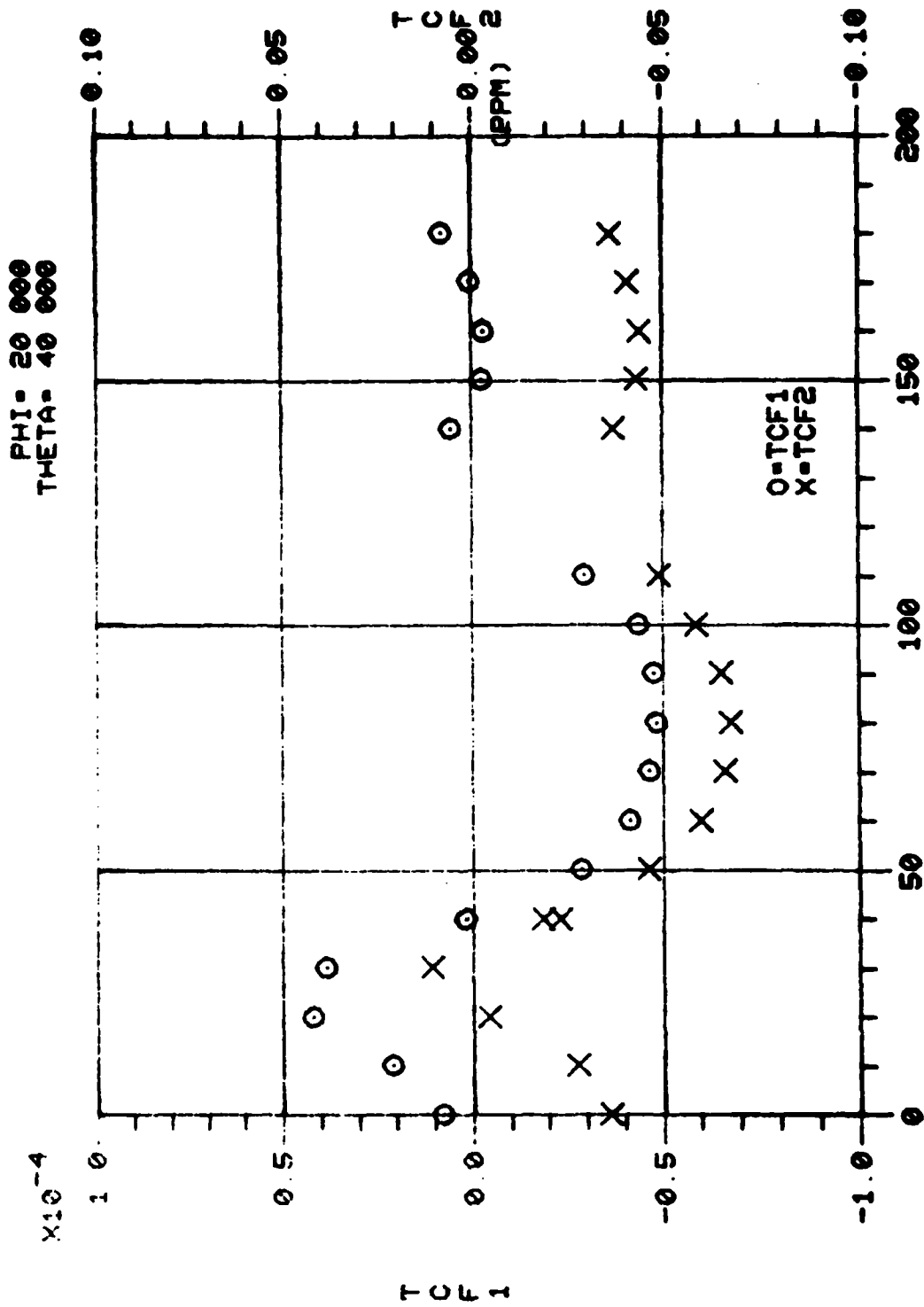
Figure 4W. Calculated Values of TCF⁽¹⁾ Versus Propagation Angles

PHI = 20.000
 THETA = 30.000



PSI

Figure 4X. Calculated Values of TCF⁽¹⁾ Versus Propagation Angles



PSI

Figure 4Y. Calculated Values of TCF⁽¹⁾ Versus Propagation Angles

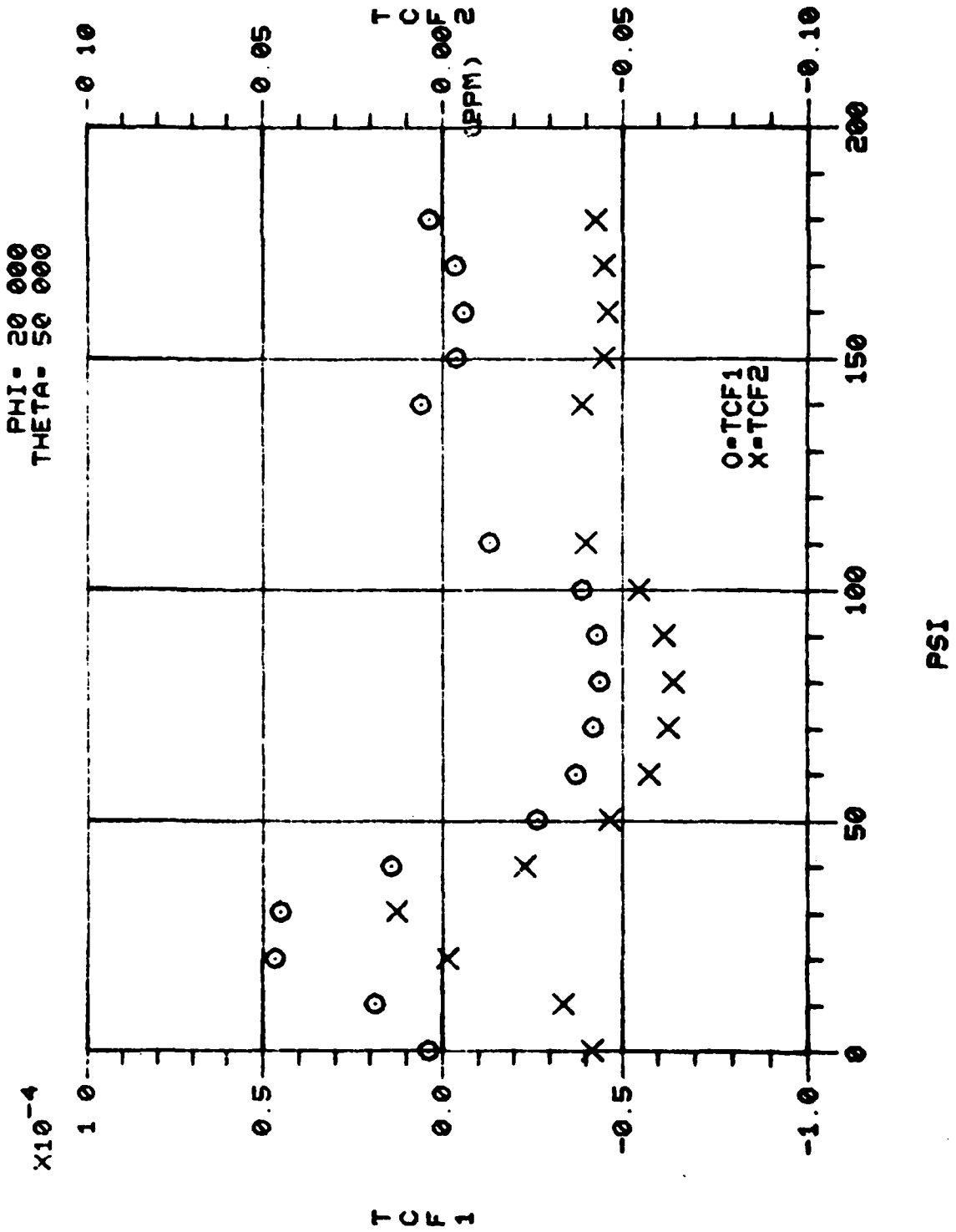
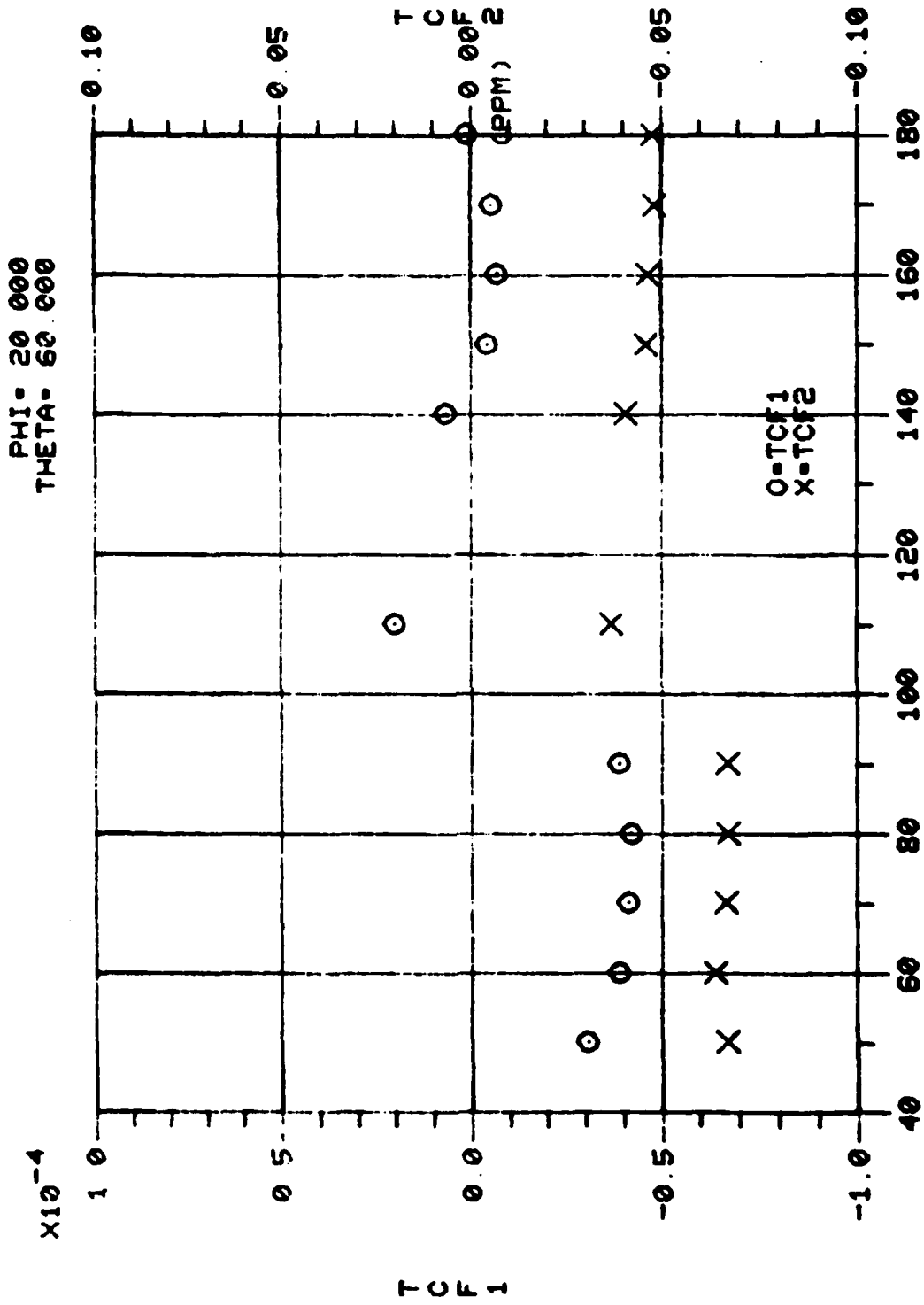
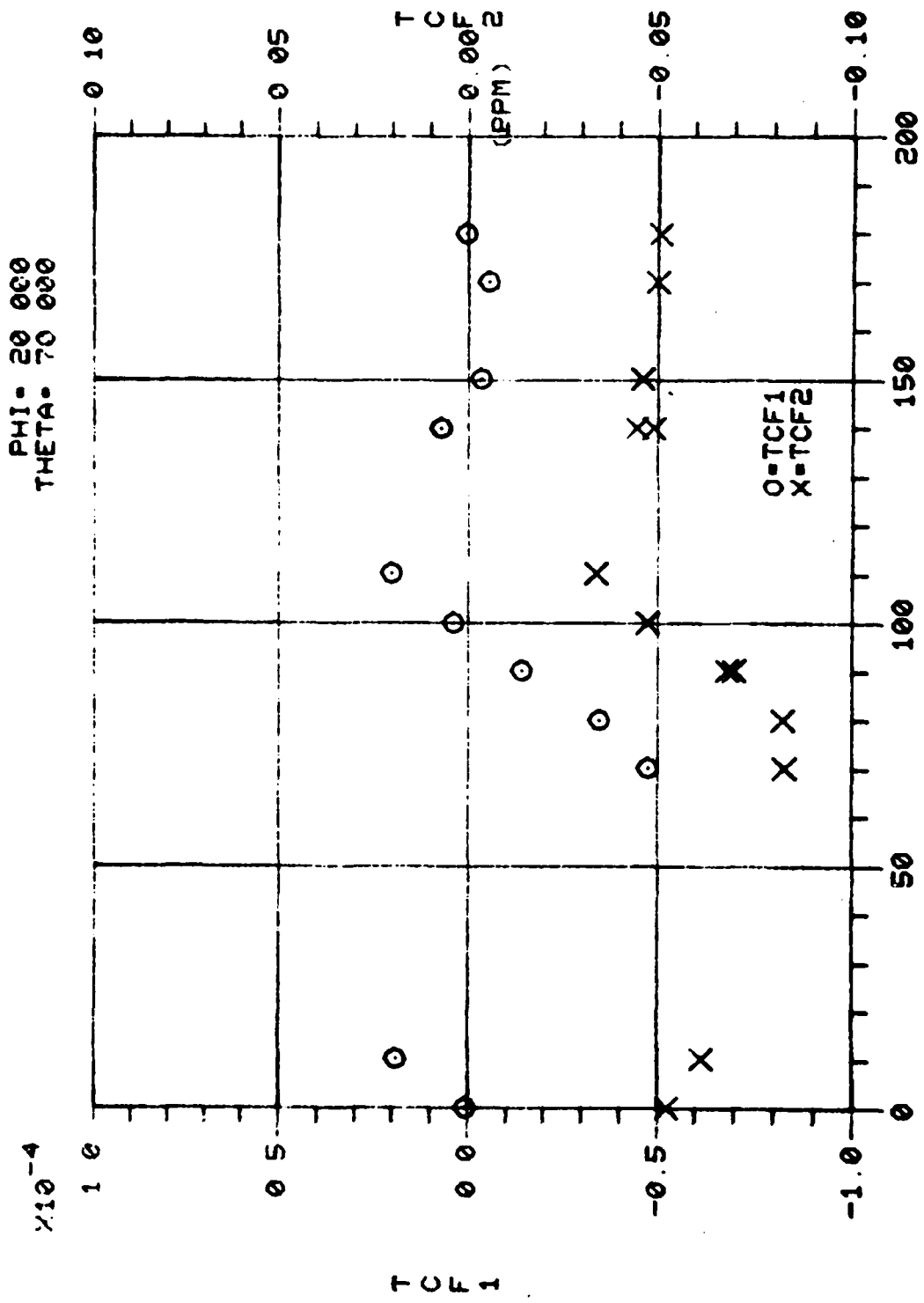


Figure 4Z. Calculated Values of TCF⁽¹⁾ Versus Propagation Angles



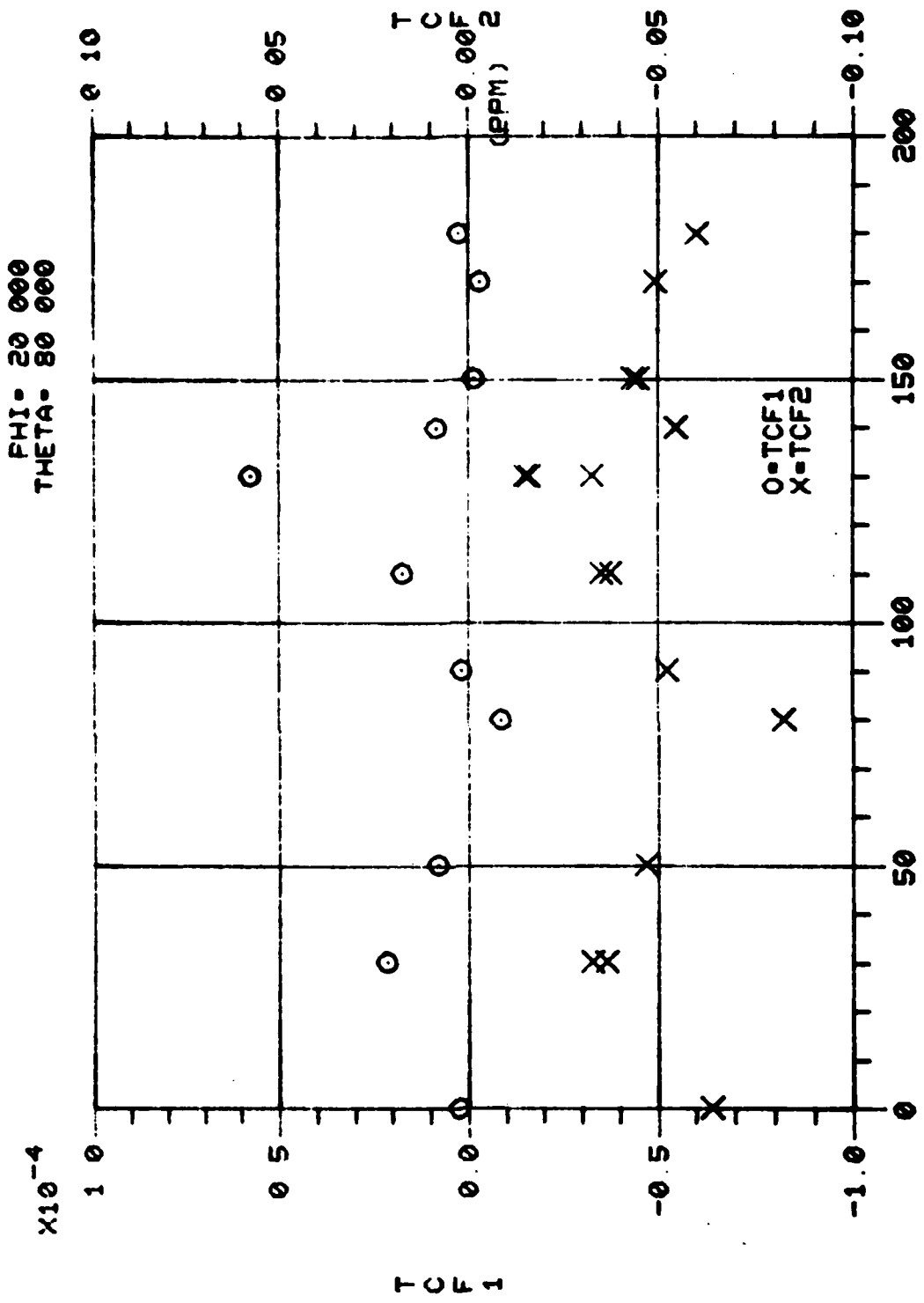
PSI

Figure 4AA. Calculated Values of TCF⁽¹⁾ Versus Propagation Angles



PSI

Figure 4BB. Calculated Values of TCF⁽¹⁾ Versus Propagation Angles



PSI
Figure 4CC. Calculated Values of TCF⁽¹⁾ Versus Propagation Angles

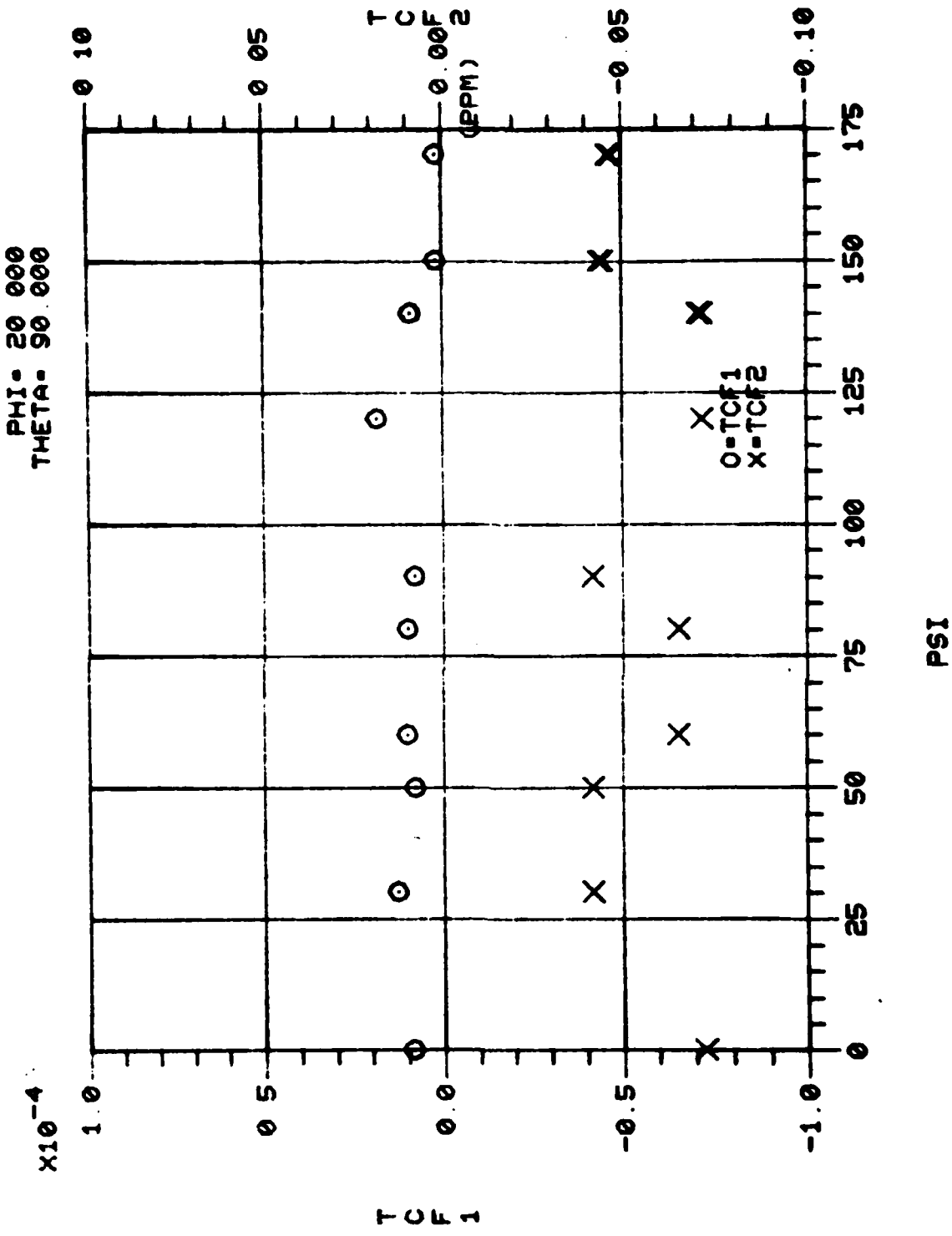
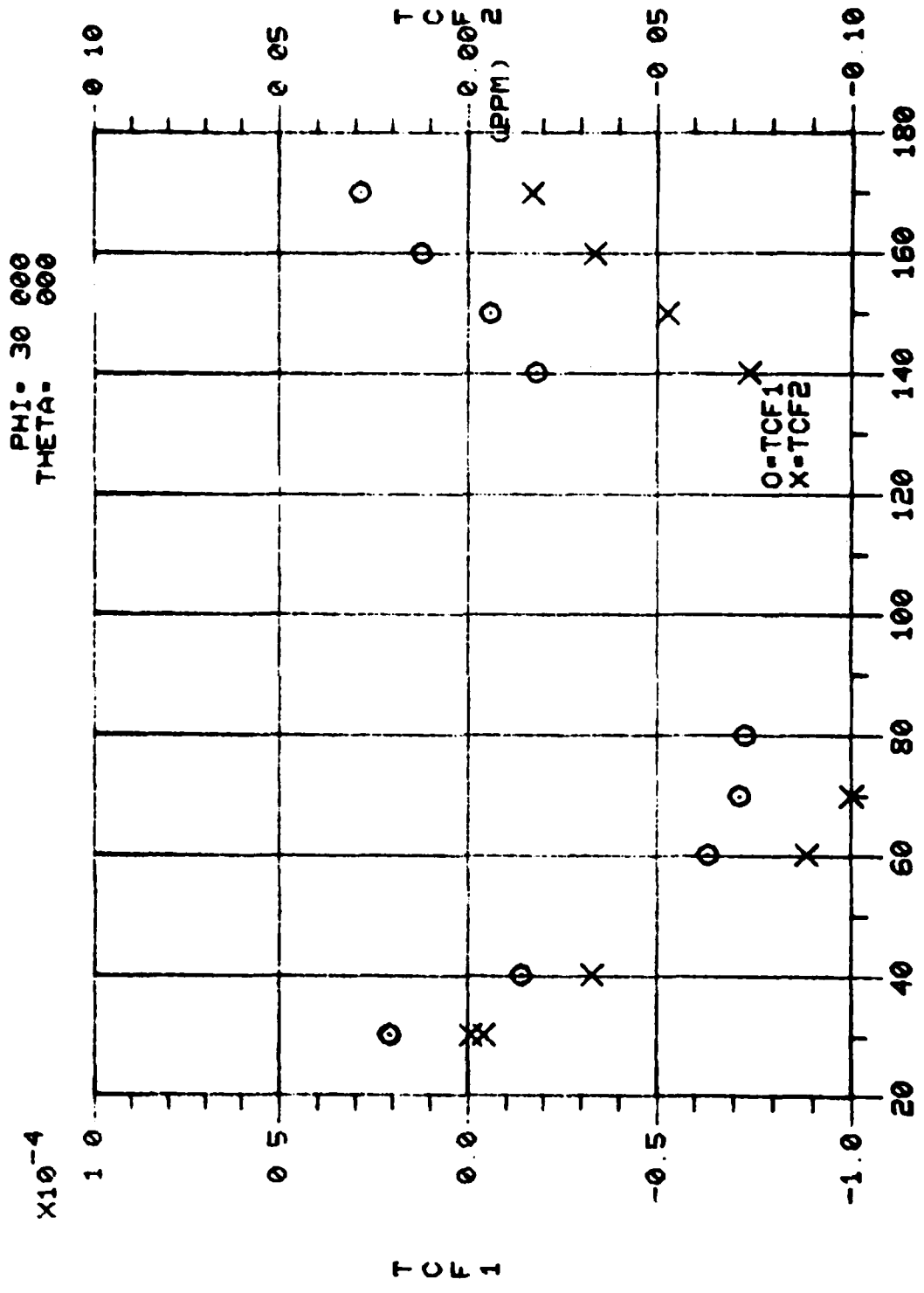


Figure 4DD. Calculated Values of TCF⁽¹⁾ Versus Propagation Angles



PSI
Figure 4EE. Calculated Values of TCF⁽¹⁾ Versus Propagation Angles

PHI = 30 000
 THETA = 10 000

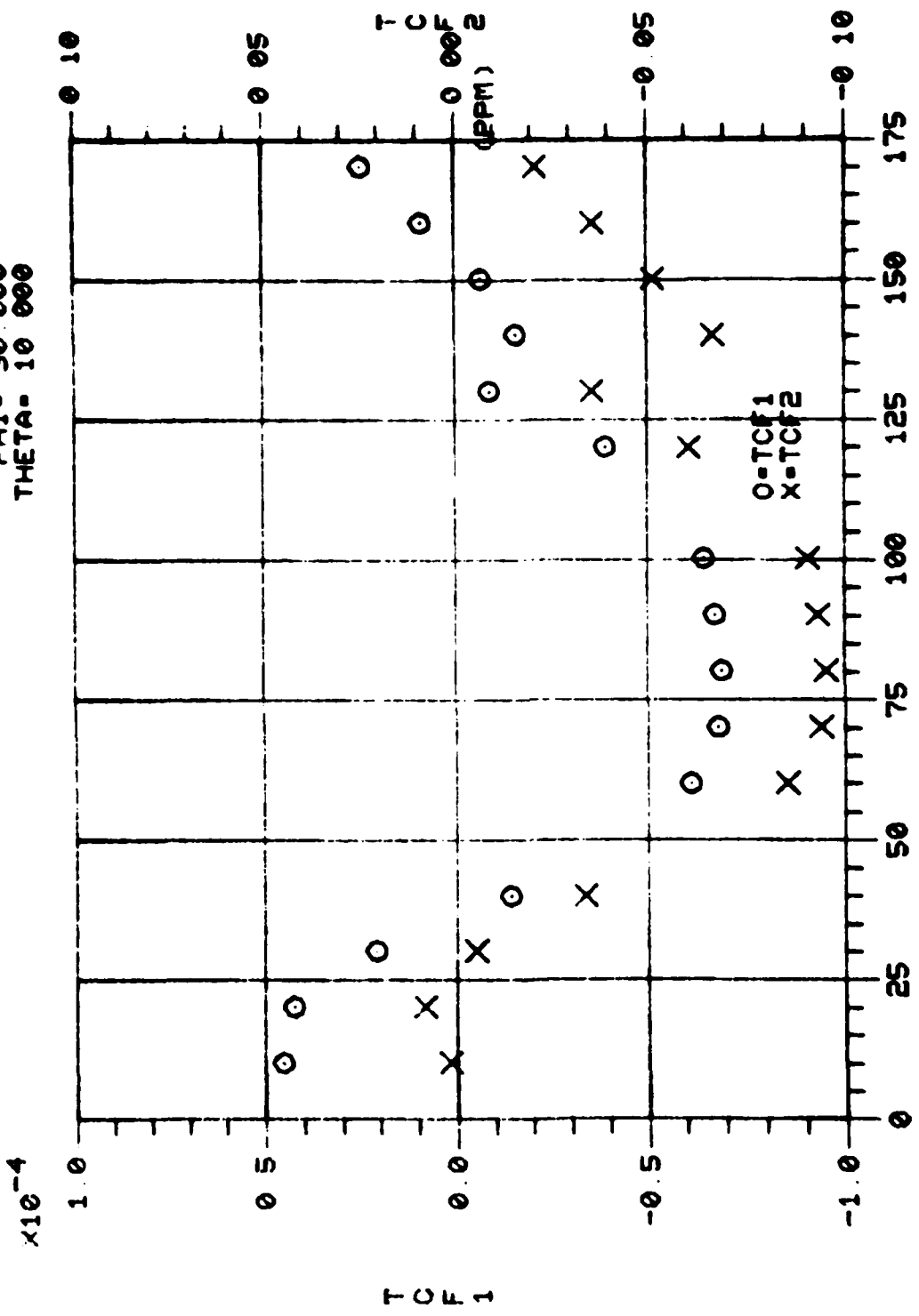


Figure 4FF. Calculated Values of TCF⁽¹⁾ Versus Propagation Angles

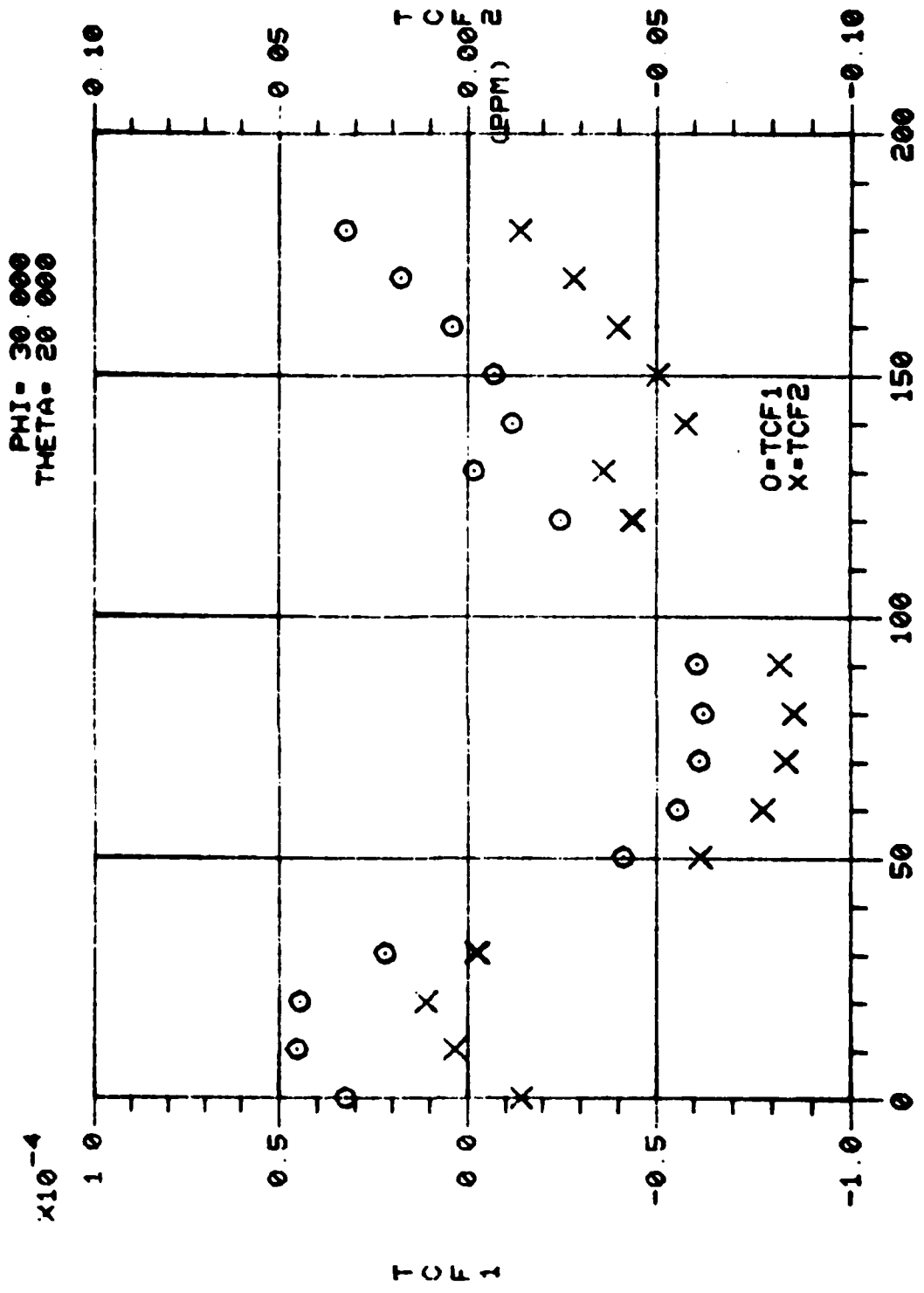


Figure 4GG. Calculated Values of TCF⁽¹⁾ Versus Propagation Angles

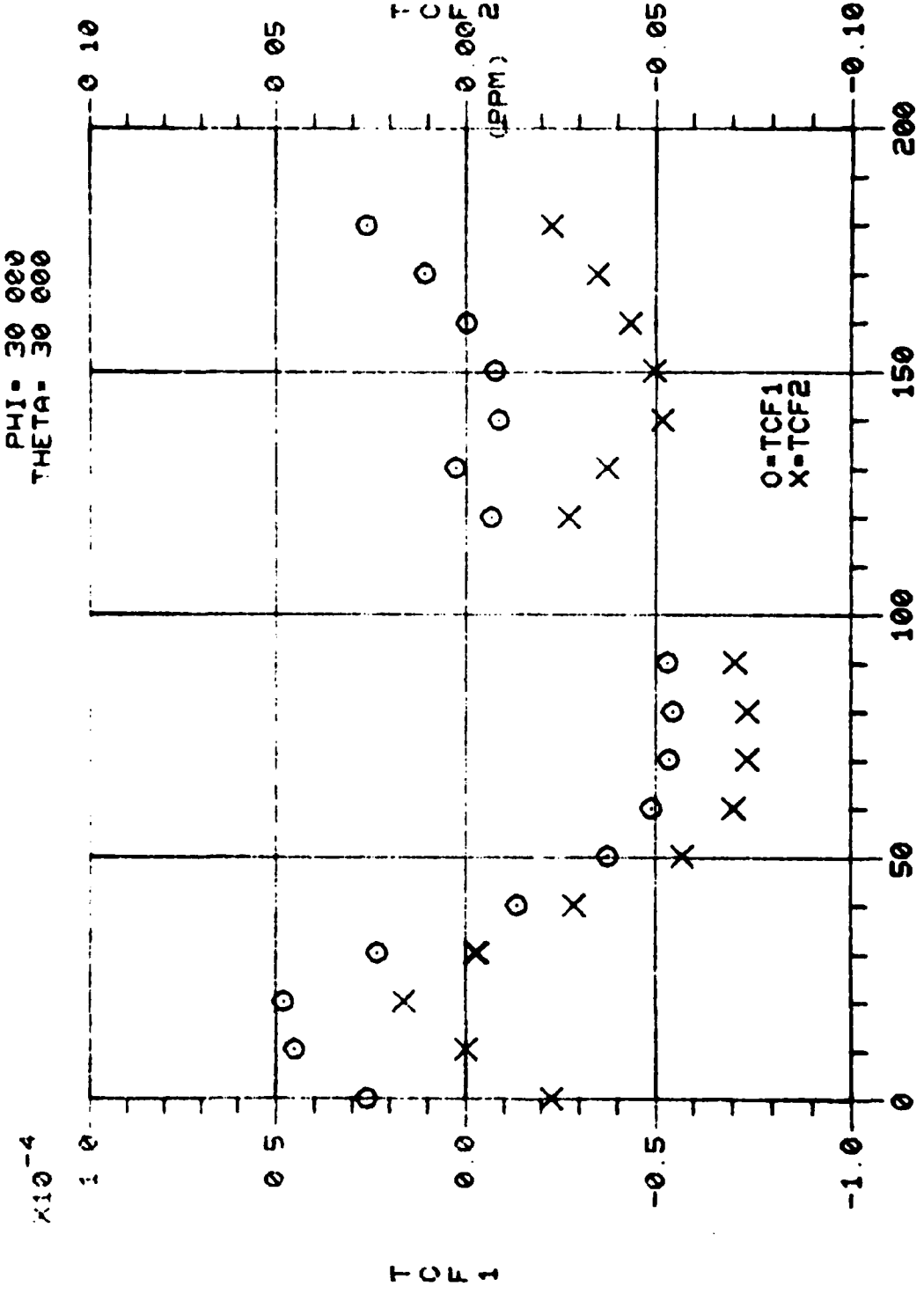
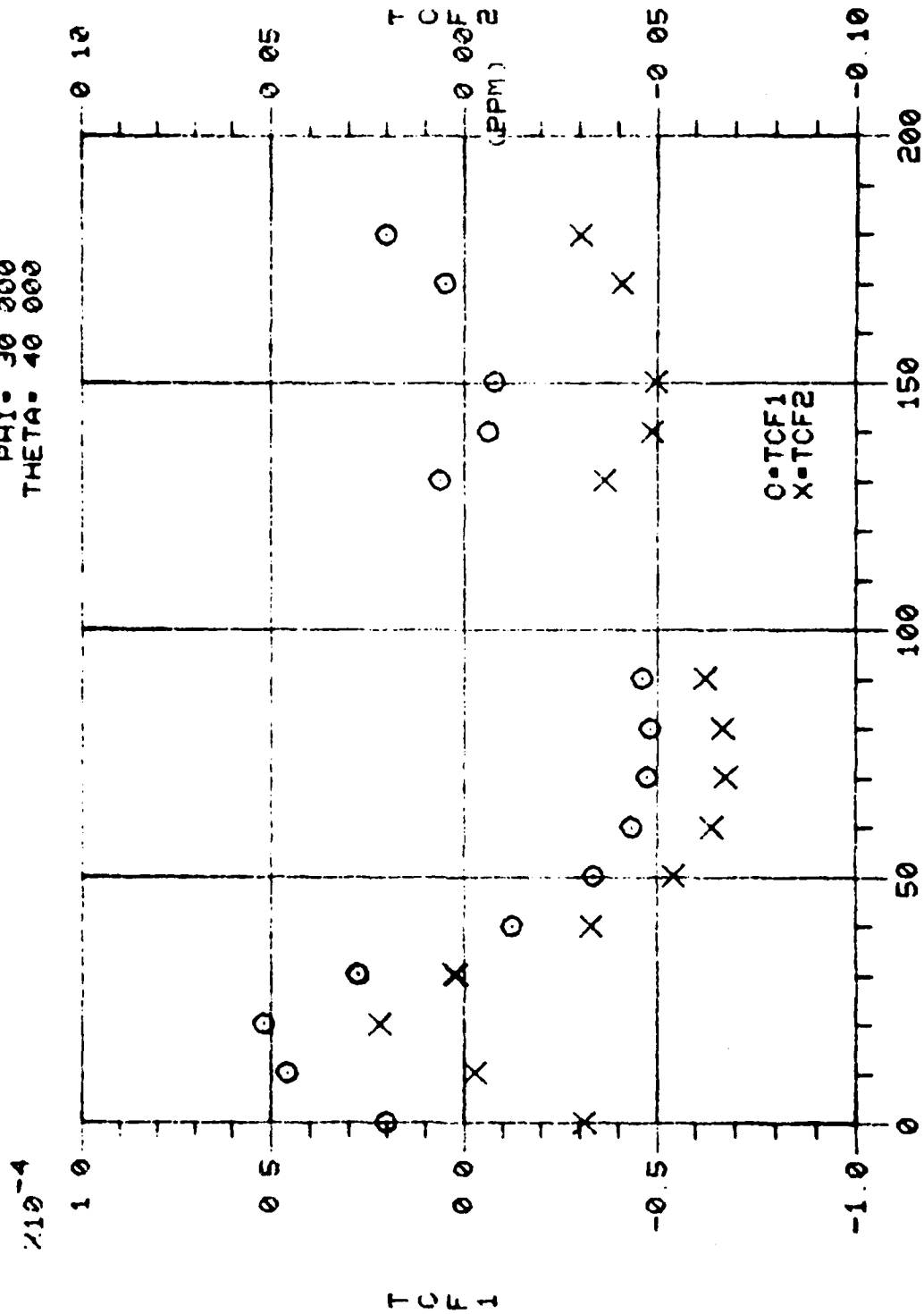


Figure 4HH. Calculated Values of TCF⁽¹⁾ Versus Propagation Angles

PHI = 30 200
 THETA = 40 000



PSI
 Figure 4II. Calculated Values of TCF⁽¹⁾ Versus Propagation Angles

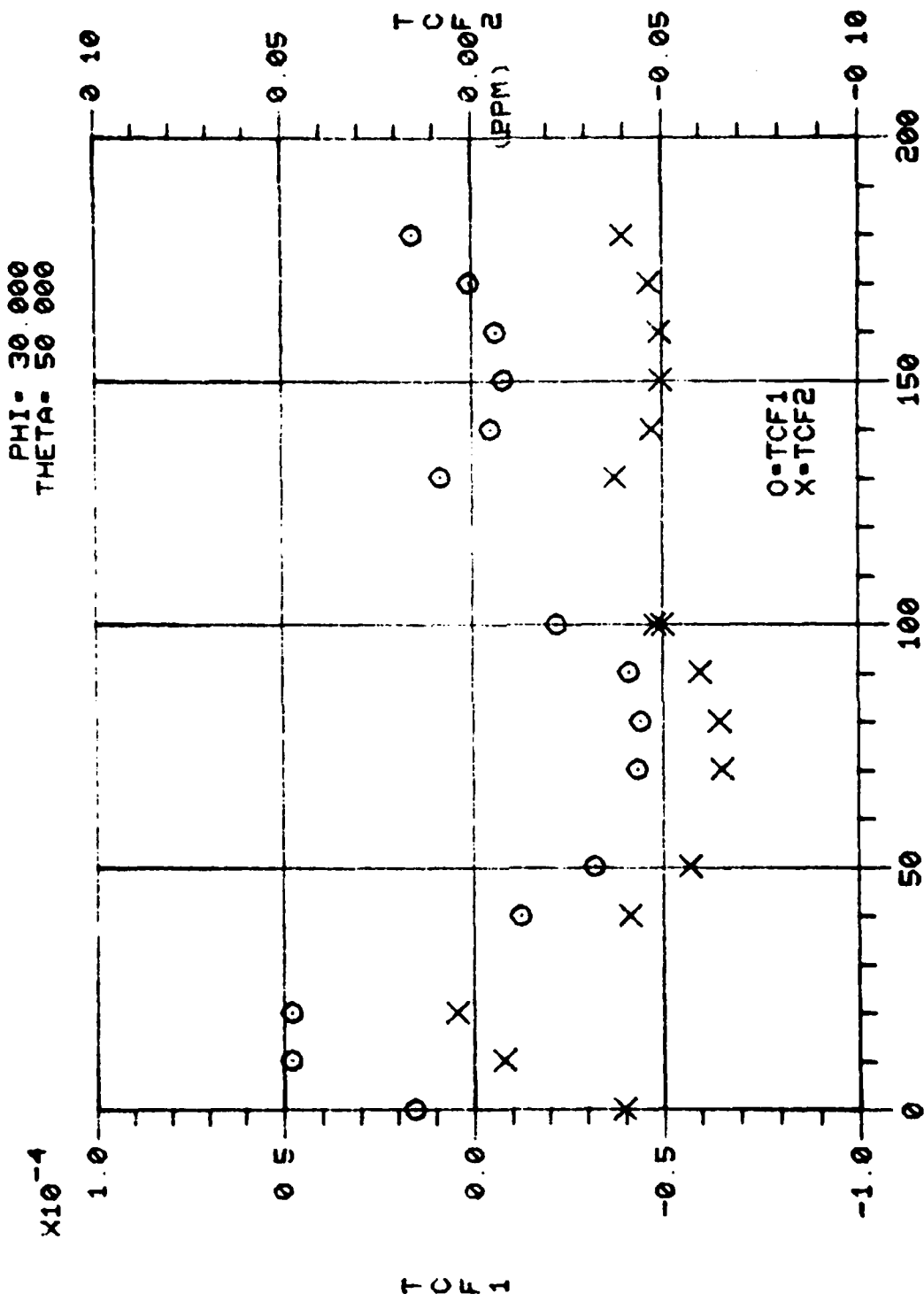
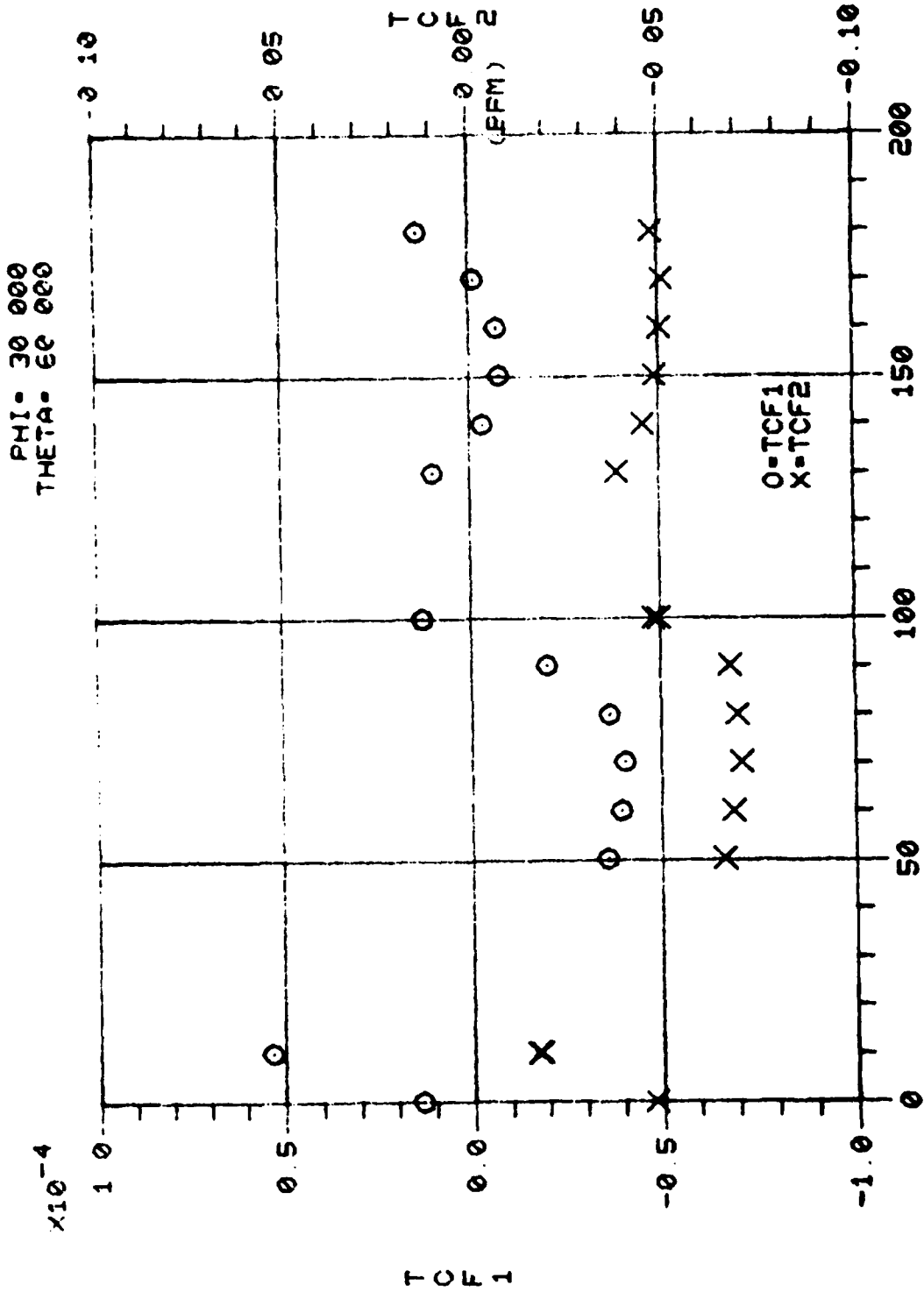


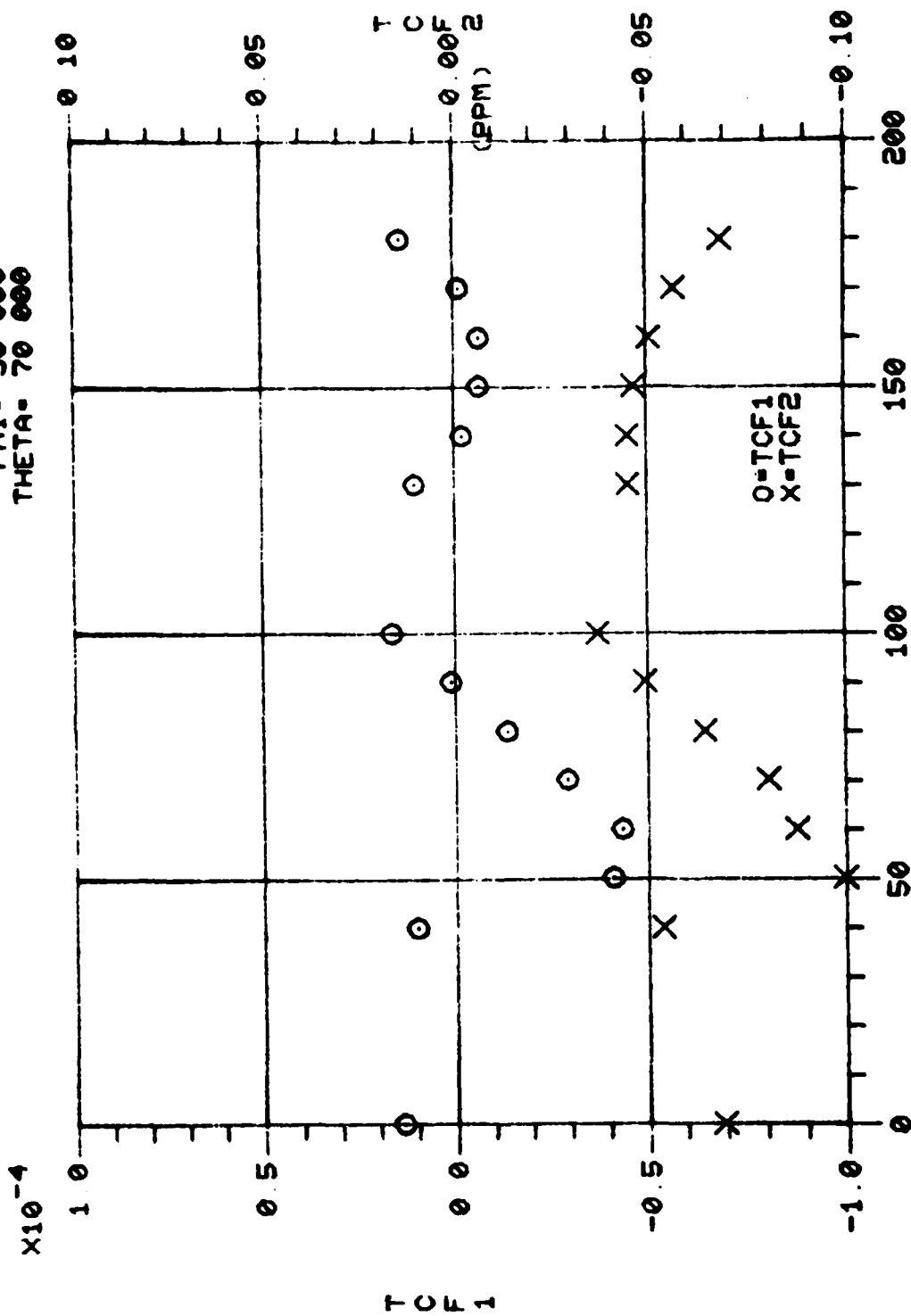
Figure 4JJ. Calculated Values of TCF⁽¹⁾ Versus Propagation Angles



PSI

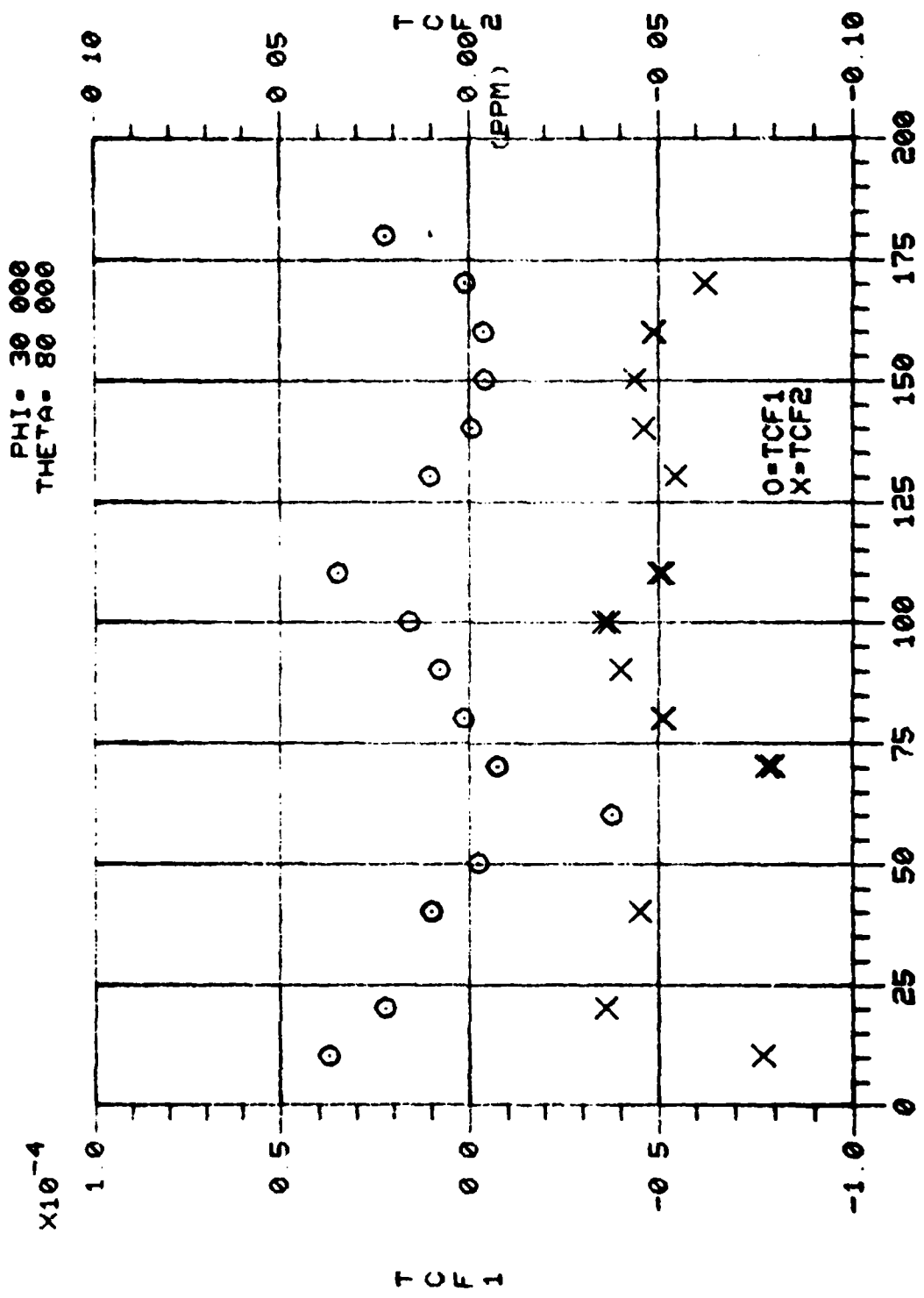
Figure 4KK. Calculated Values of TCF⁽¹⁾ Versus Propagation Angles

PHI = 30 000
 THETA = 70 000



PSI

Figure 4LL. Calculated Values of TCF⁽¹⁾ Versus Propagation Angles



PSI
Figure 4MM. Calculated Values of TCF⁽¹⁾ Versus Propagation Angles

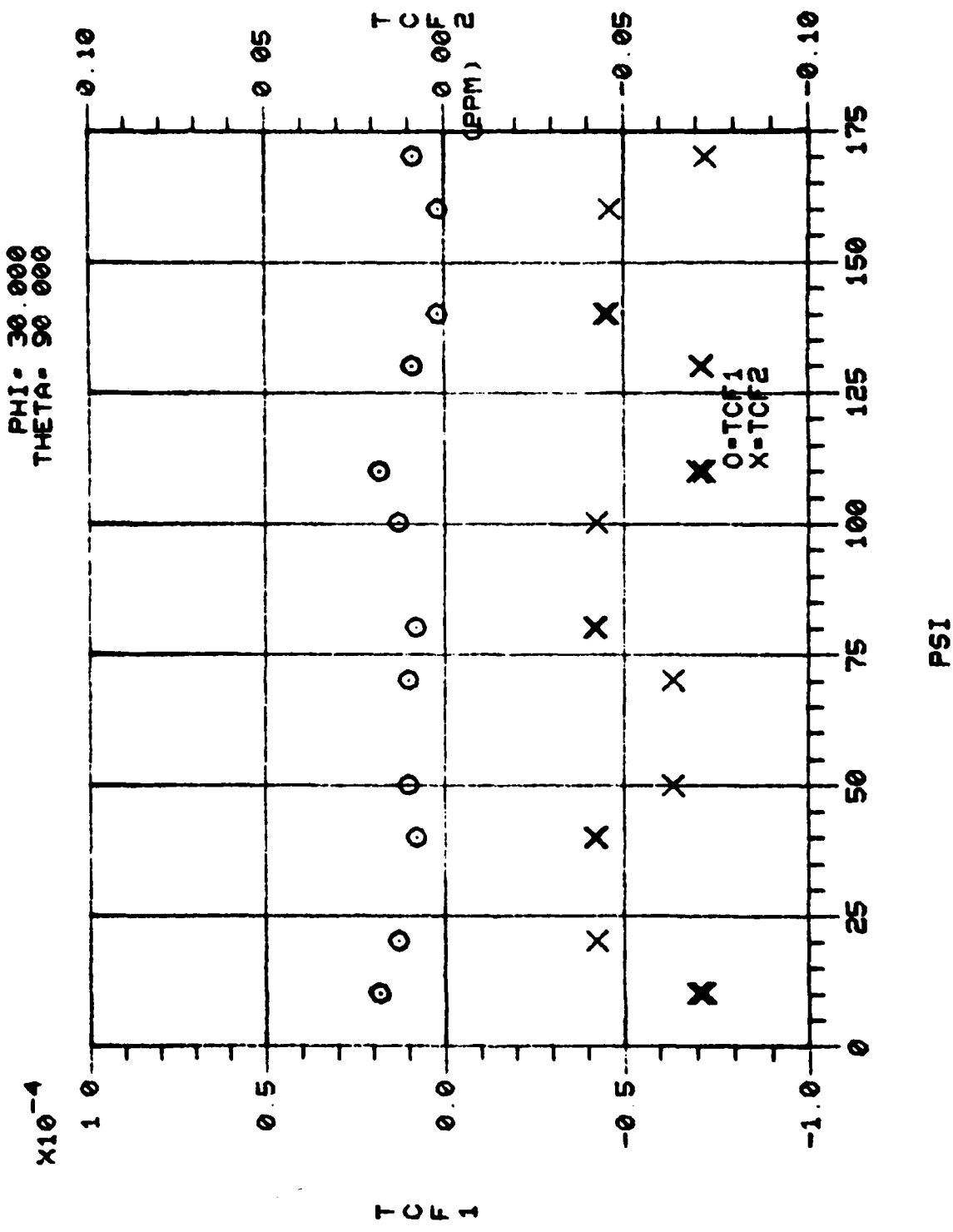


Figure 4NN. Calculated Values of TCF⁽¹⁾ Versus Propagation Angles

Calculations were performed on a $10^\circ \times 10^\circ \times 10^\circ$ grid over the angular ranges $0 \leq \text{PHI} \leq 30^\circ$, $0 \leq \text{PSI} \leq 180^\circ$, and $-90^\circ \leq \text{THETA} \leq 90^\circ$. These angular ranges, due to the symmetry of quartz, include all possible angular orientations. These initial calculations defined the "angular volumes" of low TCF orientations. Calculations were then performed on a $2.5^\circ \times 2.5^\circ \times 2.5^\circ$ grid near promising orientations. In this way, the entire angular range was explored and a large computer-based data file built. Maps of first and second order TCF's are shown in Figure 5. Zero first order TCF contours are drawn. In addition, contours of the second order TCF are drawn and shaded in areas where the second order TCF is less than $0.01 \text{ PPM}/^\circ\text{C}^2$. This represents a substantial improvement over ST quartz, for which the second order for TCF is approximately $0.03 \text{ PPM}/^\circ\text{C}^2$. Where data points were missing, lines were connected by interpolation.

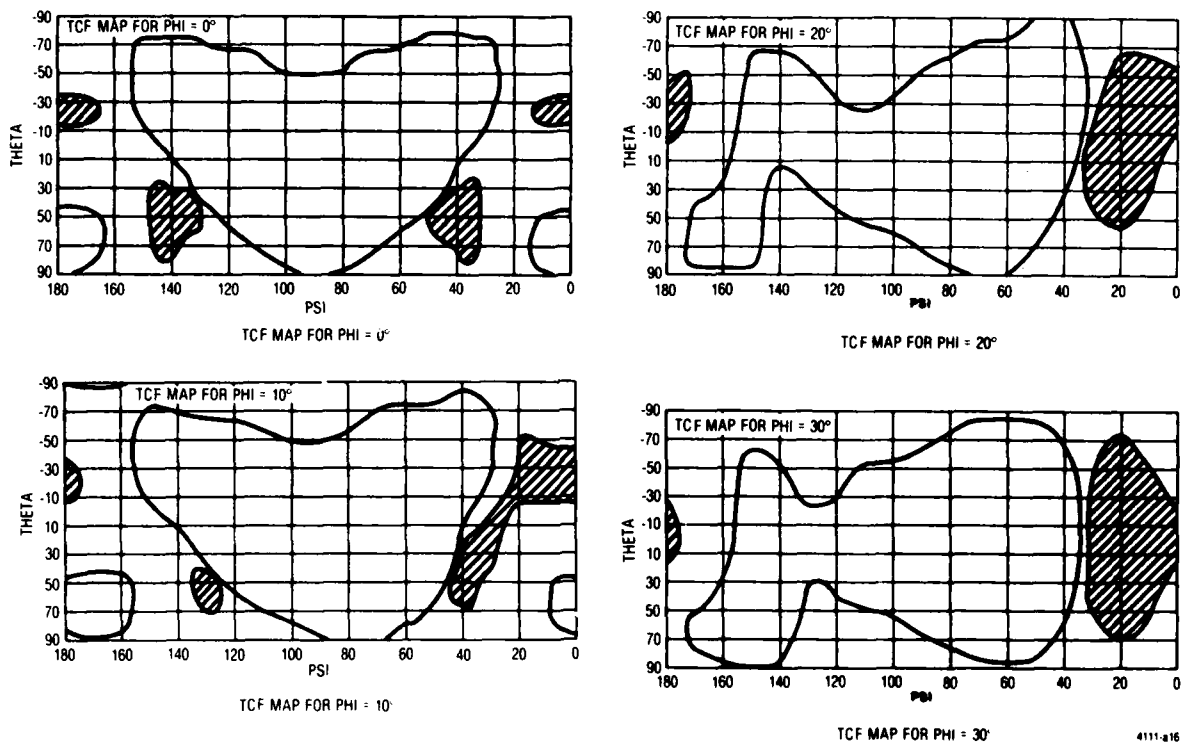


Figure 5. TCF Map of SAW Device on Quartz

Despite the number and density of points at which the first and second order TCFs were calculated, wherever $\text{TCF}^{(1)}$ was found to be less than or equal to zero, we found $\text{TCF}^{(2)}$ to be less than 0. The reason for this probably lies in the lack of independence of the crystal constants themselves. Using the volume perturbation approach of Auld¹, one obtains equation A-8 of Appendix A.

¹"Acoustic Fields and Waves in Solids," Auld, B. A., Vol. II, John Wiley & Sons, 1973, N. Y., p. 297.

For small changes in ρ and $c^{(j)}$, one might expect that the TCFs are well correlated with the temperature derivatives of the fundamental constants for Rayleigh waves in quartz. A list of some of the crystal elastic constants¹¹ temperature derivatives is in Table 1.

TABLE 1. CRYSTAL ELASTIC CONSTANTS' TEMPERATURE DERIVATIVES

	TC ⁽¹⁾	TC ⁽²⁾	TC ⁽³⁾
C ₁₁	-48.5 × 10 ⁶	-107 × 10 ⁹	-70 × 10 ⁻¹²
C ₁₂	-3000	-3050	-1260
C ₁₃	-550	-1150	-750
C ₁₄	101	-48	-590
C ₃₃	-160	-275	-250
C ₄₄	-177	-216	-216
C ₆₆	178	118	21
ρ	-34.92	-15.9	5.3
α_{11}	13.7	6.5	-1.9
α_{33}	7.5	2.9	-1.5

Figure 6 shows a plot of these values. The correlation is quite high, except for the case of C₁₄ and suggests that the TCFs should be correlated also. Plots of TCF⁽¹⁾ and TCF⁽²⁾ versus angles shown in Figure 4A through 4NN reflect this correlation.

Of course, if the two TCF surfaces do not intersect to form a line of zero TCF⁽¹⁾ and TCF⁽²⁾, we must use a slightly different approach to finding temperature stable cuts. The largest variation in constants occurs for C₁₂. As we are interested in the temperature range from -50°C to 100°C, the maximum deviation of T from T₀ = 25°C is |T - T₀| = 75°C. Calculating the changes in the constant C₁₂ for this maximum temperature change gives:

$$\frac{1}{C_{12}} |\Delta C_{12}^{(1)}| = 2.25 \times 10^{-1}$$

$$\frac{1}{C_{12}} |\Delta C_{12}^{(2)}| = 1.72 \times 10^{-2}$$

$$\frac{1}{C_{12}} |\Delta C_{12}^{(3)}| = 5.32 \times 10^{-4}$$

¹¹"Higher Order Temperature Coefficients of the Elastic Stiffnesses and Compliances of Alpha-Quartz", Bechmann, Ballato, Lukaszek, Proc. IRE, Aug 1962, pp. 1812-1922.

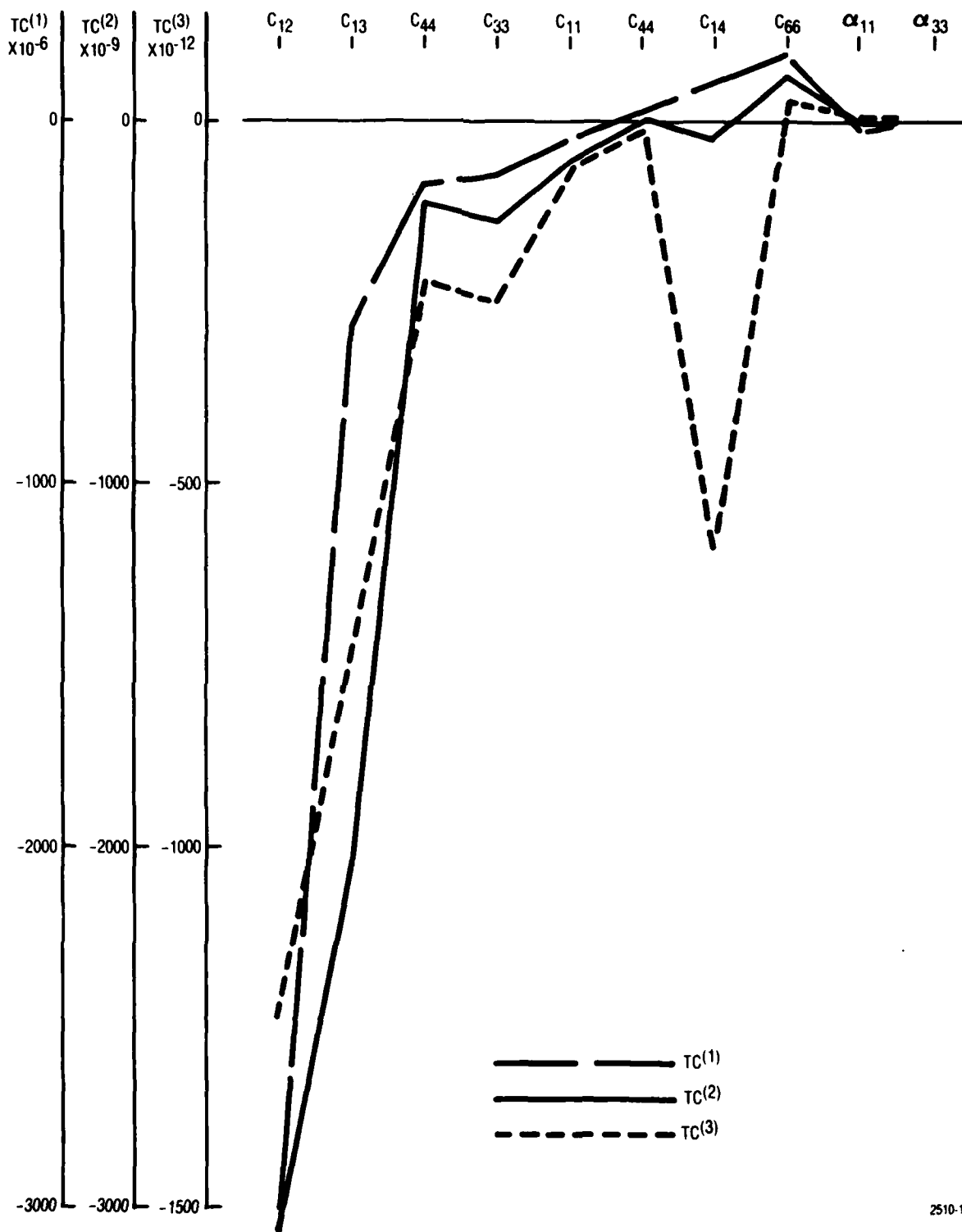


Figure 6. Temperature Coefficients of the Fundamental Constants of Quartz

Thus the most significant term is the first order term. The second order term is still quite significant but one order of magnitude below the first, while the third order term is almost three orders of magnitude below the first. Since the delay time τ is dependent on the crystal constants, the most significant term should be $TCF^{(1)}$. The least significant term should be $TCF^{(3)}$. After numerous calculations of the TCFs for many orientations, this appears to be the case.

The investigative approach used has been to first locate the surfaces of zero $TCF^{(1)}$ (the most significant term) with the finite difference program. Near these surfaces of zero $TCF^{(1)}$, low values of $TCF^{(2)}$ are sought, using already calculated results of the finite difference programs. Where low values of $TCF^{(2)}$ have been found, the perturbation approach was used to more accurately locate the zero $TCF^{(1)}$ surface, this being the most significant term in the total temperature dependence. $TCF^{(3)}$'s are then calculated to assure that their effect on the total temperature dependence is small. To date, this has always been found to be the case.

(8) Results of the Investigative Approach

Table 2 consists of a summary of the results of using the investigative approach described in paragraph (7) above. There are three areas where low TCF cuts have been located. These areas are centered near (YX wlt) 0/27/138, (YX wlt) 7/27/135.5, and (YX wlt) 15/40/40. These orientations have zero $TCF^{(1)}$, calculated by the Sinha and Tiersten approach, with $TCF^{(2)}$ and $TCF^{(3)}$ calculated with Finite Difference approach. These areas were chosen because of zero $TCF^{(1)}$, low $TCF^{(2)}$, and a low $TCF^{(3)}$ which can be mostly cancelled out by the first order TCF if the propagation direction is slightly rotated away from the zero $TCF^{(1)}$ direction. Then the $TCF^{(2)}$ term will dominate the performance characteristics. The angular resolution in these areas is $1^\circ \times 1^\circ \times 1^\circ$. The cuts potentially have one half to one third the temperature coefficients of ST-Cut quartz.

TABLE 2. PROPAGATION CHARACTERISTICS OF SELECTED ORIENTATIONS

Angles of ZTCF ⁽¹⁾ , Degrees (S & T's Program)			TCF ⁽²⁾ /°C ² (x10 ⁻⁸) Finite Difference Program	TCF ⁽³⁾ /°C ³ (x10 ⁻¹⁰) Finite Difference Program
Phi	Theta	Psi		
6	26	136.31	-1.4	
6	27	135.93	-1.3	0.67
6	28	135.59	-1.3	0.57
7	26	135.99	-1.5	
7	27	135.64	-1.4	
7	28	135.27	-1.3	0.65
8	26	135.74	-1.4	0.65
8	27	135.36	-1.4	
8	28	134.97	-1.3	
1	26	137.78	-1.2	0.68
1	27	137.48	-1.2	0.65
1	28	137.17	-1.1	0.67
0	26	138.07	-1.2	0.67
0	27	137.78	-1.1	0.68
0	28	137.49	-1.1	0.62
-1	26	138.37	-1.2	0.60
-1	27	138.09	-1.2	0.62
-1	28	137.80	-1.1	0.73
14	39	40.195	-1.0	0.64
14	40	40.415	-1.0	0.66
14	41	40.64	-1.0	0.75
15	39	39.79	-1.0	0.63
15	40	40	-1.0	0.74
15	41	40.23	-1.0	0.73
16	39	39.4	-1.0	0.68
16	40	39.605	-1.0	0.66
16	41	39.825	-1.1	0.60

d. Piezoelectric Coupling Factor

The piezoelectric coupling factor, denoted by k^2 , is a measure of the coupling efficiency for an interdigitated electrode.

We can express k^2 in terms of the interdigital transducer's input conductance¹ as

$$G_{in}(\omega_n) = -\pi^2 \omega_n M^2 W \epsilon_s^{(\infty)^2} G_s P_{n-1}^2 (\cos \eta \pi) / K^2 (\cos \eta \pi / 2) \quad (18)$$

where $\omega_n = 2\pi(2n-1)/\lambda s_0$, M is the number of electrode pairs, w is the length of the electrodes, λ is the spatial periodicity of the array, the width of each electrode is $\eta\lambda/2$, $\epsilon_s^{(\infty)}$ is the value of the effective permittivity at zero velocity, K is the complete elliptic integral of the first kind, and P_m are the Legendre polynomials. G_s is the residue of $1/(|s|\epsilon_s)$.

k^2 is defined by

$$k^2 = -2\epsilon_s^{(\infty)} G_s \quad (19)$$

Thus (18) becomes

$$G_{in}(\omega_n) = (1/2) \pi^2 \omega_n M^2 W \epsilon_s^{(\infty)} k_s^2 P_{n-1}^2 (\cos \eta \pi) / K^2 (\cos \eta \pi / 2) \quad (20)$$

and we see that k^2 is related to the input conductance and hence to the coupling efficiency. A good approximation to k^2 is given by

$$k_s^2 \cong 2(V_0 - V_s)/V_s = 2\Delta V/V \quad (21)$$

where V_s is the shorted Rayleigh wave velocity and V_0 is the free Rayleigh wave velocity.

It is seen that the quantity $\Delta V/V$ is an important parameter as it is a direct measure of the coupling efficiency and conductance of an interdigitated electrode pair on a piezoelectric substrate. Furthermore, $\Delta V/V$ is easily determined once the shorted and free surface problems have been solved. Programs are available for calculating the Rayleigh wave velocity with either shorted or free boundary conditions.

The shorted velocity calculations assumes a massless, perfectly conducting layer on the surface of the crystal. The boundary condition which must be satisfied is that $\phi = 0$ at $x_3 = 0$. The free surface boundary conditions are such that the potential ϕ and the normal component of the displacement, D_3 , are continuous at the surface. Furthermore, ϕ must satisfy Laplace's equation above the surface, resulting in

$$\phi = \phi_0 \exp(-kx_3) \exp(-ik(x_1 - Vt)), \quad (x_3 \geq 0) \quad (22)$$

¹"Surface Wave Filters," Matthews, Herbert, John Wiley & Sons, New York (1977).

In both calculations the mechanical boundary conditions are the same, that there be no force component in the x_1 direction, or

$$T_{11} = T_{12} = T_{13} = 0 \text{ at } x_1 = 0 \quad (23)$$

$\Delta V/V$ for different crystal types with various orientations were calculated. Results have been found to be in good agreement with experiments.

For example, on ST-quartz,

$$\begin{aligned} V_o &= 3.1586 \times 10^3 \text{ m/s} \\ V_s &= 3.1569 \times 10^3 \text{ m/s} \\ \Delta V/V &= 5.4 \times 10^{-4} \end{aligned} \quad (24)$$

To insure the suitability of the cuts described in paragraph (8) above for SAW applications, the coupling coefficients have been calculated for these cuts and are summarized in Table 3.

TABLE 3. PROPAGATION CHARACTERISTICS OF SELECTED ORIENTATIONS

Angles of ZTCF ⁽¹⁾ , degrees (S & T's program)			Velocity (msec)	K ² (x10 ⁻³)	Power Flow Angle (Degrees)
Phi	Theta	Psi			
6	26	136.31	3296.84	1.12	-0.3
6	27	135.93	3293.60	1.12	-0.2
6	28	135.59	3290.63	1.12	-0.1
7	26	135.99	3303.33	1.12	-0.5
7	27	135.64	3299.70	1.12	-0.4
7	28	135.27	3296.33	1.12	-0.3
8	26	135.74	3310.15	1.12	-0.7
8	27	135.36	3306.11	1.12	-0.6
8	28	134.97	3302.32	1.10	-0.5
1	26	137.78	3268.80	1.10	+0.7
1	27	137.48	3267.44	1.10	+0.9
1	28	137.17	3266.36	1.10	+1.0
0	26	138.07	3264.09	1.12	+0.9
0	27	137.78	3263.09	1.10	+1.1
0	28	137.49	3262.35	1.10	+1.2
-1	26	138.37	3259.65	1.10	+1.1
-1	27	138.09	3259.01	1.10	-1.3
-1	28	137.80	3258.64	1.08	+1.5

TABLE 3. PROPAGATION CHARACTERISTICS OF SELECTED ORIENTATIONS (CONT)

Angles of ZTCF ⁽¹⁾ , degrees (S & T's program)			Velocity (msec)	K _z ² (x10 ⁻⁴)	Power Flow Angle (Degrees)
Phi	Theta	Psi			
14	39	40.195	3298.60	0.96	-7.7
14	40	40.415	3306.67	0.96	-8.1
14	41	40.64	3315.19	0.94	-8.6
15	39	39.79	3301.82	0.96	-7.8
15	40	40.00	3310.14	0.94	-8.3
15	41	40.23	3319.09	0.98	-8.6
16	39	39.4	3305.38	0.96	-8.0
16	40	39.605	3314.03	0.98	-8.4
16	41	39.825	3323.15	0.92	-9.0

e. Power Flow Angle

The power flow angle for a particular direction of propagation is an important design parameter. While the phase fronts always remain parallel to the source transducer, the wave, as a whole, does not propagate perpendicular to the wave fronts (see Figure 7). This is a characteristic of anisotropic substrates where the phase velocity is asymmetric about the propagation direction; i.e., $V(\psi + \Delta\psi) \neq V(\psi - \Delta\psi)$. The major problem which arises is that the acoustic beam may steer off of the desired propagation track, missing the output transducer unless it is properly designed.

The power per unit width carried in a surface wave is found by integrating the mechanical and electrical Poynting vectors to obtain

$$P_i = -\frac{1}{2} \operatorname{Re} \left\{ \int_{-\infty}^0 T_{ij} \mu_j^* dx_3 - i\omega \int_{-\infty}^{\infty} \phi D_i dx_3 \right\}, i = 1, 2 \quad (25)$$

P_1 gives the power flow perpendicular to the wave front and P_2 gives the power flow parallel to the wave front. $P_1 = 0$ for the Rayleigh wave which is confined to the surface. The power flow angle may be defined as

$$\theta = \arctan(P_2/P_1) \cong P_2/P_1 \text{ for } P_2 \ll P_1 \quad (26)$$

The power flow angles are calculated using either the perturbation programs or the finite difference routine. Table 4 gives results of calculations for the ST-Cut quartz. Note that for $\psi = 0$, the power

flow angle is zero, within the single precision accuracy used, as a result of the crystal symmetry. Power flow angles as high as 20 degrees are not uncommon on quartz.

TABLE 4. POWER FLOW ANGLES ST-CUT

ψ	Transverse/Incident Power	Power Flow Angle θ
0°	6.159×10^{-3}	0
10°	6.145×10^{-3}	3.5 degrees
20°	9.502×10^{-3}	5.4 degrees

The beam steering angle will be calculated for the selected cut of quartz with TCF = 0. The analytical results will be compared with experimental measurements. Table 3 contains the results of calculations for the selected orientations described in paragraph (8) above.

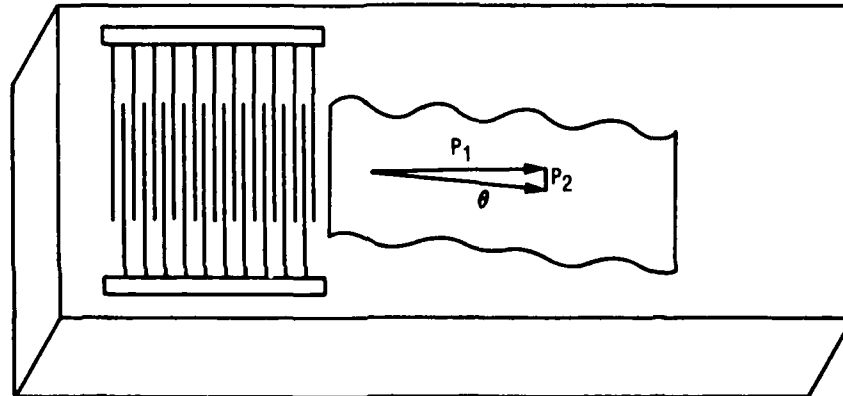


Figure 7. Nonzero Power Flow Angle

f. Proximity and Excitation Strength of Bulk Acoustic Waves (BAW) Spectrum

The purpose of this task is to analytically determine the strength of spurious signals caused by BAW. With this knowledge, one can predict the quality of the SAW device which has been selected for its zero TCD cut.

Interdigital transducers do not couple all of their field energy into surface waves. Bulk waves are also generated at various frequencies in the piezoelectric medium. These bulk waves can bounce off of the bottom surface, undergoing mode conversions in the process, and be received by the output transducer, resulting in unacceptable spurious signals. In most cases, this problem can be virtually eliminated by proper preparation of the bottom surface.

A transducer with periodicity λ excites surface waves at center frequencies

$$f_{SAW} = (2n + 1)V_{SAW}/\lambda \quad (27)$$

where V_{SAW} is the surface wave velocity and n is an integer, $n = 0, 1, 2, \dots$. The coupling to higher harmonics depends on transducer design. Bulk waves are radiated into the medium at an angle θ at a center fundamental frequency

$$f_b = V_b(\theta) / [\lambda \cos(\theta)] \quad (28)$$

where $V_b(\theta)$ is the velocity of the bulk wave in that particular direction. Equation 28 is a statement of the Bragg condition (see Figure 8). If the medium is isotropic for each mode, V_b is a constant. In the general case, V_b depends on the direction of propagation and hence on θ . To calculate $V_b(\theta)$, the matrix of elastic constants are rotated through the angle θ in the standard way. The quasi-longitudinal velocity and quasi-shear velocities are calculated as¹:

$$\begin{aligned} V_l &= \{ [C_{11}(\theta) + e_{11}^2(\theta) / \epsilon_{11}(\theta)] / \rho \}^{1/2} \\ V_{SH} &= \{ [C_{66}(\theta) + e_{16}^2(\theta) / \epsilon_{11}(\theta)] / \rho \}^{1/2} \\ V_{SV} &= \{ [C_{55}(\theta) + e_{15}^2(\theta) / \epsilon_{11}(\theta)] / \rho \}^{1/2} \end{aligned} \quad (29)$$

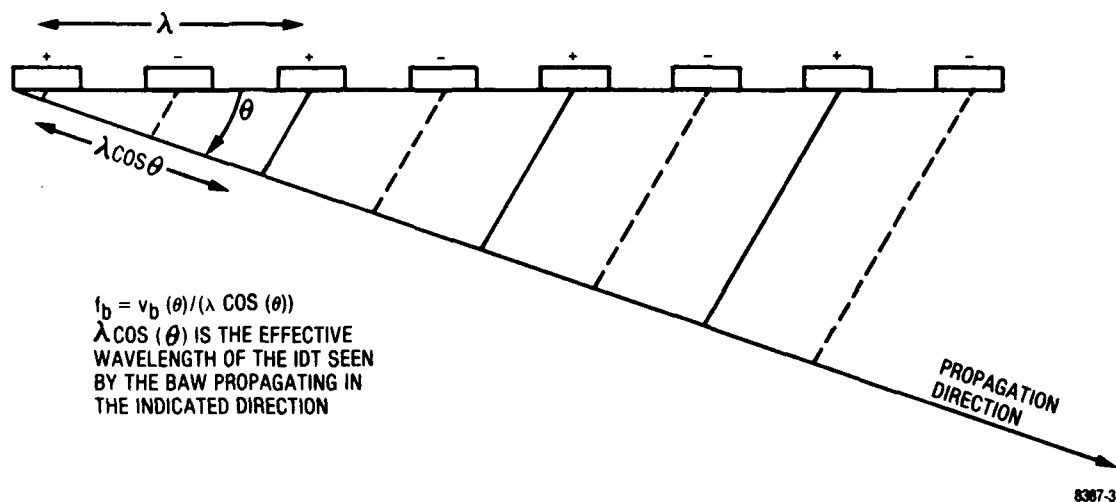


Figure 8. Bragg Condition for Excitation of BAW

The inverse values of these velocities, plotted as a function of θ , form the inverse velocity curves.

Inverse velocity plots as a function of propagation are particularly useful, for as long as $V_b / \cos \theta$, the effective velocity of the bulk wave on the surface, is greater than V_{SAW} , the effects of bulk mode generation may be suppressed by appropriate design and by proper conditioning of the bottom surface. Should $V_b / \cos \theta$ be less than V_{SAW} for any bulk mode, the SAW may couple to the BAW, resulting in a

¹"Physical Acoustics," Mason, Academic Press, NY, Vol. 1, Part A, 1964

leaky surface wave. Inverse velocity plots have been made for orientations with promising SAW temperature characteristics to check for the possibility of leaky surface waves and minimum values of f_s calculated and compared with f_{SAW} .

The polar plots of the inverse velocities for a (YX wlt) 0/27/137.8 and 7/27/135.59 are shown in Figure 9 and Figure 10, respectively. The values of $(1/v_{bulk})$ for the two shear modes and one longitudinal mode for different propagation directions (θ) into the crystal are also shown in Figures 9 and 10. The inverse surface wave velocity for 0/27/137.8 is 3.06×10^{-4} , that for 7/27/137.8 is 3.03×10^{-4} . These values are larger than the maximum $(1/v_{bulk}) \cos \theta (< 2.9 \times 10^{-4})$, therefore, the analysis indicates that a leaky mode does not exist (see Table 3 for the SAW velocities).

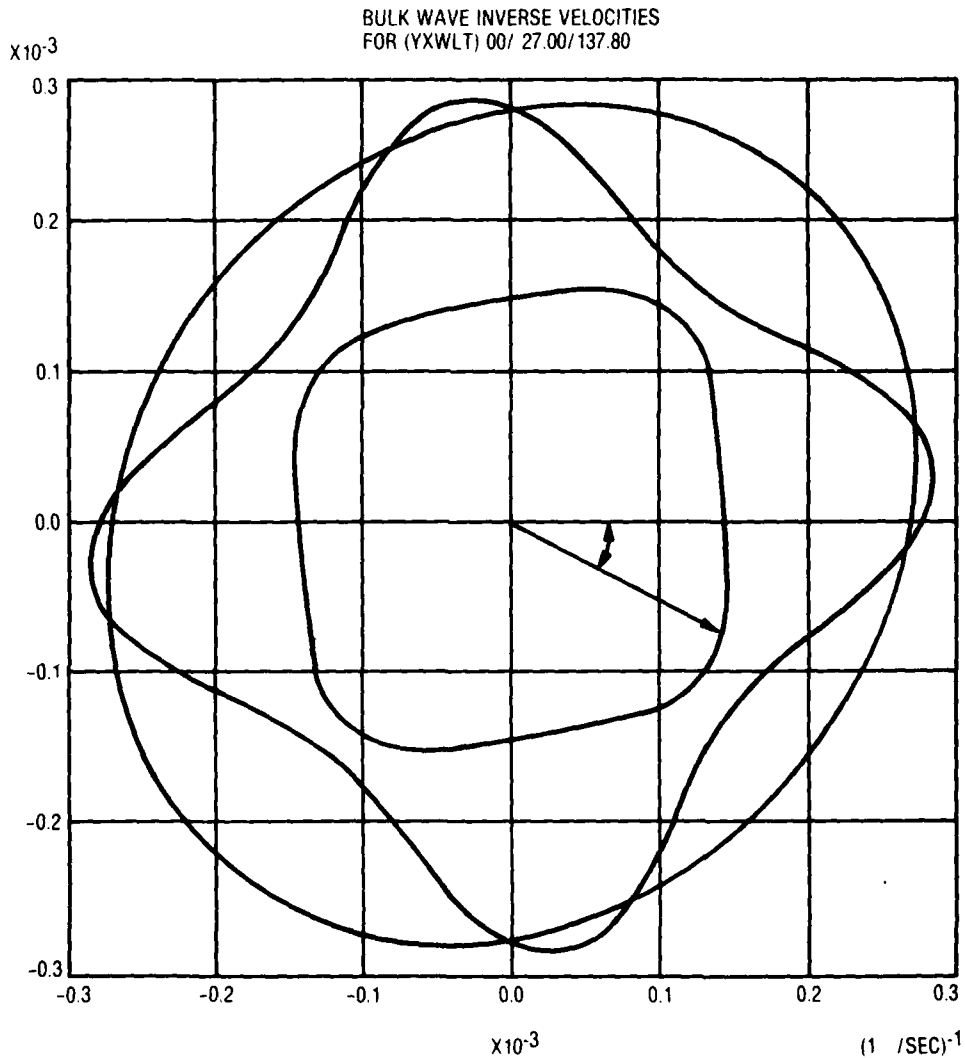


Figure 9. Polar Plots of Inverse Velocities for a (YXwlt) 0/27/137.8

2510-2

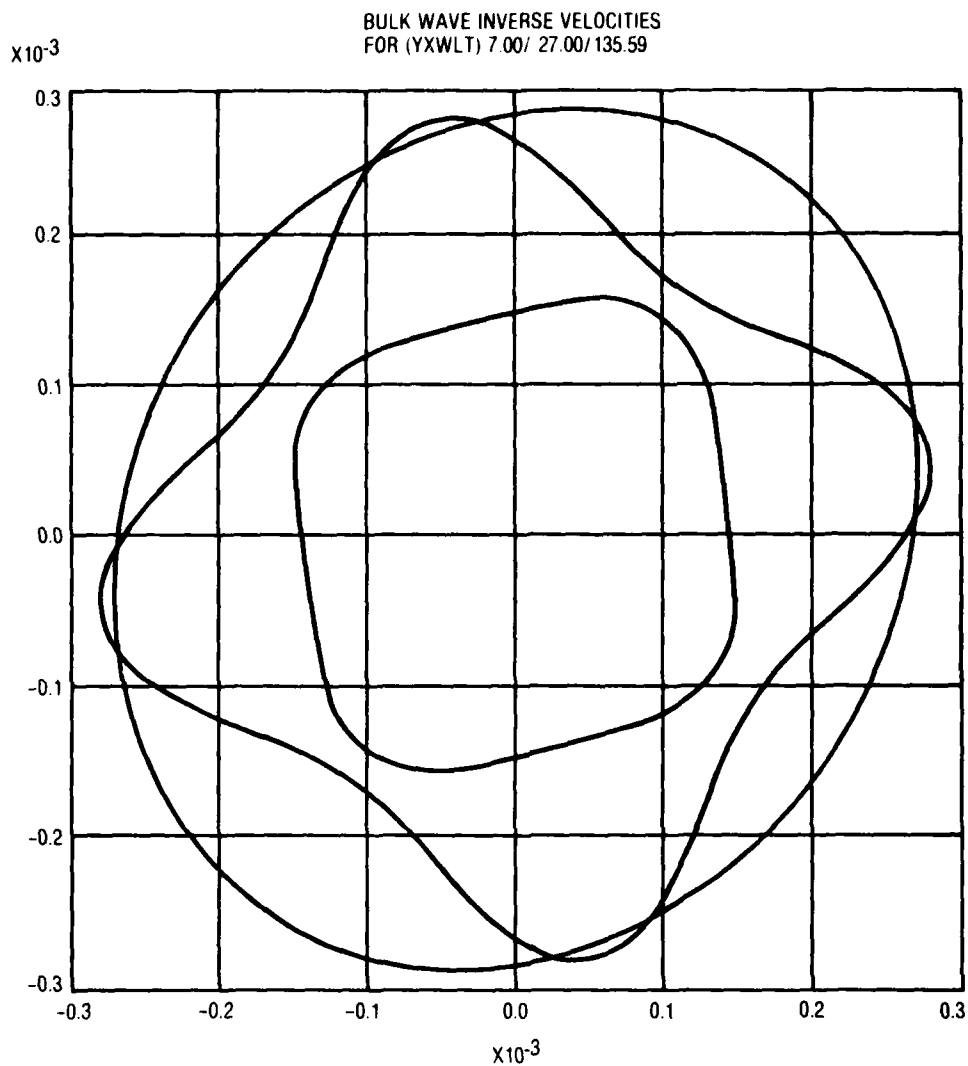


Figure 10. Polar Plots of Inverse Velocities for a (YXWLT) 7/27/135.59 2510-3

g. Degeneracies

Degenerate waves occur when the physical constants are such that equations (30) and (32) decouple.

$$\begin{bmatrix}
 \Gamma_{11} - \rho V_s^2 & \Gamma_{12} & \Gamma_{13} & \Gamma_{14} \\
 \Gamma_{12} & \Gamma_{22} - \rho V_s^2 & \Gamma_{23} & \Gamma_{24} \\
 \Gamma_{13} & \Gamma_{23} & \Gamma_{33} - \rho V_s^2 & \Gamma_{34} \\
 \Gamma_{14} & \Gamma_{24} & \Gamma_{34} & \Gamma_{44}
 \end{bmatrix}
 \begin{bmatrix}
 \alpha_1 \\
 \alpha_2 \\
 \alpha_3 \\
 \alpha_4
 \end{bmatrix}
 = 0
 \tag{30}$$

where

$$\begin{aligned}
 \Gamma_{11} &= c_{55} b^2 + 2c_{15} b + c_{11} \\
 \Gamma_{22} &= c_{44} b^2 + 2c_{46} b + c_{66} \\
 \Gamma_{33} &= c_{33} b^2 + 2c_{35} b + c_{55} \\
 \Gamma_{12} &= c_{45} b^2 + (c_{14} + c_{56}) b + c_{16} \\
 \Gamma_{13} &= c_{35} b^2 + (c_{13} + c_{55}) b + c_{15} \\
 \Gamma_{23} &= c_{34} b^2 + (c_{36} + c_{45}) b + c_{56} \\
 \Gamma_{44} &= -(e_{33} b^2 + 2e_{13} b + e_{11}) \\
 \Gamma_{14} &= e_{35} b^2 + (e_{15} + e_{31}) b + e_{11} \\
 \Gamma_{24} &= e_{34} b^2 + (e_{14} + e_{36}) b + e_{16} \\
 \Gamma_{34} &= e_{33} b^2 + (e_{13} + e_{35}) b + e_{15}
 \end{aligned} \tag{31}$$

The boundary conditions become, in matrix form,

$$\begin{bmatrix}
 \dots (c_{3311} + c_{3313} b^{(m)}) \alpha_1^{(m)} + (e_{133} + e_{333} b^{(m)}) \alpha_4^{(m)} \dots \\
 \dots (c_{3111} + c_{3113} b^{(m)}) \alpha_1^{(m)} + (e_{131} + e_{331} b^{(m)}) \alpha_4^{(m)} \dots \\
 \dots (c_{3211} + c_{3213} b^{(m)}) \alpha_1^{(m)} + (e_{132} + e_{332} b^{(m)}) \alpha_4^{(m)} \dots \\
 \dots (e_{311} + e_{313} b^{(m)}) \alpha_1^{(m)} - (e_{31} + e_{33} b^{(m)} - i\epsilon_0) \alpha_4^{(m)} \dots
 \end{bmatrix}
 \begin{bmatrix}
 C_1 \\
 C_2 \\
 C_3 \\
 C_4
 \end{bmatrix}
 = 0 \tag{32}$$

The definition of the constants and derivation of the equations are given in Appendix C. The condition for decoupling requires that the matrix in equation 30 has zero elements such that independent, non-Rayleigh wave solutions may exist. Equation 30 may decouple in many ways. If, for example, $\Gamma_{12} = \Gamma_{14} = \Gamma_{34} = 0$, u_1 and u_3 are found to be coupled and u_2 and ϕ are found to be coupled, however u_1 and u_3 are decoupled from u_2 and ϕ . If the physical constants are such that these two solutions are not coupled through the boundary conditions (equation 32) then we find the Rayleigh like wave (u_1 and u_3) is not coupled to ϕ , the potential term, and cannot be excited by electrodes in this cut.

The displacement u_2 which is coupled to ϕ is called the Bleustein — Gulyaev wave and is excited by interdigital transducers. These two waves (u_3 , u_1 and u_2 , ϕ) are degenerate as they propagate with the same velocity. The simplest method to determine whether equation 30 has decoupled for a particular orientation is to calculate the matrix of equation 30. This is presently accomplished using the Rayleigh wave velocity calculation program, which calculates and prints the matrix in equation 30. Because of the variety of special cases¹ which may arise, some of which may ultimately prove useful, each case in which we find the wave equation decouples will be considered on an individual basis.

¹"Propagation of Piezoelectric Surface Waves on Cubic and Hexagonal Crystals," Cambell & Jones, J.A.P., Vol. 41:2796-2801 (1970).

The analytical results of this section allow us to determine which modes can be generated on the selected zero TCD cut of quartz. At the three areas tabulated in Table 2, only Rayleigh wave modes were found.

h. Sensitivities Due to Crystal Misorientation

In cutting quartz and aligning masks on it, there is always some maximum achievable accuracy. Thus it is useful to know how all of the acoustic quantities considered vary with angle. Quantities such as TCD, phase velocity, power flow angle, $\Delta V/V$, bulk wave spectrums, and bulk wave velocity surfaces, are of interest to this program. These quantities can be accurately determined by directly calculating the quantities at $\phi = (\phi_0 + \Delta\phi)$, $\theta = (\theta_0 + \Delta\theta)$, and $\psi = (\psi_0 + \Delta\psi)$ with the same computer program discussed in paragraph 1, where ϕ_0 , θ_0 and ψ_0 are the desired angles, $\Delta\phi$, $\Delta\theta$ and $\Delta\psi$ are the actual directional deviation from the desired direction due to the fabrication tolerance. It is important to calculate the sensitivity of the parameters to the crystal misorientation; i.e., amount of change of a function as a result of small angular misorientation.

For case of the power flow angle (PFA)

$$\begin{aligned} d[\text{PFA}(\phi = 0, \theta = 42.75, \psi = 10^\circ)]/d\psi & \quad (33) \\ \cong (\text{PFA}(\psi = 20^\circ) - \text{PFA}(\psi = 0^\circ))/20^\circ \\ \cong 0.27^\circ/\text{degree}. \end{aligned}$$

The quantities $d[\text{PFA}(\phi = 0^\circ, \theta = 42.75, \psi = 10^\circ)]/d\phi$ and $d[\text{PFA}(\phi = 0^\circ, \theta = 42.75^\circ, \psi = 10^\circ)]/d\theta$ are computed in an equivalent manner.

In the case of TCD:

$$d(\text{TCD}) = \frac{\partial(\text{TCD})}{\partial\theta} d\theta + \frac{\partial(\text{TCD})}{\partial\phi} d\phi + \frac{\partial(\text{TCD})}{\partial\psi} d\psi \quad (34)$$

$$\frac{\partial(\text{TCD})}{\partial\theta} = [\text{TCD}(\phi_0, \theta_0, \psi_0) - \text{TCD}(\phi_0, \theta_0 + \Delta\theta, \psi_0)]/\Delta\theta \quad (35)$$

$$\frac{\partial(\text{TCD})}{\partial\phi} = [\text{TCD}(\phi_0, \theta_0, \psi_0) - \text{TCD}(\phi_0 + \Delta\phi, \theta_0, \psi_0)]/\Delta\phi$$

$$\frac{\partial(\text{TCD})}{\partial\psi} = [\text{TCD}(\phi_0, \theta_0, \psi_0) - \text{TCD}(\phi_0, \theta_0, \psi_0 + \Delta\psi)]/\Delta\psi$$

All the TCD (ϕ, θ, ψ) and TCD ($\phi, \theta, \psi + \Delta\psi$) etc., are calculated with the computer programs discussed in paragraph 1. Therefore, all the $\partial(\text{TCD})/\partial\theta$, $\partial(\text{TCD})/\partial\psi$, $\partial(\text{TCD})/\partial\phi$ can be accurately calculated. Hence the sensitivities due to crystal misorientation are determined.

Calculation of the angular dependence on the first, second, and third order TCDs is, of course, our primary task. Of these three quantities, the first order TCF is most sensitive to angular variation. The

angular dependence on these parameters will be calculated in the same way as all of the other quantities but on a much smaller angular grid ($\Delta\theta$, $\Delta\phi$ and $\Delta\psi$) about the zero TCD locus. The size of this grid will vary, depending on the magnitude and smoothness of the variation about each point on the locus of zero first order TCD orientations as verified by experiment and calculation. In case the function is smooth or linearly varying with angles, large Δ angles may be used.

By performing the above mentioned calculations, we have precise information on the sensitivities due to crystal misorientation. This information will allow us to impose a practical tolerance limit on fabrication and still be able to achieve the required superior performance specification.

Quantities such as velocity (Table 3), power flow angles (Table 3), BAW spectrum (Figures 50 and 51), coupling coefficients (Table 3), and second and third order TCFs (Table 2) do not vary quickly with angle. This is not the case for $TCF^{(1)}$. Table 5 contains a summary of $\partial TCF^{(1)}/\partial\psi$. The large values of $\partial TCF^{(1)}/\partial\psi$ impose strict fabrication tolerances on the SAW cuts and mask alignment. Fabrication accuracy to within 6 minutes is required to keep the total temperature variation due to $TCF^{(1)}$ within 45 ppm for $\partial TCF^{(1)}/\partial\psi = 3(\text{PPM}/^\circ\text{C})/\text{degree}$ over the temperature range -50°C to 100°C . Table 6 contains summaries of $\partial TCF^{(1)}/\partial\phi$ and $\partial TCF^{(1)}/\partial\theta$. These values impose fabrication tolerances on the rotated quartz plate angles ϕ and θ of 12 minutes to keep the total temperature variation due to $\partial TCF^{(1)}(15/40/40)/\partial\phi$ within 45 ppm over the temperature range -50°C to 100°C . This linear temperature variation may be compensated for by varying ψ on any particular cut if all other cut parameters vary slowly with angle.

TABLE 5. $\partial TCF^{(1)}/\partial\psi$ FOR SELECTED CUTS

Angles of ZTCF ⁽¹⁾ , degrees (S & T's program)			$\partial TCF^{(1)}/\partial\psi$
Phi	Theta	Psi	
6	26	136.31	+2.7 (ppm/°C)/degree
6	27	135.93	+2.7
6	28	135.59	+2.7
7	26	135.99	+2.7
7	27	135.64	+2.7
7	28	135.27	+2.7
8	26	135.74	+2.7
8	27	135.36	+2.7
8	28	134.97	+2.7
1	26	137.78	+2.8

TABLE 5. $\partial TCF^{(1)}/\partial \psi$ FOR SELECTED CUTS (CONT)

Angles of ZTCF ⁽¹⁾ , degrees (S & T's program)			$\partial TCF^{(1)}/\partial \psi$
Phi	Theta	Psi	
1	27	137.48	+2.8
1	28	137.17	+2.8
0	26	138.07	+3.0
0	27	137.78	+3.0
0	28	137.49	+3.0
-1	26	138.37	+3.0
-1	27	138.09	+3.0
-1	28	137.80	+3.0
14	39	40.195	-3.5
14	40	40.415	-3.5
14	41	40.64	-3.5
15	39	39.79	-3.5
15	40	40	-3.5
15	41	40.23	-3.5
16	39	39.4	-3.7
16	40	39.605	-3.7
16	41	39.825	-3.7

TABLE 6. $\partial TCF^{(1)}/\partial \phi$ AND $\partial TCF^{(1)}/\partial \theta$ FOR SELECTED CUTS

Angles of ZTCF ⁽¹⁾ (S&T's Program), Degrees			$\partial TCF^{(1)}/\partial \phi$	$\partial TCF^{(1)}/\partial \theta$
Phi	Theta	Psi		
7	27	135.64	-0.7(ppm/C°)/degree	-0.5(ppm/C°)/degree
0	27	137.78	-0.8	-0.8
15	40	40.00	+1.5	-0.7

2. WAFER FABRICATION

During the developmental phase of the doubly rotated cut SAW Devices program, a large number of wafers with 30 different crystal orientations will be fabricated and evaluated. To perform this task with good quality control, minimum cost and in a short time, Motorola has developed the techniques and processes to fabricate the doubly rotated cut of quartz wafers internally. The crystal boules are supplied by Motorola.

Carlisle, Pennsylvania; the X-ray wafer cutting is performed at Motorola's Semiconductor Group; polishing, fabrication and testing are performed at the Motorola Government Electronics Division. The methods used to fabricate the quartz wafers are described in the following sections.

A computer program was developed to calculate the incident angles and reflected angles for any given cut of crystal. The basic mathematical relations were derived in R.A. Heising's "Quartz Crystals for Electrical Circuits." The relations were formulated to computer programs. The flow diagram is shown in Figure 11. The results are shown in the printout (see Appendix F). The incident angle G , exit angle $(G + G')$, are defined for each plate position. The plate positions are determined by the direction of the rotated axis. (± 1 , ± 2 , ± 3), relative to the measuring stage. Once the angles of (YX wlt) $\phi/\theta/\psi$ are defined, all of the reflection angles will be calculated for the different reflection planes, defined by Miller indicies. The useful reflection planes that provide intense reflection with low skewed angles (< 5 degrees) are selected for printout. These results, after modification due to change in standards, are used to check the accuracy of the cuts.

a. Face Definitions

The following is an outline of the procedure to be used in this program to make a doubly rotated cut (YX wlt) $\phi/\theta/0$. The quartz bars have four lumbered faces with the minus X axis marked. The opposite face is marked by coloring it with a magic marker (blue). One other face not opposite the $-X$ face is colored also with a magic marker (red). The red face is now defined to be the $+Z$ axis as in Figure 12. The direction of the $+Y$ axis may be found by using the right-hand rule ($+X$ crossed into $+Y$ gives $+Z$). The $+Y$ axis will lie along the length of the crystal. Note that there are two ways to set up the axes on the crystal corresponding to choice of the red face (see Figure 12).

b. Running the X-Ray Program

The X-ray orientation program XRAY is run with the angles $\phi/\theta/0$. The sequence of instructions on the Honeywell 560 under the CP-V operating system is as follows:

```
!SET F:103 DC/MILDAT .538; IN
```

(This instruction assigns to unit 103 the file containing all of the Miller indicies to be searched.)

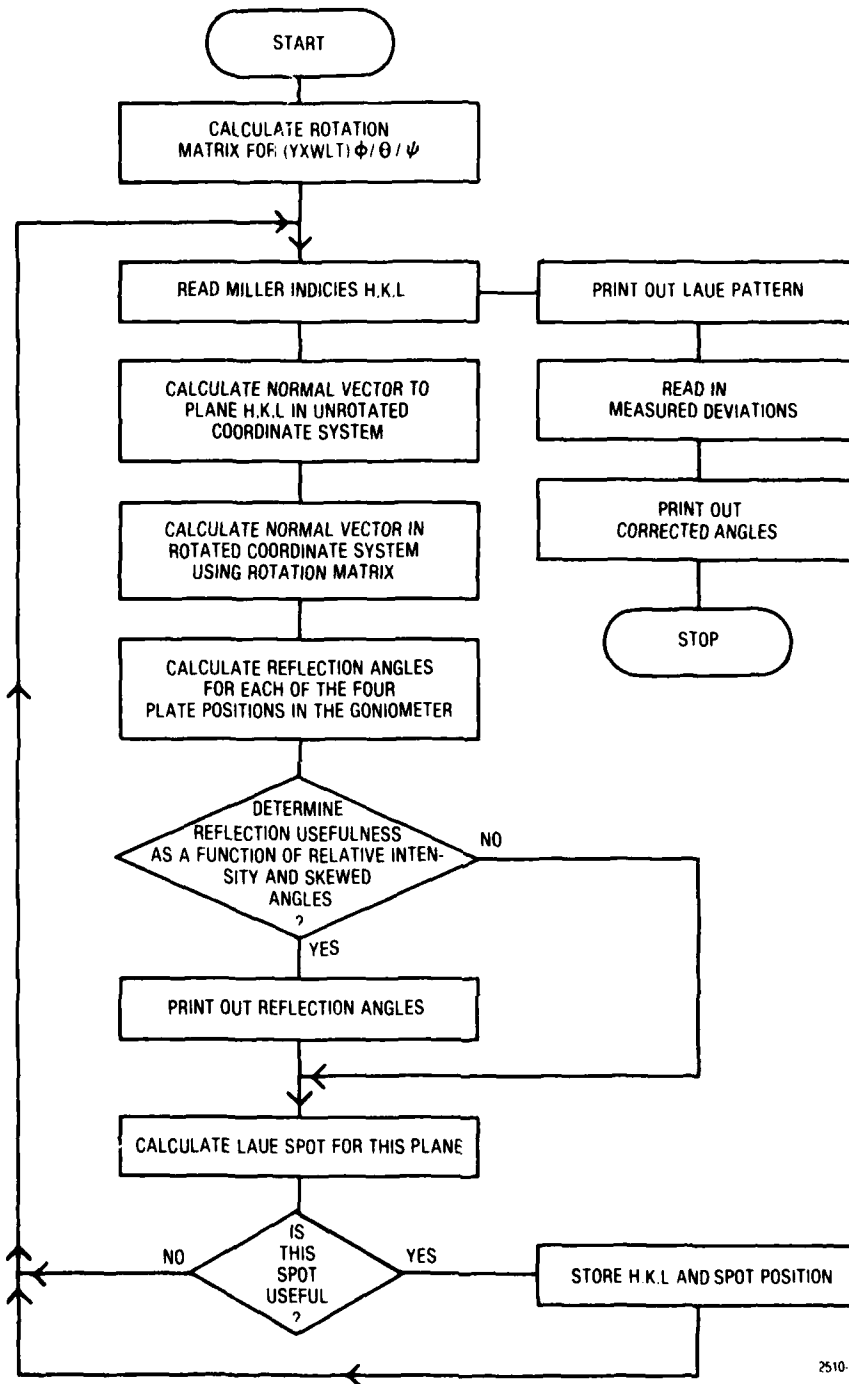
```
!SET F:104 DC/ERRDAT .538;IN
```

(This instruction assigns to unit 104 the file containing all of the angle perturbations defined in Heising for use with the Laue photographs.)

```
!XRAYL M.538
```

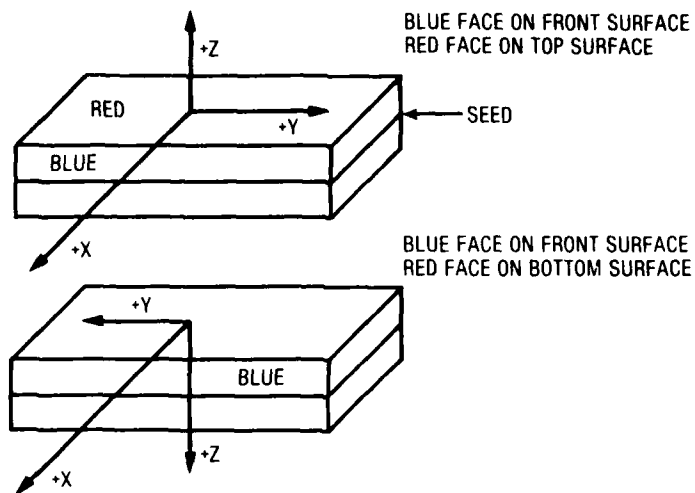
(This instruction loads and begins execution of the program.)

The program will ask for the angles $\phi/\theta/0$. These angles are entered in 3G format [i.e., 10.0, 3.0, 0.0 (carriage return)] and the results of the X-ray analysis printed.



2510-4

Figure 11. Flow Diagram of Calculation for Reflected Angles in Doubly Rotated Cut of Quartz



. 510-5

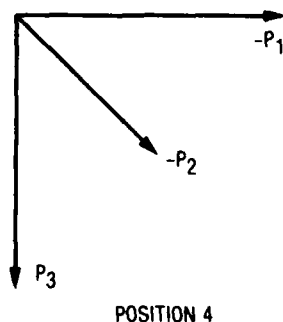
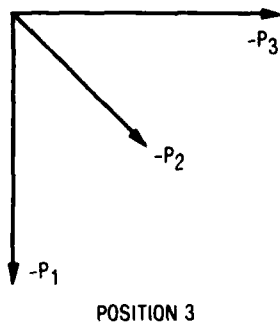
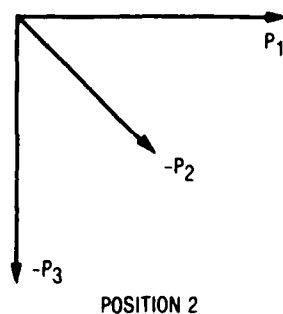
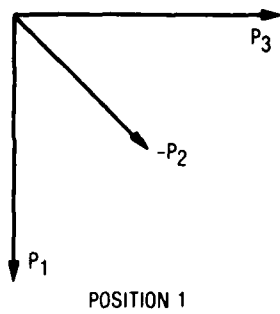
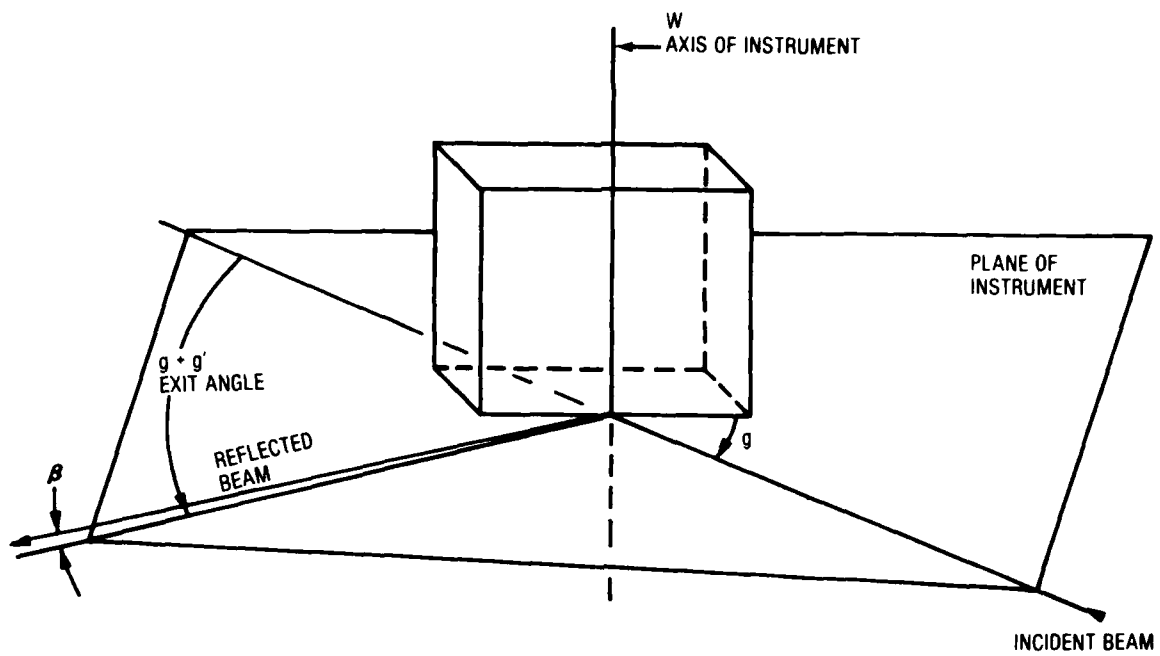
Figure 12. Two Possible Ways of Defining the Crystal Axes on a Lumbered Bar

c. Analysis of X-Ray Program

The X-ray program used follows the development of Heising's which uses a book written before the 1949 IRE Standard we use now. His X, Y, and Z axes will be denoted as \bar{X} , \bar{Y} , and \bar{Z} . The relation to our standard is as follows:

<u>Heising</u>	<u>1949 IRE Standard</u>
$+\bar{X}$	-X
$+\bar{Y}$	-Y
$+\bar{Z}$	+Z

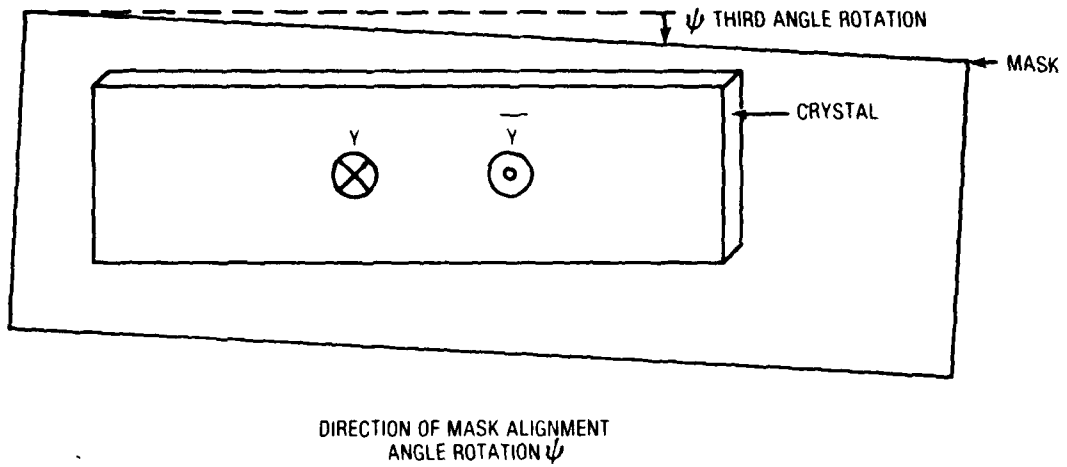
Furthermore, Heising's incident beam comes from the left, while our incident beam comes from the right. When these differences are accounted for, the "position chart" shown in Figure 13 must be used instead of the charts Heising uses in order that our X-ray machine and the 1949 standard may be used. P_1 , P_2 , and P_3 in the "position chart" are the +X, +Y, and +Z axes of the rotated plate. An important note of caution: the ϕ crystal face off of which we reflect the X-ray beam has \bar{Y} or $-Y$ as its normal. Since we may not assume that the crystal faces are parallel, we must propagate the surface wave on this face. This is important, because to achieve the same crystal properties, we must rotate by ψ about the +Y axis, resulting in a change of the sign of the third rotation (see Figure 14).



2510-7

P_1 , P_2 , and P_3 are the rotated plate axes X, Y, and Z.

Figure 13. X-ray Position Chart

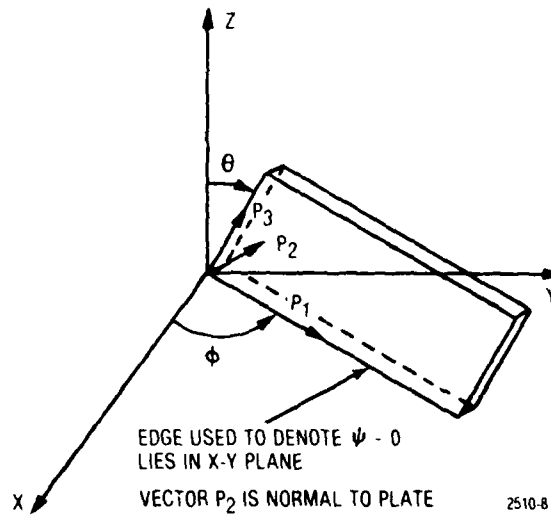


2510-6

Figure 14. Direction of Mask Alignment Angle Rotation ψ

d. Determination of the Actual ψ Angle

The third angle of rotation must be measured from a reference. The reference used is the face opposite the red face of the crystal ($-Z$ face). To determine the actual orientation of the finished crystal edge, we must know the orientation of this plane exactly (see Figure 15).



2510-8

Figure 15. Crystal Rotation (YX wlt) $\phi/\theta/0$

If the angles α and β in Figure 16 are measured using the (003) plane, which is parallel to the X and Y axes, $\Delta\psi$ is given by:

$$\Delta\psi = -\tan^{-1} \left[\frac{-\cos \phi \sin \alpha - \sin \phi \sin \beta}{(\sin \theta \sin \phi \sin \alpha - \sin \theta \cos \phi \sin \beta + \cos \theta \sqrt{1 - \sin^2 \alpha - \sin^2 \beta})} \right] \quad (36)$$

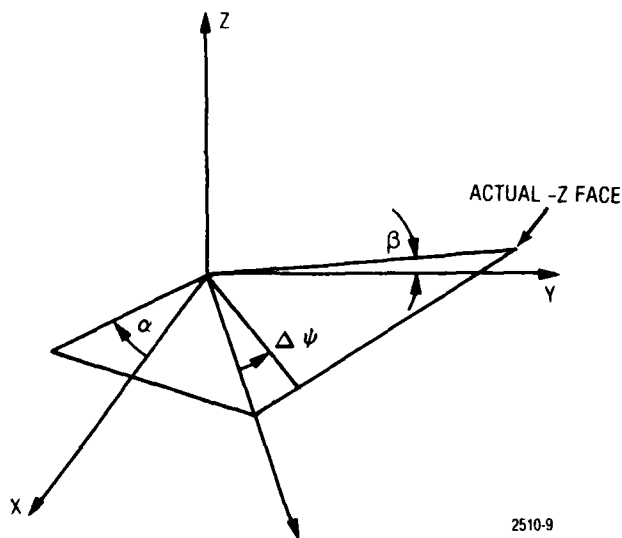


Figure 16. Actual -Z Face, Crystalline Axes, α , β , and $\Delta\psi$

Thus, given a ψ desired which we wish to obtain, we must actually rotate the mask by $\psi_{\text{ACTUAL}} = \psi_{\text{DES}} - \Delta\psi$ as shown in Figure 17.

e. Determination of α and β

The most appropriate crystal plane to use for determining α and β is the 003 plane. This plane has all of its atoms lying in planes perpendicular to the Z axis, and for a perfect Z face the X-ray deflection angles will be:

$$G = \text{Angle of incidence} = 25 \text{ degrees } 19 \text{ minutes}$$

$$G + G' = \text{Exit angle} = 50 \text{ degrees } 38 \text{ minutes}$$

For all positions on the X-ray machine with the +Z or -Z face being X-rayed. To determine α and β for the -Z face, we use the following relationships.

$$\alpha = 1/2 (G_{\cdot X \text{ TOWARD INCIDENT}} - G_{\cdot X \text{ TOWARD INCIDENT}}) \quad (37)$$

$$\beta = 1/2 (G_{\cdot Y \text{ TOWARD INCIDENT}} - G_{\cdot Y \text{ TOWARD INCIDENT}}) \quad (38)$$

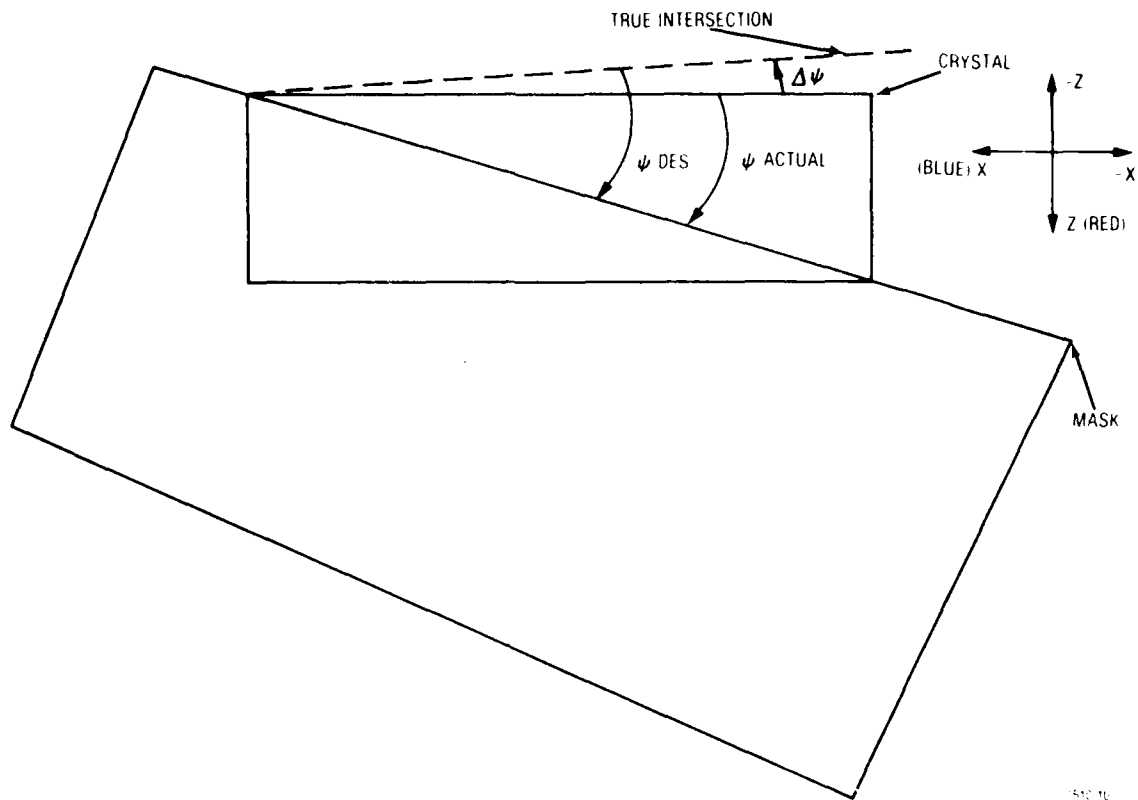


Figure 17. Mask Rotation to Obtain Desired ψ

To determine α and β for the $+Z$ face we use

$$\alpha' = 1/2 (G_{-X \text{ TO INCIDENT}} - G_{-X \text{ TO INCIDENT}}) \quad (39)$$

$$\beta' = 1/2 (G_{-Y \text{ TO INCIDENT}} - G_{-Y \text{ TO INCIDENT}}) \quad (40)$$

α' and β' are the α and β we would have measured for a $-Z$ face that is parallel to the $+Z$ face measured, which means that equation (36) is still valid for α' and β' .

The quartz crystal will now have the orientation $(YX \text{ wlt}) \phi/\theta/ - \Delta\psi(\alpha, \beta)$ if we use the $-Z$ edge as a reference and $(YX \text{ wlt}) \phi/\theta/ - \Delta\psi(\alpha', \beta')$ if we use the $+Z$ edge as a reference. The computer X-ray program for these angular orientations must be used if we are to get an accurate measurement. The integrity of these measurements of α and β is checked by comparing $1/2 (G_{-X} + G_{+X})$ and $1/2 (G_{-Y} + G_{+Y})$ with the theoretical result, $G_{AVC} = 25$ degrees 19 minutes.

f. Procedure Used to Zero X-Ray Machine:

- (1) Use reference quartz plate marked 10.1

- (2) Set X-ray exit angle to 26.5 degrees (marked AT cut on machine)
- (3) Set plate in X-ray machine with marking toward you (X-ray bounces off unmarked surface) and blue line up (width direction vertical). (See Figure 18).
- (4) Adjust with clutch till X-ray reading occurs at incident angle 13 degrees 18 minutes
- (5) Set plate in X-ray machine with marking toward you (X-ray bounces off unmarked surface) and blue line down (width direction vertical). (See Figure 19).
- (6) Angle of incidence should occur at 13 degrees 18 minutes + Δ angle.
- (7) Adjust clutch until angle of incidence is at 13 degrees 18 minutes + $1/2 \Delta$ angle.
- (8) Check alignment by measuring in positions of steps 3 and 5. The average of the two readings should be 13 degrees 18 minutes. Any discrepancy represents error in zeroing the machine and may be made less than less than 1 minute.
- (9) If the 10.1 cut is not available, the same procedure may be used if, for the cut to be used, the theoretical angles of incidence are equal for the particular crystal plane used in both positions.

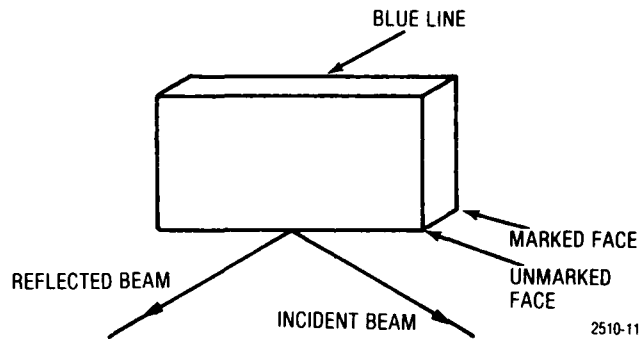


Figure 18. Position of Step 3, 10.1 Alignment Wafer

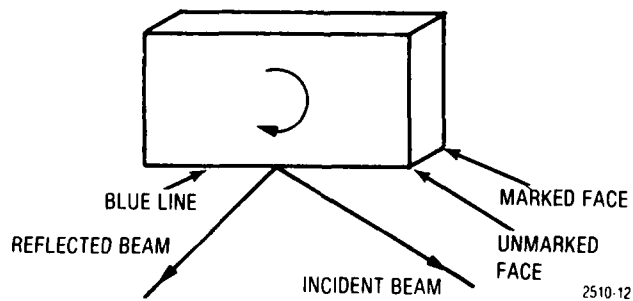


Figure 19. Position of Step 5, 10.1 Alignment Wafer Rotated by 180 Degrees About -Y Axis

g. Cutting Techniques for Doubly Rotated Orientations

A slicing machine built by Meyer and Burger Company, model TS3, was used to slice the quartz boule. The 6 inch diamond impregnated blade is supplied by Maurice Dessau, New York. The drift accuracy of the 2 inch cut is approximately 3 mils (~5 minutes).

The stage of the saw has the capability to rotate in two dimensions; it is designed to make the doubly rotated cut. The adjustment accuracies are graded to 0.5 minute. The X-ray beam resolution is about 2 minutes.

The combined accuracy of the wafers obtained experimentally has been better than 15 minutes. Iterative adjustment of the cutting stage can bring the cutting accuracy to within 10 minutes. The cutting procedures are the following:

- (1) Heat brass plate, glass plate and quartz boule.
- (2) Melt wax on brass plate and mount glass plate.
- (3) Melt wax on glass and mount quartz boule on glass.
- (4) Let cool to room temperature.
- (5) Screw mount brass plate to slice machine.
- (6) Initial cut of boule along the XZ plane (or directly to the desired angle if the boule was lumbered).
- (7) Determine true atomic plane using diffractometer and X-ray computer program.
- (8) Adjust stage to correct for true atomic planes, and obtain the desired rotation.
- (9) Perform doubly rotated cut of quartz.
- (10) Measure the reflection angle and check against the calculated result of the X-ray program. Iterative adjustment of stage can be done if cut accuracy is critical.

These procedures are presently used to cut the wafers with low TCF orientation required for this program.

h. Wafer Polishing

The polishing process for the quartz wafers was established during this period. The procedure includes the following:

- (1) The crystal axis orientation is marked on the back surface of the wafers with marking ink and baked dry. The markings have been demonstrated to stay on the crystal throughout the photolithographic process for easy identification.

(2) The corners of the wafers are ground prior to lapping and polishing to prevent corner breakage.

(3) The polishing is a two step process. The first step is a 15 μm lapping to obtain surface flatness with Microgrit, type WCA, Size 15, on a LAPMASTER, Model 24. The second step is to polish the surface with Cerium oxide on a LogiTech, Ltd. Model PM2 polisher. The polish wheel is made of pitch wax supplied by Hacker Instruments, Inc. The polished wafers have a surface finish with no observable grains or pits under a 50X microscope. The wafers are suitable for surface wave application. X-ray orientation was performed before and after the lapping and polishing processes. The change is normally less than 6 minutes. At the present time, wafers of the following cuts are polished; these are $\phi/\theta/\psi$ of 6/27/135.9, 6/28/135.6, 7/27/135.6, 7/28/135.3, 8/26/135.7, 8/27/135.4, and 8/28/134.9.

In the coming period, SAW devices will be fabricated on these wafers. Experimental results will be obtained and compared with the theoretical calculations.

SECTION III CONCLUSION

The temperature coefficients of frequency (TCF) have been analyzed for doubly rotated cuts of quartz for surface acoustic wave devices. The analysis procedure is shown below:

- (1) Using Finite Difference program, identify angular areas with zero $TCF^{(1)}$ and low $TCF^{(2)}$ on $10^\circ \times 10^\circ \times 10^\circ$ grid.
- (2) Calculate in these areas with $2.5^\circ \times 2.5^\circ \times 2.5^\circ$ grid to locate the rotation with minimum $TCF^{(2)}$ which has $TCF^{(1)} = 0$.
- (3) Identify the accurate zero $TCF^{(1)}$ with Sinha and Tiersten's program in areas obtained in (2).
- (4) Calculate $TCF^{(1)}$, $TCF^{(2)}$ and $TCF^{(3)}$ in selected areas obtained in (3) with $1^\circ \times 1^\circ \times 1^\circ$ span.
- (5) Calculate the coupling coefficients, propagation velocities, power flow angles and inverse bulk wave velocities for these angles.

The conclusions of the initial study are:

(a) The zero $TCF^{(1)}$ surface and zero $TCF^{(2)}$ surface data does not show an intersection in the $10^\circ \times 10^\circ \times 10^\circ$ grid. However, orientations with frequency variation ≈ 100 ppm from -50°C to 100°C , *better than ST Cut by a factor of two*, have been found in several areas where $TCF^{(1)} = 0$ and $TCF^{(2)}$ is less than $1.5 \times 10^{-8}/\text{C}^\circ$.

(b) The $\Delta TCF/\Delta$ angle is normally very large in the areas with zero $TCF^{(1)}$ and low $TCF^{(2)}$, therefore accurate crystal orientation is critical. It is estimated that the orientation accuracy of 6 minutes is required to obtain a $TCF^{(1)}$ of ≈ 50 ppm in the -50°C to 100°C temperature range in the three areas investigated. These are $\phi/\theta/\psi$ of 6/27/135.93 (4.45×10^{-2} ppm/ $^\circ\text{C} \cdot \text{minute}$), 14/40/40.415 (5.83×10^{-2} ppm/ $^\circ\text{C} \cdot \text{minute}$) and 0/27/137.78 (5.00×10^{-2} ppm/ $^\circ\text{C} \cdot \text{minute}$). Orientations with less sensitivity to orientation accuracy have been evaluated. These are the cuts that have $\partial[TCF^{(1)}]/\partial\psi = 0$ when $TCF^{(1)} = 0$. The cuts evaluated were $\phi/\theta/\psi = 20/30/155$, 20/20/150, 10/40/168. The $TCF^{(2)}$ of these cuts are approximately $4 \times 10^{-8}/\text{C}^\circ$, comparable or higher than ST cut.

(c) Coupling coefficients, velocities and beam steering angles were defined for the selected areas, no leaky modes were found in these areas.

(d) Methods to X-ray orient the quartz crystals, cut the doubly rotated wafers and polish such crystal wafers were developed. The wafers are ready for SAW device fabrication. The effort in the coming period is to design and fabricate single mode oscillators and to experimentally measure the TCF's of these selected orientations.

APPENDIX A

VOLUME PERTURBATION OF AULD

Perturbation techniques, as used here, allow calculations of small changes in the solutions to a problem caused by small changes in the physical parameters of the problem, once the solution to the unperturbed problem is known.

Our general approach to the problem of determining the temperature dependence of V_s will be as follows. First, the Rayleigh wave propagation problem will be solved in the standard way in its entirety at room temperature, T_0 . Given the solution of problem at T_0 and the dependence of the physical constants (such as c_{ij}) on temperature at T_0 , we will apply the volume perturbation formula, calculating the temperature dependence of V_s . The dependence of V_s on T is then used to calculate the frequency characteristics of the actual device given the thermal expansion coefficients as a function of temperature. At this point, the frequency temperature dependence of the substrate as a function of crystal cut and direction can be thoroughly explored.

The Volume Perturbed Formula.

Denoting $u_i(T_0)$ by u_i , etc., the volume perturbation formula is given by¹:

$$\beta_R = \omega \int_0^{\infty} [A] dy / \int_0^{\infty} (-u^* \cdot T' - u' \cdot T^* + \phi^* (i\omega D') + \phi' (i\omega D)^*) \cdot z dy \quad (A-1)$$

$$[A] = [\Delta\rho u^* \cdot u' + T^* : (\Delta s^E : T' + \Delta d \cdot E') + E^* \cdot (\Delta\epsilon^T \cdot E' + \Delta d : T')]$$

This equation is exact, but involves knowing the solution u' . However, we can set $u = u'$ if the temperature dependence of the solution is small and use $P = (1/2) \text{Re} \int (-u^* \cdot T + E \cdot H^*) dy$ to obtain the approximate solution

$$\Delta\beta_R = (\omega/4P) \int_0^{\infty} [\Delta\rho |u|^2 + S : \Delta c : S + E^* \cdot \Delta\epsilon^T \cdot E + E^* \cdot \Delta e : S + S : \Delta e \cdot E] dy \quad (A-2)$$

The u 's and E 's, and ρ come directly from the computer solution at T_0 .

¹Auld, B.A., "Acoustic Fields and Waves in Solids," Vol. II.

The Δ terms can be written as expansions of the form:

$$\Delta\beta_R = \beta_R(T_0)(\alpha_\beta^{(1)} dT + \alpha_\beta^{(2)} dT^2 + \alpha_\beta^{(3)} dT^3) \quad (A-3)$$

$$\Delta\rho = \rho(T_0)(\alpha_\rho^{(1)} dT + \alpha_\rho^{(2)} dT^2 + \alpha_\rho^{(3)} dT^3) \quad (A-4)$$

$$= \rho^{(1)} dT + \rho^{(2)} dT^2 + \rho^{(3)} dT^3 \quad (A-5)$$

$$\Delta C_{ijkl} = C_{ijkl}^{(1)} dT + C_{ijkl}^{(2)} dT^2 + C_{ijkl}^{(3)} dT^3, \text{ etc.} \quad (A-6)$$

to obtain

$$\begin{aligned} \Delta\beta_R &= \beta_R(T_0) (\alpha_\beta^{(1)} dT + \beta_R(T_0) \alpha_\beta^{(2)} dT^2 + \beta_R(T_0) \alpha_\beta^{(3)} dT^3) \\ &= (\omega dT/4P) \int_0^\infty (\rho(T_0) \alpha_\rho^{(1)} |u|^2 + S:c^{(1)}:S + E^* \cdot \epsilon^{(1)} \cdot E \\ &\quad + E^* \cdot e^{(1)} \cdot S + S:e^{(1)} \cdot E) dy \\ &\quad + (\omega dT^2/4P) \int_0^\infty (\rho(T_0) \alpha_\rho^{(2)} |u|^2 + S:c^{(2)}:S + \dots) dy \\ &\quad + (\omega dT^3/4P) \int_0^\infty (\rho(T_0) \alpha_\rho^{(3)} |u|^2 + S:c^{(3)}:S + \dots) dy \end{aligned} \quad (A-7)$$

or

$$\alpha_\beta^{(j)} = (\omega/4P\beta_R(T_0)) \int_0^\infty (\rho(T_0) \alpha_\rho^{(j)} |u|^2 + S:c^{(j)}:S + \dots) dy \quad (A-8)$$

For the problem of quartz, the electrostatic coupling is small and the electric terms can be ignored. Thus Δd and $\Delta\epsilon$ in (A-8) may be set to zero resulting in the simplified equation.

$$\alpha_\beta^{(j)} = (\omega/4P\beta_R) \int_0^\infty (\rho(T_0) \alpha_\rho^{(j)} |u|^2 + S : c^{(j)} : S) dy \quad (A-9)$$

The integrals are calculable, for instance, from (14),

$$\begin{aligned} &\int_0^\infty \rho(T_0) \alpha_\rho^{(1)} |u|^2 dy \\ &= \rho(T_0) \alpha_\rho^{(1)} \sum_n \int_0^\infty \left[\sum_m C_m \alpha_i^{(m)} \exp(-i \beta_R b^{(m)} y) \right] \\ &\quad \left[\sum_n C_n^* \alpha_i^{(n)*} \exp(i \beta_R b^{(n)} y) \right] dy \end{aligned} \quad (A-10)$$

The problem can easily be extended to multi-layered media by simply performing the integral over each layer separately. For the double layer (A-9) becomes:

$$\int_0^{\alpha} \rho_1 (T_0) \alpha_{\rho_1}^{(1)} |u|^2 dy + \int_{\alpha}^{\infty} \rho_2 (T_0) \alpha_{\rho_2}^{(2)} |u|^2 dy + \dots \quad (\text{A-11})$$

Because the dependence of u , is given explicitly by (13), it is not necessary to use numerical integration procedures, as demonstrated in (A-10).

Once the $\alpha_{\beta}^{(j)}$ have been calculated from (A-9) the $\alpha_v^{(j)}$ are simply determined. Using $\beta = \omega/V_0$, and (A-9) we determine $\alpha_r^{(j)}$.

APPENDIX B

VOLUME PERTURBATION FORMULA OF SINHA AND TIERSTEN

The approach used by Sinha and Tiersten includes the effects of distortion caused by heating a substrate of quartz and is based in the coordinate system to which the fundamental elastic constants refer. In this reference system, the density is constant and the $\alpha_i^{(i)}$ are equivalent to the $\alpha v^{(i)}$.

In this new reference system, the perturbation formula becomes¹

$$(\Delta v/v_s) = (1/2\beta_R^2 v^2) (H/N^2), \quad (B-1)$$

$$N^2 = (\rho^0 \pi i / \beta_R^2) \sum_{m=1}^4 \sum_{n=1}^4 (c^{(m)} \alpha^{(m)} c^{(n)*} \alpha^{(n)*}) / (\beta_m - \beta_n^*) \quad (B-2)$$

$$H = -\int_0^\infty dy \int_{-\pi/\beta_R}^{\pi/\beta_R} dz (K_{zz} u_{z,z} + K_{zy} u_{y,z} + K_{zx} u_{z,x} + K_{yz} u_{z,y} + K_{yy} u_{y,y} + K_{yx} u_{x,y}) \quad (B-3)$$

$$K_{L\gamma} = (c_{L\gamma M\alpha} + \Delta c_{L\gamma M\alpha}) u_{\alpha, M} \quad (B-4)$$

For the first order perturbation in T we have:

$$c_{L\gamma M\alpha} = (c_{L\gamma M\nu AB} \alpha_{AB} + c_{L\gamma KM} \alpha_{\nu K} + c_{LK M\nu} \alpha_{\gamma K}) dT \quad (B-5)$$

$$\Delta c_{L\gamma M\alpha} = (d c_{L\gamma M\alpha} / dT) dT \quad (B-6)$$

Where $c_{L\gamma M\alpha}$ are the second order elastic constants previously denoted simply as $c_{L\gamma M\alpha}$ and $c_{L\gamma M\nu AB}$ are the third order elastic constants. The terms $\Delta c_{L\gamma M\alpha}$ as calculated by Tiersten² is available only to first order in T, and the higher order elastic constants $c_{L\gamma M\nu ABCD}$ have never been determined.

¹"On The Temperature Dependence Of The Velocity Of Surface Waves On Quartz," B.K. Sinha and H.F. Tiersten, 1978 Ultrasoncs Symposium Proceeding, IEEE, pp. 662-665.

²"Temperature dependence of the Fundamental Elastic Constants of Quartz," B.K. Sinha and H.F. Tiersten, Proceedings of the 32nd Annual Symposium on Frequency Control, 1978, pp. 150-153.

APPENDIX C

THE DIFFERENTIATION METHOD

A method for determining the theoretical temperature dependence of Rayleigh Surface Waves consists of formally differentiating the wave equation and boundary conditions. The boundary conditions and wave equation must be true at all temperatures, placing restraints on how the parameters of the wave equation may vary. In this technique, the derivatives of these equations with respect to temperature are set to zero and solved for the velocity temperature dependence. This method follows the methods used by Bechmann, Ballato, and Lukaszek¹ to compute the temperature dependence of the fundamental elastic constants from frequency data, except that the simplifying assumptions of assuming bulk wave solutions cannot be made. This method was later used by Hauden² to search for temperature stable cuts of quartz.

Christoffel's wave equation can be written in matrix form as

$$\begin{bmatrix} \Gamma_{11} - \rho V_s^2 & \Gamma_{12} & \Gamma_{13} & \Gamma_{14} \\ \Gamma_{12} & \Gamma_{22} - \rho V_s^2 & \Gamma_{23} & \Gamma_{24} \\ \Gamma_{13} & \Gamma_{23} & \Gamma_{33} - \rho V_s^2 & \Gamma_{34} \\ \Gamma_{14} & \Gamma_{24} & \Gamma_{34} & \Gamma_{44} \end{bmatrix} \begin{bmatrix} \alpha_1 \\ \alpha_2 \\ \alpha_3 \\ \alpha_4 \end{bmatrix} = 0 \quad (C-1)$$

where

$$\begin{aligned} \Gamma_{11} &= c_{55} b^2 + 2c_{15} b + c_{11} & \Gamma_{23} &= c_{34} b^2 + (c_{36} + c_{45}) b + c_{36} \\ \Gamma_{22} &= c_{44} b^2 + 2c_{46} b + c_{66} & \Gamma_{34} &= -(e_{33} b^2 + 2e_{13} b + e_{11}) \\ \Gamma_{33} &= c_{33} b^2 + 2c_{35} b + c_{55} & \Gamma_{14} &= e_{35} b^2 + (e_{15} + e_{31}) b + e_{11} \\ \Gamma_{12} &= c_{45} b^2 + (c_{14} + c_{56}) b + c_{16} & \Gamma_{24} &= e_{34} b^2 + (e_{14} + e_{36}) b + e_{16} \\ \Gamma_{13} &= c_{35} b^2 + (c_{13} + c_{55}) b + c_{15} & \Gamma_{34} &= e_{33} b^2 + (e_{13} + e_{35}) b + e_{15} \end{aligned} \quad (C-2)$$

¹"Higher Order Temperature Coefficients of the Elastic Stiffnesses and Compliances of Alpha Quartz." Bechmann, Ballato, and Lukaszek, Proc. IRE, Aug 1962, pp. 1812-1822.

²"Higher Order Temperature Coefficients of Quartz SAW Oscillators," D. Handen, M. Michael, J.J. Gagnepain, Proc. Frequency Control Symposium (1978), pp. 77-86.

following the notation used in the previous section and in Matthews¹. This equation holds for each of the four modes, hereafter designated by a superscript m.

The boundary conditions become, in matrix form,

$$\begin{bmatrix} \dots(C_{33,1} + C_{33,3} b^{(m)}) \alpha_1^{(m)} + (e_{133} + e_{333} b^{(m)}) \alpha_4^{(m)} \dots \\ \dots(C_{31,1} + C_{31,3} b^{(m)}) \alpha_1^{(m)} + (e_{131} + e_{331} b^{(m)}) \alpha_4^{(m)} \dots \\ \dots(C_{32,1} + C_{23,3} b^{(m)}) \alpha_1^{(m)} + (e_{132} + e_{332} b^{(m)}) \alpha_4^{(m)} \dots \\ \dots(e_{3,1} + e_{3,3} b^{(m)}) \alpha_1^{(m)} - (\epsilon_{31} + \epsilon_{33} b^{(m)} - i\epsilon_0) \alpha_4^{(m)} \dots \end{bmatrix} \begin{bmatrix} C_1 \\ C_2 \\ C_3 \\ C_4 \end{bmatrix} = 0 \quad (C-3)$$

where only the m'th column is shown and the C_m 's are the amplitudes of each mode. This formulation assumes a normalization of the α 's

$$(\alpha_1^{(m)})^2 + (\alpha_2^{(m)})^2 + (\alpha_3^{(m)})^2 + (\alpha_4^{(m)})^2 = 1. \quad (C-4)$$

The first condition we can place on the wave equation is that the determinant of Christoffel's equation vanishes for all temperature, or

$$d/dT \begin{vmatrix} \Gamma_{11} - \rho V_s^2 & \Gamma_{12} & \Gamma_{13} & \Gamma_{14} \\ \Gamma_{12} & \Gamma_{22} - \rho V_s^2 & \Gamma_{23} & \Gamma_{24} \\ \Gamma_{13} & \Gamma_{23} & \Gamma_{33} - \rho V_s^2 & \Gamma_{34} \\ \Gamma_{14} & \Gamma_{24} & \Gamma_{34} & \Gamma_{44} \end{vmatrix} = 0 \quad (C-5)$$

For each of the four modes, this equation is valid, resulting in four equations in five unknowns, dV_s/dT , and $db^{(m)}/dT$ of the form $F_1^{(m)}(dV_s/dT, db^{(m)}/dT) = 0$, $m = 1, 2, 3, 4$.

For each mode, Christoffel's matrix equation (C-1) must vanish, yielding the set of equations

$$\begin{aligned} (d/dT) (\alpha_1^{(m)} (\Gamma_{11}^{(m)} - \rho V_s^2) + \alpha_2^{(m)} \Gamma_{12}^{(m)} + \alpha_3^{(m)} \Gamma_{13}^{(m)} + \alpha_4^{(m)} \Gamma_{14}^{(m)}) &= 0 \\ (d/dT) (\alpha_1^{(m)} \Gamma_{12}^{(m)} + \alpha_2^{(m)} (\Gamma_{22}^{(m)} - \rho V_s^2) + \alpha_3^{(m)} \Gamma_{23}^{(m)} + \alpha_4^{(m)} \Gamma_{24}^{(m)}) &= 0 \\ (d/dT) (\alpha_1^{(m)} \Gamma_{13}^{(m)} + \alpha_2^{(m)} \Gamma_{23}^{(m)} + \alpha_3^{(m)} (\Gamma_{33}^{(m)} - \rho V_s^2) + \alpha_4^{(m)} \Gamma_{34}^{(m)}) &= 0 \\ (d/dT) (\alpha_1^{(m)} \Gamma_{14}^{(m)} + \alpha_2^{(m)} \Gamma_{24}^{(m)} + \alpha_3^{(m)} \Gamma_{34}^{(m)} + \alpha_4^{(m)} \Gamma_{44}^{(m)}) &= 0. \end{aligned} \quad (C-6)$$

This results in 16 equations (four per mode) and an additional 16 unknowns (the $\alpha_i^{(m)}$'s) of the form

$$F_{2i}^{(m)}(dV_s/dT, db^{(m)}/dT, d\alpha_1^{(m)}/dT, d\alpha_2^{(m)}/dT, d\alpha_3^{(m)}/dT, d\alpha_4^{(m)}/dT) = 0$$

¹"Surface Wave Filters," H. Matthews, John Wiley and Sons, New York (1977).

Using (C-3) we obtain the single equation

$$(d/dt) \begin{vmatrix} \dots\dots (C_{3311} + C_{3313}b^{(m)}) \alpha_1^{(m)} + (e_{133} + e_{333}b^{(m)}) \alpha_4^{(m)} \dots\dots \\ \dots\dots (C_{3111} + C_{3113}b^{(m)}) \alpha_1^{(m)} + (e_{131} + e_{331}b^{(m)}) \alpha_4^{(m)} \dots\dots \\ \vdots \\ \vdots \\ \vdots \end{vmatrix} = 0 \quad (C-7)$$

of the form $F_1^{(m)} (db^{(1)}/dT, db^{(2)}/dT, \dots, d\alpha_1^{(m)}/dT) = 0$

and four equations of the form

$$(d/dT) \sum_m C_m [(C_{3311} + C_{3313}b^{(m)}) \alpha_1^{(m)} + (e_{133} + e_{333}b^{(m)}) \alpha_4^{(m)}] = 0 \quad (C-8)$$

$$(d/dT) \sum_m C_m [(C_{3111} + C_{3113}b^{(m)}) \alpha_1^{(m)} + (e_{131} + e_{331}b^{(m)}) \alpha_4^{(m)}] = 0$$

of the form $F_4^{(m)} (db^{(m)}/dT, d\alpha_1^{(m)}/dT, dC_m/dT) = 0$ (C-9)

From (5) $\alpha_1^{(m)} (d\alpha_1^{(m)}/dT) + \alpha_2^{(m)} (d\alpha_2^{(m)}/dT) + \alpha_3^{(m)} (d\alpha_3^{(m)}/dT)$ (C-10)

$$+ \alpha_4^{(m)} (d\alpha_4^{(m)}/dT) = 0$$

or

$$F_5^{(m)} (d\alpha_i^{(m)}/dT) = 0 \quad (C-11)$$

Combining the above results gives 25 equations in the 25 unknowns.

$$dV./dT, db^{(m)}/dT, d\alpha_i^{(m)}/dT, dC_m/dT$$

which are solved simultaneously. Once the temperature dependence of the Rayleigh wave velocity is found, the frequency dependence is found in the usual way.

To obtain the second order dependence of V_s , the 25 equations are differentiated again. The values of $dV./dT, db^{(m)}/dT, d\alpha_i^{(m)}/dT$ and dC_m/dT previously obtained are used to obtain $d^2V./dT^2$, etc.

APPENDIX D

SOLUTION METHOD

Calculating the velocity of a Rayleigh wave requires a complete solution of the problem to be performed. All of the constants in equation (13) must be evaluated. The standard used at Motorola as developed by Campbell and Jones is outlined below.

First the fundamental constants are rotated into the coordinate system of interest.

Next a value of V_r is picked. The coefficients τ_{ij} of equation (C-2) are evaluated and the determinant of the matrix in equation (C-1) is set to zero, as it must be if a solution of (C-1) is to be found. This results in an eighth order equation in b . This equation is solved for the eight complex roots. The four roots $b^{(m)}$ in the lower complex plane are retained, the four discarded roots not satisfying the boundary conditions at infinity. Equation (C-1) is then solved for the four eigenvectors $\alpha_i^{(m)}$. The $b_i^{(m)}$ and the corresponding eigenvector $\alpha_i^{(m)}$ are substituted into equation (C-3) and the determinant of the matrix in equation (C-3) is evaluated. This determinant must be zero for a solution to (C-3) exist. If it is not zero, V_r is varied, and the whole procedure repeated, until it is. Once a value of V_r is found such that the determinant in equation (C-3) vanishes, the solution to (C-3) is found, giving the values for C_m . These constants completely describe the solution of equation (13), as well as providing the exact velocity.

APPENDIX E

EQUIVALENCE OF TEMPERATURE COEFFICIENTS OF FREQUENCY AND DELAY

In the following section, the relations relating the first, second, and third order temperature coefficients of delay and frequency will be derived. These relations show implicitly the equivalence of each representation of the device temperature characteristics, and justify their interchangeable usage.

In the text, we have used the following notation:

$$\tau = \text{delay time of delay line oscillator} \quad (\text{E-1})$$

$$i\text{th order temperature coefficient of delay} = \text{TCD}^{(i)} = \alpha_{\tau}^{(i)} \quad (\text{E-2})$$

$$F = \text{frequency of delay line oscillator} \quad (\text{E-3})$$

$$i\text{th order temperature coefficient of frequency} = \alpha_F^{(i)} \quad (\text{E-4})$$

$$\tau = \tau_0 (1 + \alpha_{\tau}^{(1)} (T - T_0) + \alpha_{\tau}^{(2)} (T - T_0)^2 + \alpha_{\tau}^{(3)} (T - T_0)^3 + \dots) \quad (\text{E-5})$$

$$F = F_0 (1 + \alpha_F^{(1)} (T - T_0) + \alpha_F^{(2)} (T - T_0)^2 + \alpha_F^{(3)} (T - T_0)^3 + \dots) \quad (\text{E-6})$$

where T is temperature and T_0 is a reference temperature, 25°C in our case. For a SAW oscillator, $F\tau = \text{constant}$ or

$$\begin{aligned} \tau/\tau_0 &= F_0/F \\ &= 1/(1 + \alpha_F^{(1)} (T - T_0) + \alpha_F^{(2)} (T - T_0)^2 + \alpha_F^{(3)} (T - T_0)^3 + \dots) \end{aligned} \quad (\text{E-7})$$

Using the relation

$$1/(1 + X) \cong 1 - X + X^2 - X^3 \text{ for } X \ll 1 \quad (\text{E-8})$$

we can write

$$\begin{aligned} \tau/\tau_0 &= 1 - [\alpha_F^{(1)} (T - T_0) + \alpha_F^{(2)} (T - T_0)^2 + \alpha_F^{(3)} (T - T_0)^3] \\ &\quad + [(\alpha_F^{(1)} (T - T_0))^2 + 2\alpha_F^{(1)} (T - T_0) \alpha_F^{(2)} (T - T_0)^2] \\ &\quad - [\alpha_F^{(1)} (T - T_0)]^3 + \text{higher order terms} \end{aligned} \quad (\text{E-9})$$

$$= 1 - \alpha_F^{(1)} (T - T_0) + (-\alpha_F^{(2)} + (\alpha_F^{(1)})^2) (T - T_0)^2 + (-\alpha_F^{(3)} + 2\alpha_F^{(1)} \alpha_F^{(2)} - (\alpha_F^{(1)})^3) (T - T_0)^3 \quad (\text{E-10})$$

Equating powers of $T - T_0$ in (E-5) and (E-10), we obtain

$$\alpha_{\tau}^{(1)} = -\alpha_f^{(1)} \quad (E-11)$$

$$\alpha_{\tau}^{(2)} = -\alpha_f^{(2)} + (\alpha_f^{(1)})^2 \quad (E-12)$$

$$\alpha_{\tau}^{(3)} = -\alpha_f^{(3)} + 2\alpha_f^{(1)}\alpha_f^{(2)} - (\alpha_f^{(1)})^3 \quad (E-13)$$

As the only assumption on F and τ used is that of equation (E-7) which is symmetric in F and τ , we immediately obtain

$$\alpha_f^{(1)} = -\alpha_{\tau}^{(1)} \quad (E-14)$$

$$\alpha_f^{(2)} = -\alpha_{\tau}^{(2)} + (\alpha_{\tau}^{(1)})^2 \quad (E-15)$$

$$\alpha_f^{(3)} = -\alpha_{\tau}^{(3)} + 2\alpha_{\tau}^{(1)}\alpha_{\tau}^{(2)} - (\alpha_{\tau}^{(1)})^3 \quad (E-16)$$

Using (E-11) through (E-16), we can always relate one set of temperature coefficients to the other.

AD-A086 734

MOTOROLA INC SCOTTSDALE ARIZ GOVERNMENT ELECTRONICS DIV F/G 20/2
DOUBLY ROTATED CUT SAW DEVICES.(U)
JUN 80 D F WILLIAMS, F Y CHO

DAAK20-79-C-0275

UNCLASSIFIED

DELET-TR-79-0275-1

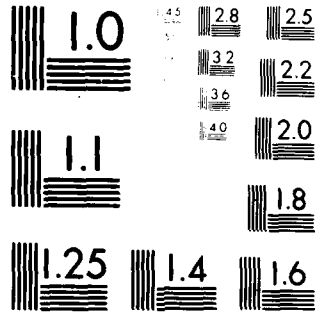
NL

2 of 2

AD-A086 734



END
DATE
FILMED
8-80
DTIC



MICROCOPY RESOLUTION TEST CHART
NATIONAL BUREAU OF STANDARDS-1963-A

APPENDIX F

X-RAY RUN

The following is an example of the computer results from the FORTRAN X-ray orientation computer program for the doubly rotated cut 7/27/0. File MILDAT contains only the two Miller indices shown on the printout on this run.

16105 APR 19 '60 1000047
JOB 536,WILLIAMS(352200),7, FILEXRAYJOB, ID63, LINE22
LIMIT (TIME,2),(CO,30),(UO,30)
ASSIGN P1103,(FILE,MILDAT),(IN)
ASSIGN P1104,(FILE,ERRDAT),(IN)
RUN (LMN,XRAYLH)
INPUT THE THREE ANGLES PHI,THETA,PSI

***** ANGLES ARE (YXHLT)7.0000 (0 MIN.)/27.0000 (0 MIN.)/.00000 (0 MIN.)

MILLER INDICIES: 0 -1 1

NORMAL VECTOR =.97534E-01 -.975690 .197133
THETA= 13.3213

PLATE IN POSITION 1 (-1 AXIS VERTICAL, 2 AXIS NORMAL)
G = ANGLE OF INCIDENCE:24.0064 (48 MIN.)
BETA=2.52901 (32 MIN.)
G PLUS G PRIME:EXIT ANGLE:126.5310 (32 MIN.)
INTENSITY FACTOR:1.70921E-01 INTENSITY:1.00000

PLATE IN POSITION 3 (1 AXIS VERTICAL, 2 AXIS NORMAL)
G = ANGLE OF INCIDENCE:1.96138 (58 MIN.)
BETA=-2.52901 (32 MIN.)
G PLUS G PRIME:EXIT ANGLE:126.5310 (32 MIN.)
INTENSITY FACTOR:1.924245 INTENSITY:1.00000

MILLER INDICIES: 0 -2 1

NORMAL VECTOR =.113399 -.980196 -.929136E-01
THETA= 22.8995

PLATE IN POSITION 2 (-3 AXIS VERTICAL, 2 AXIS NORMAL)
G = ANGLE OF INCIDENCE:29.5843 (33 MIN.)
BETA=1.16657 (9 MIN.)
G PLUS G PRIME:EXIT ANGLE:145.6526 (39 MIN.)
INTENSITY FACTOR:1.362103 INTENSITY:1.00000

PLATE IN POSITION 4 (3 AXIS VERTICAL, 2 AXIS NORMAL)
G = ANGLE OF INCIDENCE:16.4650 (28 MIN.)
BETA=-1.16657 (9 MIN.)
G PLUS G PRIME:EXIT ANGLE:145.6526 (39 MIN.)
INTENSITY FACTOR:1.633495 INTENSITY:1.00000

```

*****
LAUE ANGLES DEFINED SUCH THAT ALPHA = ANGLE FROM BEAM,
BETA = ROTATION CLOCKWISE FROM P1, DIST TO CRYSTAL = 10.0000
MILLER INDICES: 0 = 1 1 LAUE SPOT ANGLES: ALPHA=25.3188  BETA=64.0927  X=2.06704  Y=4.25554
MILLER INDICES: 0 = 2 1 LAUE SPOT ANGLES: ALPHA=16.0600  BETA=30.3295  X=2.34422  Y=1.92073
*****
LAUE ANGLES DEFINED SUCH THAT ALPHA = ANGLE FROM BEAM,
BETA = ROTATION CLOCKWISE FROM P1.
FOR ROTATIONS E(1) = .000000 E(2) = .000000 E(3) = .000000  ACTUAL ANGLES ARE
(VX=176.99998 (60 MIN.)/27.0000 (60 MIN.)/.000000 ( 0 MIN.))
FOR ROTATIONS E(1) = .500000 E(2) = -.116660 E(3) = .000000  ACTUAL ANGLES ARE
(VX=176.99998 (60 MIN.)/27.5011 (30 MIN.)/.117251 ( 7 MIN.))
*STOP* NORMAL
DATA INFORMATION=IGNORED

```

APPENDIX G

X-RAY PROGRAM

The following is the FORTRAN computer program used to calculate X-ray diffraction angles for a doubly rotated cut of quartz.


```

41 000 SUBROUTINE CLEAR
42 000 COMMON/CLEAN/N
43 000 COMMON /ANGLE/A1,A2,A3
44 000 NSD
45 000 WRITE(100,10)
46 000 FORMAT(' INPUT THE THREE ANGLES PHI,THETA,PBI')
47 000 READ(105,30)A1,A2,A3
48 000 FORMAT(3E)
49 000 WRITE(100,20)A1,MI(A1),A2,MI(A2),A3,MI(A3)
50 000 COMMON /NORM/PHI,THETA
51 000 COMMON /MILLER/M,K,L
52 000 REAL RM(3),RMI(3),R(3,3)
53 000 IERR=0
54 000 RETURN
55 000 END
56 000 SUBROUTINE NORMAL(IERR)
57 000 INTEGER M
58 000 COMMON /RNT/R
59 000 COMMON /NORM/PHI,THETA
60 000 COMMON /MILLER/M,K,L
61 000 REAL RM(3),RMI(3),R(3,3)
62 000 IERR=0
63 000 RMI(1)=R(1,1)
64 000 RMI(2)=R(2,2)/SQRT(3.0)
65 000 RMI(3)=R(3,3)/1.09997
66 000
67 000 DO 10 I=1,3
68 000 RM=RM+RMI(I)*RMI(I)
69 000 SQRT(0)
70 000 DO 20 I=1,3
71 000 RMI(I)=RMI(I)/8
72 000 DO 30 I=1,3
73 000 RMI(I)=0.
74 000 DO 30 J=1,3
75 000 R(1,1)=R(1,1)+RMI(I)*RMI(J)
76 000 A=0.993
77 000 CDIV=1.09997
78 000 D=SQRT((A./3.)*R(1,1)+R(2,2)+R(3,3))
79 000 RLAN=1.5378
80 000 IF (RLAN>.05) D=ABS(D)/16010.40
81 000 THETASIN(PLAND=1/(2.*D))
82 000 THETASIN(METAN=100./3.141592654)
83 000 RETURN
84 000 CONTINUE

```

```

83,000 IERR01
84,000 RPTURN
85,000 PND
86,000 SUBROUTINE SPOTS
87,000 COMMON /CLEAN/N
88,000 DIMENSION IREM(3,250),REM(2,250)
89,000 INTEGER N
90,000 COMMON /NORM/RN,THETA
91,000 COMMON /MILLER/M,K,L
92,000 REAL RN(3)
93,000 HERE WE USE TWICE THE VALUE PUT IN BY WEISING, WHICH HE TAKES
94,000 INTO ACCOUNT BY USE OF HIS SPECIAL SCALE ON THE FILM ITSELF.
95,000 ALPHA=2.0*ACOS(-RN(2))/100./3.141592654
96,000 IP(ARB(ALPHA).GT.60.)RETURN
97,000 BETAS=0
98,000 IF(RN(3).LT.0)BETAS=90.
99,000 IF(RN(1).EQ.0.)GO TO 10
100,000 BETAS=ATAN(RN(3)/RN(1))*100./3.141592654
101,000 CONTINUE
102,000 N=N+1
103,000 IF(N.GT.250)STOP'ARRAY SIZE TOO SMALL'
104,000 IRFM(1,N)=N
105,000 IREM(2,N)=K
106,000 IREM(3,N)=L
107,000 REM(1,N)=ALPHA
108,000 REM(2,N)=BETA
109,000 RETURN
110,000 ENTRY LAST
111,000 DIST=10.0
112,000 WRITE(100,40)DIST
113,000 FORMAT('1 *****')
114,000 ** LAUE ANGLES DEFINED SUCH THAT ALPHA & ANGLE FROM BEAM, **
115,000 ** BETA & ROTATION CLOCKWISE FROM P1, DIST TO CRYSTAL = **, **
116,000 DO 30 I=1,N
117,000 CALL SCFUN(REM(1,I),ALB,ALC)
118,000 ALTB=ALC
119,000 X=DIST*ALTB*SEC
120,000 Y=DIST*ALTB*SEC
121,000 WRITE(100,20)(IREM(J,I),J=1,3),REM(1,I),REM(2,I),X,Y
122,000 CONTINUE
123,000
124,000
125,000
126,000
127,000

```

```

120 - 110,000
121 - 110,000
122 - 120,000
123 - 121,000
124 - 122,000
125 - 123,000
126 - 124,000
127 - 125,000
128 - 126,000
129 - 127,000
130 - 128,000
131 - 129,000
132 - 130,000
133 - 131,000
134 - 131,100
135 - 131,150
136 - 131,200
137 - 131,300
138 - 131,400
139 - 131,500
140 - 132,000
141 - 133,000
142 - 134,000
143 - 135,000
144 - 136,000
145 - 137,000
146 - 138,000
147 - 139,000
148 - 140,000
149 - 141,000
150 - 142,000
151 - 143,000
152 - 144,000
153 - 145,000
154 - 146,000
155 - 147,000
156 - 148,000
157 - 149,000
158 - 150,000
159 - 151,000
160 - 152,000
161 - 153,000

```

```

** LAUE ANGLES DEFINED SUCH THAT ALPHA = ANGLE FROM BEAM, **
** BETA = ROTATION CLOCKWISE FROM P1, **
** FOMMAY, ** MILLER INDICES I, J, K, L, ** LAUE SPOT ANGLES: ALPHA, **
** G, ** BETA, ** G, ** XE, ** G, ** YE, ** G, **
RETURN
END
SUBROUTINE SONIOM
  INTFGR H
  COMMON /INTFN/REF
  COMMON /MILLER/M,K,L
  COMMON /NORM/RN,THETA
  LOGICAL NO1,NO2,NO3,NO4
  DIMENSION RN(3)
  DATA PHI/3.141592654/,BETAMAX/5.0/
  IF(ABS(RN(2))).LT. 0.9)RETURN
  IF(L.LT.0)RETURN
  IF(K.GT.0)GOTO 12
  IF(K.EQ.0 .AND. M.GT.0)GOTO 12
  RETURN
CONTINUE
  NO1=.TRUE.
  NO2=.TRUE.
  CALL SCFUN(THETA,TTS, TTC)
  T1=2.*TTS*RN(1)
  T2=2.*TTS*RN(3)
  IF(ABS(T1).GT.1.0)NO1=.FALSE.
  IF(ABS(T2).GT.1.0)NO2=.FALSE.
  IF(NO1)RET1=180.*ASIN(T1)/PHI
  IF(NO2)RET2=180.*ASIN(T2)/PHI
  IF(ABS(RET1).GT.BETAMAX)NO1=.FALSE.
  IF(ABS(RET2).GT.BETAMAX)NO2=.FALSE.
  IF(.NOT.NO1) .AND. .NOT.NO2)RETURN
  DELT1=180.*ATAN(RN(3)/RN(2))/PHI
  DELT2=180.*ATAN(RN(1)/RN(2))/PHI
  T=180.*ASIN(RN(1))/PHI
  CALL SCFUN(THETA, TTS, TTC)
  T=TTS/TC
  IF(ABS(T).GT.1.0)NO1=.FALSE.
  IF(NO1)THEY=180.*ASIN(T)/PHI
  T=180.*ASIN(RN(3))/PHI
  CALL SCFUN(T, TTS, TTC)

```



```

214 . 186,000
215 . 187,000
216 . 188,000
217 . 189,000
218 . 190,000
219 . 191,000
220 . 192,000
221 . 193,000
222 . 194,000
223 . 195,000
224 . 196,000
225 . 197,000
226 . 198,000
227 . 199,000
228 . 200,000
229 . 201,000
230 . 202,000
231 . 203,000
232 . 204,000
233 . 205,000
234 . 206,000
235 . 207,000
236 . 208,000
237 . 209,000
238 . 210,000
239 . 211,000
240 . 212,000
241 . 213,000
242 . 214,000
243 . 215,000
244 . 216,000
245 . 217,000
110
111
112
113
114
115
116
117
118
119
120
121
122
123
124
125
126
127
128
129
130
131
132
133
134
135
136
137
138
139
140
141
142
143
144
145
146
147
148
149
150
151
152
153
154
155
156
157
158
159
160
161
162
163
164
165
166
167
168
169
170
171
172
173
174
175
176
177
178
179
180
181
182
183
184
185
186
187
188
189
190
191
192
193
194
195
196
197
198
199
200
201
202
203
204
205
206
207
208
209
210
211
212
213
214
215
216
217
218
219
220
221
222
223
224
225
226
227
228
229
230
231
232
233
234
235
236
237
238
239
240
241
242
243
244
245
246
247
248
249
250
251
252
253
254
255
256
257
258
259
260
261
262
263
264
265
266
267
268
269
270
271
272
273
274
275
276
277
278
279
280
281
282
283
284
285
286
287
288
289
290
291
292
293
294
295
296
297
298
299
300
301
302
303
304
305
306
307
308
309
310
311
312
313
314
315
316
317
318
319
320
321
322
323
324
325
326
327
328
329
330
331
332
333
334
335
336
337
338
339
340
341
342
343
344
345
346
347
348
349
350
351
352
353
354
355
356
357
358
359
360
361
362
363
364
365
366
367
368
369
370
371
372
373
374
375
376
377
378
379
380
381
382
383
384
385
386
387
388
389
390
391
392
393
394
395
396
397
398
399
400
401
402
403
404
405
406
407
408
409
410
411
412
413
414
415
416
417
418
419
420
421
422
423
424
425
426
427
428
429
430
431
432
433
434
435
436
437
438
439
440
441
442
443
444
445
446
447
448
449
450
451
452
453
454
455
456
457
458
459
460
461
462
463
464
465
466
467
468
469
470
471
472
473
474
475
476
477
478
479
480
481
482
483
484
485
486
487
488
489
490
491
492
493
494
495
496
497
498
499
500
501
502
503
504
505
506
507
508
509
510
511
512
513
514
515
516
517
518
519
520
521
522
523
524
525
526
527
528
529
530
531
532
533
534
535
536
537
538
539
540
541
542
543
544
545
546
547
548
549
550
551
552
553
554
555
556
557
558
559
560
561
562
563
564
565
566
567
568
569
570
571
572
573
574
575
576
577
578
579
580
581
582
583
584
585
586
587
588
589
590
591
592
593
594
595
596
597
598
599
600
601
602
603
604
605
606
607
608
609
610
611
612
613
614
615
616
617
618
619
620
621
622
623
624
625
626
627
628
629
630
631
632
633
634
635
636
637
638
639
640
641
642
643
644
645
646
647
648
649
650
651
652
653
654
655
656
657
658
659
660
661
662
663
664
665
666
667
668
669
670
671
672
673
674
675
676
677
678
679
680
681
682
683
684
685
686
687
688
689
690
691
692
693
694
695
696
697
698
699
700
701
702
703
704
705
706
707
708
709
710
711
712
713
714
715
716
717
718
719
720
721
722
723
724
725
726
727
728
729
730
731
732
733
734
735
736
737
738
739
740
741
742
743
744
745
746
747
748
749
750
751
752
753
754
755
756
757
758
759
760
761
762
763
764
765
766
767
768
769
770
771
772
773
774
775
776
777
778
779
780
781
782
783
784
785
786
787
788
789
790
791
792
793
794
795
796
797
798
799
800
801
802
803
804
805
806
807
808
809
810
811
812
813
814
815
816
817
818
819
820
821
822
823
824
825
826
827
828
829
830
831
832
833
834
835
836
837
838
839
840
841
842
843
844
845
846
847
848
849
850
851
852
853
854
855
856
857
858
859
860
861
862
863
864
865
866
867
868
869
870
871
872
873
874
875
876
877
878
879
880
881
882
883
884
885
886
887
888
889
890
891
892
893
894
895
896
897
898
899
900
901
902
903
904
905
906
907
908
909
910
911
912
913
914
915
916
917
918
919
920
921
922
923
924
925
926
927
928
929
930
931
932
933
934
935
936
937
938
939
940
941
942
943
944
945
946
947
948
949
950
951
952
953
954
955
956
957
958
959
960
961
962
963
964
965
966
967
968
969
970
971
972
973
974
975
976
977
978
979
980
981
982
983
984
985
986
987
988
989
990
991
992
993
994
995
996
997
998
999
1000

```


**ELECTRONICS TECHNOLOGY AND DEVICES LABORATORY
MANDATORY CONTRACT DISTRIBUTION LIST**

101	Defense Technical Information Center ATTN: DTIC-TCA Cameron Station (Bldg 5) Alexandria, VA 22314	001	Arlington, VA 22212
012		602	Cdr, Night Vision & Electro-Optics ERADCOM ATTN: DELNV-D
203	GIDEP Engineering & Support Dept TE Section PO Box 398 NORCO, CA 91760	001	Fort Belvoir, VA 22060
001		603	Cdr, Atmospheric Sciences Lab ERADCOM ATTN: DELAS-SY-S
205	Director Naval Research Laboratory ATTN: CODE 2627	001	White Sands Missile Range, NM 88002
001	Washington, DC 20375	607	Cdr, Harry Diamond Laboratories ATTN: DELHD-CO, TD (In Turn) 2800 Powder Mill Road
301	Rome Air Development Center ATTN: Documents Library (TILD)	001	Adelphi, MD 20783
001	Griffiss AFB, NY 13441	609	Cdr, ERADCOM ATTN: DRDEL-CG, CD, CS (In Turn) 2800 Powder Mill Road
437	Deputy for Science & Technology Office, Asst Sec Army (R&D)	001	Adelphi, MD 20783
001	Washington, DC 20310	612	Cdr, ERADCOM ATTN: DRDEL-CT 2800 Powder Mill Road
438	HQDA (DAMA-ARZ-D/Dr. F.D. Verderame)	001	Adelphi, MD 20783
001	Washington, DC 20310	680	Commander US Army Electronics R&D Command
482	Director US Army Materiel Systems Analysis Actv ATTN: DRXSY-MP	000	Fort Monmouth, NJ 07703 1 DELET-MQ 1 DELEW-D 1 DELET-DD 1 DELSD-L (Tech Library) 2 DELSD-L-S (STINFO) 34 Originating Office 1 DELET-MF
001	Aberdeen Proving Ground, MD 21005	681	Commander US Army Communications R&D Command ATTN: USMC-LNO
563	Commander, DARCOM ATTN: DRCDE 5001 Eisenhower Avenue Alexandria, VA 22333	001	Fort Monmouth, NJ 07703
001			
564	Cdr, US Army Signals Warfare Lab ATTN: DELSW-OS Vint Hill Farms Station Warrenton, VA 22186		
001			
705	Advisory Group on Electron Devices 201 Varick Street, 9th Floor New York, NY 10014		
002			
579	Cdr, PM Concept Analysis Centers ATTN: DRCPM-CAC Arlington Hall Station		

**ELECTRONICS TECHNOLOGY AND DEVICES LABORATORY
SUPPLEMENTAL CONTRACT DISTRIBUTION LIST**

(ELECTIVE)

103	Code R123, Tech Library DCA Defense Comm Engrg Ctr 1800 Wiehle Ave Reston, VA 22090	475	Cdr, Harry Diamond Laboratories ATTN: Library 2800 Powder Mill Road Adelphi, MD 20783
104	Defense Communications Agency Technical Library Center Code 205 (P. A. Tolovi) Washington, DC 20305	477	Director US Army Ballistic Research Labs ATTN: DRXBR-LB Aberdeen Proving Ground, MD 21005
206	Commander Naval Electronics Laboratory Center ATTN: Library San Diego, CA 92152	*481	Harry Diamond Laboratories ATTN: DELHD-RCB (Dr. J. Nemarich) 2800 Powder Mill road Adelphi, MD 20783
207	Cdr, Naval Surface Weapons Center White Oak Laboratory ATTN: Library Code WX-21 Silver Spring, MD 20910	482	Director US Army Materiel Systems Analysis Actv ATTN: DRXSY-T, MP (In Turn) Aberdeen Proving Ground, MD 21005
314	Hq, Air Force Systems Command ATTN: DLCA Andrews Air Force Base Washington, DC 20331	507	Cdr, AVRADCOM ATTN: DRSAV-E PO Box 209 St. Louis, MO 63166
403	Cdr, MICOM Redstone Scientific Info Center ATTN: Chief, Document Section Redstone Arsenal, AL 35809	511	Commander, Picatinny Arsenal ATTN: SARPA-FR-5, -ND-A-4, -TS-S (In Turn) Dover, NJ 07801
406	Commandant US Army Aviation Center ATTN: ATZQ-D-MA Fort Rucker, AL 36362	515	Project Manager, REMBASS ATTN: DRCPM-RBS Fort Monmouth, NJ 07703
407	Director, Ballistic Missile Defense Advanced Technology Center ATTN: ATC-R, PO Box 1500 Huntsville, AL 35807	517	Commander US Army Satellite Communications Agcy ATTN: DRCPM-SC-3 Fort Monmouth, NJ 07703
418	Commander HQ, Fort Huachuca ATTN: Technical Reference Div Fort Huachuca, AZ 85613	518	TRI-TAC Office ATTN: TT-SE Fort Monmouth, NJ 07703

*For Millimeter & Microwave Devices Only

**ELECTRONICS TECHNOLOGY AND DEVICES LABORATORY
SUPPLEMENTAL CONTRACT DISTRIBUTION LIST (CONT)
(ELECTIVE)**

519	Cdr, US Army Avionics Lab AVRADCOM ATTN: DAVAA-D	608	Commander ARRADCOM DRDAR-TSB-S
001	Fort Monmouth, NJ 07703	001	Aberdeen Proving Ground, MD 21005
520	Project Manager, FIREFINDER ATTN: DRCPM-FF	614	Cdr, ERADCOM ATTN: DRDEL-LL, -SB, -AP (In Turn)
001	Fort Monmouth, NJ 07703		2800 Powder Mill Road
521	Commander Project Manager, SOTAS ATTN: DRCPM-STA	001	Adelphi, MD 27083
001	Fort Monmouth, NJ 07703	617	Cdr, ERADCOM ATTN: DRDEL-AQ
531	Cdr, US Army Research Office ATTN: DRXRO-PH (Dr. Lontz) DRXRO-IP (In Turn)		2800 Powder Mill Road
	PO Box 12211	001	Adelphi, MD 20783
001	Research Triangle Park, NC 27709	619	Cdr, ERADCOM ATTN: DRDEL-PA, -ILS, -ED (In Turn)
556	HQ, TCATA Technical Information Center ATTN: Mrs. Ruth Reynolds		2800 Powder Mill Road
001	Fort Hood, TX 76544	001	Adelphi, MD 20783
568	Commander US Army Mobility Eqp Res & Dev Cmd ATTN: DRDME-R	701	MTI — Lincoln Laboratory ATTN: Library (RM A-082)
001	Fort Belvoir, VA 22060		PO Box 73
604	Chief Ofc of Missile Electronic Warfare Electronic Warfare Lab, ERADCOM	002	Lexington, MA 02173
001	White Sands Missile Range, NM 88002	703	NASA Scientific & Tech Info Facility Baltimore/Washington Intl Airport
606	Chief Intel Materiel Dev & Support Ofc Electronic Warfare Lab, ERADCOM	001	PO Box 8757, MD 21240
001	Fort Meade, MD 20755	704	National Bureau of Standards Bldg 225, RM A-331
			ATTN: Mr. Leedy
		001	Washington, DC 20231
		707	TACTEC Batelle Memorial Institute
			505 King Avenue
		001	Columbus, OH 43201

**ELECTRONICS TECHNOLOGY AND DEVICES LABORATORY
SUPPLEMENTAL CONTRACT DISTRIBUTION LIST (CONT)**

(ELECTIVE)

Coordinated Science Laboratory University of Illinois Urbana, Illinois 61801 ATTN: Dr. Bill J. Hunsinger	(1)	Anderson Laboratories, Inc. 1280 Blue Hills Ave ATTN: Dr. A.A. Comparini Bloomfield, Conn. 06002	(1)
Dr. J.S. Bryant OCDR ATTN: DARD-ARP Washington, DC 20310	(1)	Mr. Henry Friedman RADC/OCTE Griffiss AFB, NY 13440	(1)
Dr. R. LaRosa Hazeltine Corporation Greenlawn, New York 11740	(1)	Autonetics, Division of North American Rockwell P.O. Box 4173 3370 Miraloma Avenue Anaheim, CA 92802 ATTN: Dr. G.R. Pulliam	(1)
General Electric Co. Electronics Lab Electronics Park Syracuse, NY 13201 ATTN: Mr. S. Wanuga	(1)	General Dynamics, Electronics Division P.O. Box 81127 San Diego, CA 92138 ATTN: Mr. R. Badewitz	(1)
Air Force Cambridge Labs ATTN: CRDR (Dr. P. Carr & Dr. A.J. Slobodnik) Bedford, MA 01730	(2)	Texas Instruments, Inc. P.O. Box 5936 13500 N. Central Expressway Dallas, Texas 75222 ATTN: Dr. L.T. Clairborne	(2)
Mr. R. Weglein Hughes Research Laboratories 3011 Malibu Canyon Road Malibu, California 90265	(1)	Raytheon Company Research Division 28 Seyon Street Waltham, Massachusetts 02154 ATTN: Dr. M.B. Schulz	(1)
Mr. H. Bush CORC RADC Griffiss Air Force Base New York 13440	(1)	Sperry Rand Research Center 100 North Road Sudbury, Massachusetts 01776 ATTN: Dr. H. Van De Vaart	(1)
Dr. Tom Bristol Hughes Aircraft Company Ground Systems Group Bldg 600/MS D235 1901 W. Malvern Fullerton, CA 92634	(2)	Microwave Laboratory W.W. Hansen Laboratories of Physics Stanford University Stanford, CA 94305 ATTN: Dr. H.J. Shaw	(2)
Commander, AFAL ATTN: Mr. W.J. Edwards, TEA Wright-Patterson AFB, Ohio 45433	(1)		

**ELECTRONICS TECHNOLOGY AND DEVICES LABORATORY
SUPPLEMENTAL CONTRACT DISTRIBUTION LIST (CONT)
(ELECTIVE)**

Polytechnic Institute of Brooklyn Route No. 110 Farmingdale, NY 11735 ATTN: Dr. A.A. Oliner (1)	Advanced Technology Center, Inc. Subsidiary of LTV Aerospace Corp. P.O. Box 6144 Dallas, Texas 75222 ATTN: Mr. A.E. Sobey (1)
Westinghouse Electric Corp. Research & Development Center Beulah Road Pittsburgh, PA 15235 ATTN: Dr. J. DeKlerk (1)	United Aircraft Research Labs ATTN: Dr. Thomas W. Grudkowski East Hartford, Conn. 06108 (1)
Stanford Research Institute Menlo Park, CA 94025 ATTN: Dr. A. Bahr (1)	Science Center Rockwell International Thousand Oaks, CA 91360 ATTN: Dr. T.C. Lim (1)
International Business Machines Corp. Research Division P.O. Box 218 Yorktown Heights, NY 10598 ATTN: Dr. F. Bill (1)	University of Southern CA Electronic Science Lab School of Engineering University Park, Los Angeles California 900 ATTN: Dr. K. Lakin, SSC 303 (1)
TRW Defense and Space Sys Group One Space Park Redondo Beach, CA 90278 ATTN: Dr. R.S. Kagiwada (1)	SAWTEK, Inc. P.O. Box 7756 2451 Shader Road Orlando, Florida 32854 ATTN: Mr. S. Miller (1)
Tektronix Inc. P.O. Box 500 Beaverton, OR 97077 ATTN: Dr. R. Li (1)	Prof. P.C.Y. Lee School of Engineering Princeton University Princeton, NJ 08540 (1)
Dr. Fred S. Hickernell Integrated Circuit Facility Motorola Government Electronics Division 8201 East McDowell Road Scottsdale, AZ 85257 (1)	Mr. John A. Kusters Hewlett-Packard 5301 Stevens Creek Boulevard Santa Clara, CA 95050 (1)
Prof. H.F. Tiersten Jonsson Engineering Center Rensselaer Polytechnic Institute Troy, NY 12181 (1)	Dr. Tom Young Sandia Laboratories P.O. Box 5800 Albuquerque, NM 87185 (1)
McGill University ATTN: G.W. Farnell Montreal 110, Canada (1)	Dr. William J. Tanski Sperry Research Center 100 North Road Sudbury, MA 01776 (1)

**ELECTRONICS TECHNOLOGY AND DEVICES LABORATORY
SUPPLEMENTAL CONTRACT DISTRIBUTION LIST (CONT)
(ELECTIVE)**

Dr. B.A. Auld E.L. Ginzton Laboratory Stanford University Stanford, CA 94305	(1)	Dr. Robert L. Rosenberg Bell Laboratories Crawfords Corner Road Holmdel, NJ 07733	(1)
Mr. Marvin E. Frerking MS 137-138 Collins Radio Company 855 35th Street, NE Cedar Rapids, IA 52406	(1)	Dr. B.K. Sinha Schlumberger-Doll Research Center P.O. Box 307 Ridgefield, CT 06877	(1)
Dr. William R. Shreve HP Laboratories 1501 Page Mill Road Palo Alto, CA 94304	(1)	Dr. Robert S. Wagers Texas Instruments, Inc. 13500 N. Central Expwy. P.O. Box 225836, MS 134 Dallas, TX 75265	(1)
Dr. Thomas M. Reeder MS 50-362 Tektronix, Inc. P.O. Box 500 Beaverton, OR 97077	(1)	Dr. Richard C. Williamson Lincoln Laboratory P.O. Box 73 Lexington, MA 02173	(1)

SUPPLEMENT TO DISTRIBUTION LIST

D. Chrissotimos, Code 763 National Aeronautics and Space Administration Goddard Space Flight Center Greenbelt, MD 20771	(1)	Army Materials and Mechanics Research Center (AMMRC) Watertown, MA 02172 ATTN: DMXMR-EO	(1)
Naval Research Laboratories Code 5237 Washington, DC 20375 ATTN: Dr. D. Webb	(1)	Commander, Picatinny Arsenal ATTN: SARPA-FR-S Bldg. 350 Dover, NJ 07801	(2)
HQ ESD (DRI) L.G. Hanscom AFB Bedford, MA 01731	(1)	A. Kahan RADC/ESE Hanscom AFB Bedford, MA 01731	(1)
Commander US Army Missile Command ATTN: DRSMI-RE (Mr. Pittman) Redstone Arsenal, AL 35899	(1)		

